2009

Effects of Water Content and Salinity on Soil Electrical Properties at 50 MHz: Structural and Textural Interactions

Tairone Paiva Leão
University of Tennessee, Knoxville

To the Graduate Council:

I am submitting herewith a dissertation written by Tairone Paiva Leão entitled "Effects of Water Content and Salinity on Soil Electrical Properties at 50 MHz: Structural and Textural Interactions." I have examined the final electronic copy of this dissertation for form and content and recommend that it be accepted in partial fulfillment of the requirements for the degree of , with a major in Geology.

Edmund Perfect, Major Professor

We have read this dissertation and recommend its acceptance:

Accepted for the Council:

Carolyn R. Hodges

Vice Provost and Dean of the Graduate School

(Original signatures are on file with official student records.)

To the Graduate Council:

I am submitting herewith a dissertation written by Tairone Paiva Leao entitled "Effects of water content and salinity on soil electrical properties at 50 MHz: structural and textural interactions." I have examined the final electronic copy of this dissertation for form and content and recommend that it be accepted in partial fulfillment of the requirements for the degree of Doctor of Philosophy, with a major in Geology.

Edmund Perfect, Major Professor

We have read this dissertation and
recommend its acceptance:

Gregory S. Baker

Larry McKay

John S. Tyner

Accepted for the Council:

Carolyn R. Hodges
Vice Provost and Dean of the Graduate School

(Original signatures are on file with official student records.)

Effects of Water Content and Salinity on Soil Electrical Properties at 50 MHz: Structural and Textural Interactions

A Dissertation
Presented for the
Doctor of Philosophy
Degree
The University of Tennessee, Knoxville

Tairone Paiva Leão
May 2009

ACKNOWLEDGEMENTS

I would like to thank everyone that made the completion of this project possible. I would like to thank Dr. Edmund Perfect for guidance and support and for giving me the opportunity to pursue my Ph.D. degree at the University of Tennessee, my committee members Drs Gregory Baker, Larry McKay and John Tyner for valuable suggestions and help with the project, Dr. Alvaro Pires da Silva of University of Sao Paulo (Brazil) for constant support and encouragement since the beginning of my graduate studies, and the US Army Corps of Engineering – Engineering Research and Development Center, for partial funding of this research.

I also wanted to thank everyone that helped with laboratory and field work, instrumentation, and data analysis: Dr. John Curtis, formerly of USACE/ERDC for suggestions, Dr. Charles Weiss of USACE/ERDC for soil mineralogical analyses, Dr. Paul Denton of UT Plant Sciences Department for help with soil sampling, Mr. Mike Newman of UT for statistical consulting, Dr. Alvaro Pires da Silva of ESALQ-University of Sao Paulo, Brazil for soil texture analysis and suggestions, Mr. Wesley Wright of UT Biosystems Engineering Department for help with instrumentation setup, Mr. Bill Deane of UT Earth and Planetary Sciences Department for XRD and XRF analysis, Drs. Craig Barnes and Geoff Eldridge of UT Chemistry Department for help with surface area measurements, and Mr. Dan Williams of UT SERF for help with soil carbon measurements. Without the help of these individuals this research would not have been possible.

Finally I would like to thank all the friends that I made along the years in Knoxville for their support and friendship through good and bad times.

ABSTRACT

The use of dielectric methods for estimating water content and electrical conductivity in saturated and partially saturated porous media is one of the major innovations in soil physics over the past decades. One example of a dielectric sensor is the 50 MHz Hydra Probe. The Hydra Probe is an impedance device that operates at a fixed frequency measuring both components of the complex soil dielectric permittivity response. The general objectives of this research were to: i. improve the understanding of the relationship between soil physical and electrical properties measured at 50 MHz using the Hydra Probe sensor, ii. evaluate the effects of texture, disturbance and salinity on the estimation of water content using the 50 MHz sensor, and iii. develop new models for predicting soil pore solution conductivity from soil electrical properties at 50 MHz. Disturbed and undisturbed duplicate samples from a range of soil textures (Clay, Silty Clay Loam, and Sandy Loam) were saturated with distilled-deionized water and saline solutions at four concentrations: KCl and $CaCl_2$ at 0.01 and 0.02 Mol L^{-1} for three days and then air dried under laboratory conditions. Real and imaginary components of the dielectric permittivity were measured every 5 minutes by the Hydra Probe. Load cells recording changes in sample weight over time, which were later converted into volumetric water content, were also logged. Soil bulk apparent conductivity was calculated from the imaginary permittivity. I found that there was no benefit in including the imaginary dielectric permittivity, or a correction for the loss tangent, in models for estimating water content at 50 MHz. Based on the results, Clay soils should be assessed independently when developing calibration equations for the Hydra Probe. Furthermore, the sensor's water content estimations are sensitive to soil disturbance. New models for estimating the pore solution conductivity were developed. These are dielectric equivalents of Rhoades type two-pathway models based on linear and power law solutions for the transmission coefficient. Overall the average soil solution conductivity predicted by the new models compared favorably to that of the saturating solutions for conductivities greater than about 1.23 dS m^{-1}.

TABLE OF CONTENTS

LIST OF TABLES

Table **Page**

LIST OF FIGURES

Figure **Page**

CHAPTER I. INTRODUCTION

Motivation

The measurement of water content in soils, rocks and other porous materials is a fundamental analysis for agriculture, engineering, environmental and Earth sciences. The accurate and precise determination of water content can be applied to estimate plant water needs in agricultural fields and it is vital to modern agriculture due to the increasing limitation on the amount and cost of water supplies around the world. It is also important for predicting trafficability and workability conditions in agricultural fields and engineering projects in order to avoid compaction in the former case or, in many instances, to optimize it as in the latter case. In hydrogeology, water content is a key parameter for modeling and predicting the fate and transport of water and contaminants in the vadose zone and also in the development of remediation efforts in contaminated underground water sources and soils.

Determination of the electrical conductivity of porous media and their pore solutions are also important features in soil and environmental sciences. The apparent (i.e. bulk) soil electrical conductivity is used in models for estimating the soil solution electrical conductivity. From the latter, the salinity of the soil solution can be directly estimated. Soil salinity is of major importance in agriculture, since it can negatively affect plant growth resulting in productivity losses, and if not controlled promptly can render agricultural fields virtually unusable due to salt build-up. This problem is especially significant in dry-land irrigated agriculture, where irrigation water has a high concentration of soluble salts. Electrical conductivity methods also have several other applications in geophysics and hydrogeology, such as the detection of contaminant plumes and also military or humanitarian applications such as the detection of landmines and unexploded ordnance.

What these two components (electrical conductivity and volumetric water content) have in common is that: i. they cannot be easily determined by direct methods which are often destructive and labor intensive ii. they can satisfactorily be determined from the electrical properties of a multi-phase system, by using sensors that can provide minimum disturbance, real-time, accurate and precise estimations, once they have been calibrated by using empirical or

semi-empirical methods. The 50 MHz Hydra Probe (Stevens Water Monitoring System Inc., 2007) has been viewed as a cheap and reliable method for measuring soil water content using soil dielectric properties. A pore solution conductivity model has not been yet evaluated or proposed for the 50 MHz Hydra Probe.

General Objectives

The general objectives of this research were to:

i. Improve understanding of the relationship between soil physical and electrical properties measured at 50 MHz using the Hydra Probe sensor

ii. Evaluate the effects of texture, disturbance and salinity on the estimation of water content using the 50 MHz sensor

iii. Develop new models for predicting soil pore solution conductivity from soil electrical properties at 50 MHz

Dissertation organization

In order to accomplish the objectives above, this dissertation is subdivided into seven chapters. Chapter II provides a literature review on methods for estimation of soil water content and electrical conductivity. Chapter III presents the methods used throughout this research. Chapter IV presents basic soil characterization and preliminary results. Chapter V presents the results of an investigation into the effects of texture, disturbance and salinity on the estimation of soil volumetric water content from electrical properties. In Chapter VI two models for the estimation of soil pore solution electrical conductivity are derived and evaluated. Finally, Chapter VII presents a summary of the previous chapters, along with general conclusions and recommendations for future studies.

CHAPTER II. BACKGROUND AND LITERATURE REVIEW

Soil Electrical Conductivity

The electrical conductivity is a measure of the ability of a material to conduct an electric current. Under natural conditions, soils are three phase media and therefore the measured conductivity is a representation of the conductivities of the soil solution, air, and solid phases. This "averaged" conductivity is often called apparent or bulk soil conductivity (σ_a) (Friedman, 2005). Apparent soil conductivity is usually determined by using electromagnetic sensors. However, the true interest is in the soil pore solution electrical conductivity. The pore solution electrical conductivity is used to estimate the salt concentration, or salinity of the soil solution (Corwin and Lesch, 2005). Salinity is a major topic in agricultural and environmental sciences; soluble salt contamination of soils has caused problems for all recorded history, primarily in arid regions where rainfall is inadequate to leach salts from the soil (Miller and Donahue, 1995).

Since the electrical conductivity of air is very low (i.e. air is a good insulator) the apparent conductivity is defined mainly by the conductivities of the solid and liquid phases. The conductivity of deionized water at 25°C is very low: 0.0545×10^{-5} dS m^{-1} (Pashley et al., 2005). As the amount of total dissolved solids (TDS) in the pore solution increases the electrical conductivity of that solution will increase in a linear way (Miller and Donahue, 1995). Since the solid phase conductivity is often constant and lower than the pore solution conductivity in the presence of salts, the soil apparent conductivity responds mainly to the salinity of soil solution. If the relationship among the solid phase conductivity, water content and geometrical arrangement of the particles is known it is, at least in theory, possible to estimate the conductivity of the pore solution, and thus its salinity by using a 'Rhoades' type model (Rhoades et al., 1976; Rhoades et al., 1989; Mualem and Friedman, 1991; Hamed et al., 2003):

$$\sigma_a = \theta_v T(\theta_v) \sigma_w + \sigma_s \qquad [2.1]$$

where: θ_v is the volumetric water content (cm^3 cm^{-3}), $T(\theta_v)$ is a transmission coefficient (also known as tortuosity, geometric or formation factor) and is a function of θ_v, σ_w is the soil pore solution electrical conductivity (dS m^{-1}) and σ_s is the soil solid phase surface electrical

conductivity (dS m^{-1}). One of difficulties in using Eq.[2.1] is that estimations of σ_a and subsequent predictions of σ_w are dependent on the knowledge of soil volumetric water content, which can cause mathematical and experimental complications. Methods for estimation of electrical conductivity that are mathematically independent of volumetric water content are discussed in depth in Chapter VI.

Soil Water Content

Soil water content is the amount of water in mass or volume per unit mass or volume of soil (Miller and Donahue, 1995). Most dynamic processes that take place in soil are directly influenced by water content, including, but not limited to: transport, adsorption and exchange of chemical and biological contaminants and nutrients, water absorption by plants and micro- and macro-organisms inhabiting the soil, rates of dissolution and precipitation of minerals, compaction and penetration resistance, unsaturated hydraulic conductivity, and ultimately crop productivity. Therefore, the accurate and precise estimation of soil water content is essential for understanding, modeling, predicting and optimizing (or preventing) the occurrence of such processes.

Soil water content can be expressed in both gravimetric and volumetric form:

$$\theta_g = \text{mass of water/mass of solids} \quad [2.2]$$

$$\theta_v = \text{volume of water/volume of solids} \quad [2.3]$$

where: θ_g is the gravimetric water content (g g^{-1}) and θ_v is the volumetric water content (cm^3 cm^{-3}). The standard method for determination of water content is the thermogravimetric method using convective oven-drying, or "gravimetric" for simplicity.

The gravimetric method was probably the first method developed to measure soil water content, being used as a standard to validate and/or calibrate most, if not all other methods developed after it. In the gravimetric method the water present in a sample is determined by recording the loss of mass in response to heating of the sample. Several methods can be used to heat the samples; the most common is the incandescent heating to a controlled temperature of 105°C to achieve a constant weight as in a conventional oven (Topp and Ferre, 2002). The

gravimetric method, which involves sampling, transporting and repeated weighing, entails practically inevitable errors. It is also laborious and time consuming, since the samples must be transported from the field to the laboratory, and a period of at least 24 h is usually considered necessary for complete oven drying. The standard oven drying method is also questionable because certain clays can retain considerable amounts of adsorbed water even at 105°C. Also the heating can cause oxidation and decomposition of organic material, causing a weight reduction not related to water loss. The errors in the gravimetric method can be minimized by increasing the size and number of samples. On the other hand, the extraction of samples from the field is an invasive and destructive process, which may disturb an observation or experimental plot sufficiently to distort the results (Hillel, 1998). The volumetric water content can be easily calculated from the gravimetric water content if the soil bulk density is known.

$$\theta_v = \theta_g \, D_b/D_w \qquad [2.4]$$

where: D_b is the soil dry bulk density (g cm^{-3}) and D_w is the water density, often assumed as 1.0 g cm^{-3} for simplicity.

The volumetric water content can also be estimated using the neutron thermalization method, commonly know as the "neutron probe". First developed in the 1950s, the neutron thermalization method has gained widespread acceptance as an efficient and reliable technique for monitoring soil moisture in the field (Hillel, 1998). These instruments include a radioactive source of high-energy, epithermal neutrons. When these epithermal neutrons collide with atoms in the soil, they lose energy becoming thermalized. Given that the H nuclei are similar in mass to neutrons, they serve particularly well in thermalizing epithermal neutrons. Thus, a measure of the quantity of thermalized neutrons returning to a detector on the probe over time can give a good measure of the saturation of H atoms in the soil. Given that most H in common soils are associated with water, this can be used to infer the volumetric water content. The main advantage of the neutron thermalization method over the gravimetric method is that it allows less laborious, faster, nondestructive (after initial installation), and periodically repeatable measurements, in the same locations and depths, of the volumetric water content of a representative volume of soil. The method is practically independent of temperature and pressure. Its main disadvantages are the high initial cost of the instrument, low degree of spatial resolution, difficulty of measuring moisture in the soil surface zone, and especially the health hazard associated with exposure to

neutron and gamma radiation (Hillel, 1998). Another problem associated with the neutron thermalization method is that in soils with high organic matter contents, the epithermal neutrons can interact with H nuclei present in organic matter, which will be accounted as H in water molecule providing an erroneous overestimated measurement of soil water content.

Many of the problems associated with estimating soil water content by the gravimetric and neutron thermalization methods can be overcome by using electromagnetic methods. Electromagnetic methods are indirect methods and will be discussed later in this chapter.

Dielectric Properties of Soils

The word dielectric is derived from the Greek prefix *dia* which can be translated as "through" or "across". The term dielectric refers to a material that permits the passage of an electric field, but not particles. This statement implies that a dielectric material does not permit the passage of any kind of particles, including electrons. Thus, it should not conduct the electric current. However, a dielectric material is generally considered nonconducting or insulating. An ideal dielectric material does not exist. The absolute vacuum is considered as to be close to the ideal dielectric, but absolute vacuum cannot be obtained on Earth. All real dielectric materials are imperfect, and thus permit, to a certain degree, the passage of particles (Kao, 2004). An important characteristic of a dielectric is its permittivity, also known as dielectric constant or dielectric permittivity (ε).

Real dielectrics are substances that have dielectric permittivity values (ε) greater than that of vacuum (ε_0). Since the permittivity of a dielectric is always greater than the permittivity of the vacuum, the relative permittivity (ε^*) of the dielectric is usually employed. The relative permittivity is the ratio of the permittivity of the material to that of vacuum (Krauss, 1992):

$$\varepsilon^* = \varepsilon/\varepsilon_0 \qquad [2.5]$$

where: ε^* = relative permittivity of the dielectric (dimensionless), ε = permittivity of the dielectric (F m^{-1}), ε_0 = permittivity of absolute vacuum (8.85 x 10^{-12} F m^{-1}).

The dielectric permittivity of materials is a complex quantity and is influenced by the frequency at which the measurements are performed (Campbell, 1990; Seyfried et al., 2005):

$$\varepsilon^* = \varepsilon_r - j\,\varepsilon_i \quad [2.6]$$

where: ε_r is the real component of ε^*, ε_i is the imaginary component of ε^*, and $j = \sqrt{-1}$. The imaginary component of ε^* is related to the loss of energy caused mainly by two factors, molecular relaxation and DC conductivity (Seyfried et al., 2005):

$$\varepsilon_i = \varepsilon_{i,mr} + (\sigma/2\pi f\varepsilon_0) \quad [2.7]$$

where: $\varepsilon_{i,mr}$ = relative permittivity due to molecular relaxation, σ = low frequency conductivity (DC) (S m^{-1}) and f = measured frequency (Hz).

For most practical applications, methods that rely on soil dielectric properties to estimate soil water content, including several TDR, capacitance and impedance devices, often rely on the assumption that the measured real dielectric permittivity (ε_r) is a good approximation for the complex permittivity of the soil (ε^*). Thus, for low-loss, nearly homogenous materials, the $j\varepsilon_i$ term in Eq.[2.6] is often neglected and the approximate complex permittivity, named apparent soil permittivity (ε_a), is used (Topp et al., 1980). The very large dielectric permittivity of water $\varepsilon_r \sim 80$, relative to that of air $\varepsilon_r \sim 1.0006$, and common soil minerals $\varepsilon_r \sim 4.5$ to 10 (Robinson, 2004) results in the permittivity of a wet soil being dominated by the volumetric water content. More precisely, the bulk dielectric permittivity of a soil will be a function of the volumetric water content, with only a slight dependence on the volume fraction of solids (Ferre and Topp, 2002). Much like in the case of electrical conductivity, the complex permittivity of a soil is therefore a representation of all three phases interacting in the bulk volume that is being measured.

The loss tangent is another critical parameter from soil dielectric response (Seyfried and Murdock, 2004). The loss tangent represents the ratio of the imaginary to the real permittivity (Robinson et al., 2003) and integrates all dielectric and conductive losses into a single parameter (Topp et al., 2000). The loss tangent is defined as:

$$\tan\delta = \varepsilon_i/\varepsilon_r \quad [2.8]$$

The higher the conductive losses, the higher the tan δ value.

History of Electromagnetic Methods

The use of dielectric techniques for measuring water content has grown enormously over the last few decades. This revolution in electromagnetic methods for water content estimation was initiated by the Time Domain Reflectometry (TDR) method which has become a standard method for measuring water content, second only to the gravimetric method (Ferre and Topp, 2002). The advances and potential problems of the TDR method are described in several publications. Some of the best descriptions of this method can be found in Topp et al. (1980) for a reference publication; Jones et al. (2002) for principles and applications; Robinson et al. (2003) for a general overview of the method, and Ferre and Topp (2002) for theory and application.

The TDR was first developed as a technique for measuring effective permittivity of materials (Ferre and Topp, 2002). The process of adaptation of TDR for measuring soil water content was lead by G. Clarke Topp and is described in detail by Topp et al. (2003). Most TDR systems currently used for soil measurements apply a fast rise time electromagnetic pulse to the soil transmission lines (usually a pair of parallel metal rods, connected to a signal receiver inserted into the soil). The time delay between the reflections of the pulse from the beginning and end of the soil transmission line is used to determine the velocity of propagation through the soil along the transmission line. The permittivity of the soil controls this velocity. The dependence of this permittivity on the water content is used to infer the water content from the velocity (Topp and Ferre, 2002).

The high cost of TDR has lead to the development of alternative electromagnetic sensors that use the principle of measuring soil dielectric properties to determine water content (Seyfried and Murdock, 2004). These alternative sensors are based on other electromagnetic techniques and usually operate at lower, fixed frequencies aiming to simplify the electronic design and thus the cost of the equipment. Examples of these techniques are capacitive and impedance type sensors (Paltineanu, 2007). This dissertation is based on data collected using an impedance type sensor, the 50 MHz Hydra Probe (Stevens Water Monitoring System Inc., 2007).

The 50 MHz Hydra Probe

The design of the Hydra Probe is based on the work of Campbell (1990). The first evaluation of commercial versions of the device was reported by Seyfried and Murdock (2004). The instrument consists of a 4 cm diameter cylindrical head with four 0.3 cm diameter tines of 5.8 cm in length (Appendix A). The tines are arranged in a way that the centrally located tine is surrounded by the other three tines in an equilateral triangle with 2.2 cm sides. The 50 MHz signal is generated in the head and transmitted via planar waveguides to the tines which constitute a coaxial transmission line (Campbell, 1990; Seyfried and Murdock, 2004). The impedance of the probe is defined by the electronic components and the $\varepsilon*$ of the material between tines (Seyfried and Murdock, 2004):

$$Z_p = \text{cotanh}(\omega L \sqrt{\varepsilon^*})/c\, j \qquad [2.9]$$

where: Z_p = probe impedance, L = electric length of the probe, and c = speed of light, ω is the angular frequency, and $j = \sqrt{-1}$. When a voltage is applied to the probe via a coaxial cable, a reflected voltage signal is produced that is related to the characteristic impedance of the coaxial cable, Z_c, by (Campbell, 1990):

$$Z_p/Z_c = (1 + \Gamma) / (1 - \Gamma) \qquad [2.10]$$

where: Γ is the complex ratio of the reflected voltage to the incident voltage. From Γ is possible to determine Z_p from Eq.[2.10] and then invert Eq.[2.9] to solve for ε^*. In the Hydra Probe, a conductor cable transmits analog DC voltages that are used to calculate ε_i, ε_r and temperature (Seyfried and Murdock, 2004). The measured temperature is used to correct the dielectric variables to a standard temperature value. Volumetric water content of the medium in which the probe is inserted is then calculated by using empirical calibration equations and the real component of soil permittivity. The most common types of calibration equations are the linear square root (Seyfried et al., 2005):

$$\theta_v = A \sqrt{\varepsilon_r} + B \qquad [2.11]$$

and the polynomial (Topp et al., 1980):

$$\theta_v = A_0 + A_1 \varepsilon_r + A_2 \varepsilon_r^2 + \ldots + A_n \varepsilon_r^n \qquad [2.12]$$

where: A, B, and A_0 to A_n are empirical coefficients that assume different values depending on the medium in which the sensor is calibrated.

With the Hydra Probe, the electrical conductivity is calculated directly from the imaginary permittivity, i.e. by rearranging and neglecting $\varepsilon_{i,mr}$ in Eq.[2.7] we get (Campbell, 1990; Seyfried et al., 2005):

$$\sigma_d = (\varepsilon_i \, 2\pi \, f \, \varepsilon_0) \qquad [2.13]$$

where: σ_d = dielectric conductivity (S m^{-1}).

Research applications of the Hydra Probe are limited to a few publications. The Hydra Probe provided accurate and precise measurements of ε_r in different fluids (air, water, and ethanol) with low variability among individual sensors, for values of $\varepsilon_i < 50$ and $\tan \delta < 1.45$ (Seyfried and Murdock, 2004). These authors also found that the calibration equations provided by the manufacturer were inadequate to describe the soils evaluated in their research (Seyfried and Murdock, 2004). Estimations of water content under field conditions using the Hydra Probe resulted in greater variability, and an increase in error components, when compared to laboratory experiments (Bosch, 2004). Under such conditions, soil specific calibration equations are recommended in order to increase the accuracy and precision of the estimations (Bosch, 2004).

Seyfried et al. (2005) were the first to employ square root linear equations (Eq.[2.11]) to calibrate Hydra Probe sensors. The default calibration equations provided by the manufacturer are high order polynomials in the form of Eq.[2.12] (Bosch, 2004). Their results showed that general and soil specific calibration equations for 19 soils performed better than the equations provided by the manufacturer (Seyfried et al., 2005). They also provided a loss corrected general calibration equation (i.e. with a linear correction term for $\tan \delta$) that resulted in a further increase in the accuracy of the Hydra Probe sensor (Seyfried et al., 2005). The Hydra Probe ε_r measurements were found to be largely insensitive to temperature variation in the range of 5 to 50 °C, while ε_i was highly responsive to temperature changes over that same range of values (Seyfried and Grant, 2007). To overcome this problem the Hydra Probe sensor offers temperature corrected readings of ε_r and ε_i (Stevens Water Monitoring System Inc., 2007).

CHAPTER III. GENERAL METHODS

Soil Sampling

Thirty undisturbed cores and three disturbed bulk soil samples were collected on June 10, 2005 at the Plant Sciences experimental farm at the University of Tennessee, Knoxville. The sampling was performed in areas encompassing three soil series, covering three contrasting soil textural classes, according to the USDA system: Etowah Clay (fine-loamy, siliceous, semiactive, thermic Typic Paleudult) Sequatchie Sandy Loam (fine-loamy, siliceous, semiactive, thermic Humic Hapludult) and Lindside Silty Clay Loam (fine-silty, mixed, active, mesic Fluvaquentic Eutrudept) (Soil Survey Staff, 2008) (Appendix B).

Ten undisturbed and one bulk disturbed samples were collected at each site. The objective of sampling in three different soil classes was to obtain different physical properties (e.g. water retention, electrical properties, bulk density, porosity, etc) improving the quality, sensitivity and applicability of the final models. The undisturbed samples were collected using a Uhland core sampler, the cores having the dimensions of 5.37 cm inner diameter and 6 cm height. The bulk disturbed samples were collected using a shovel and approximately 5 kg of soil was collected. All samples were collected at the depth of 20 to 25 cm which was beneath the layer of greatest root mass. The disturbed soil samples were air dried, broken apart by hand and used to pack 10 disturbed cores for each soil. The repacked cores and the undisturbed samples were of the same dimensions.

Soil Characterization

Particle density (Blake and Hartge, 1986a), total carbon and general chemical characterization were performed. Total carbon was measured using a PC-controlled total organic carbon analyzer Model TOC-V CSH (Shimadzu Co., Kyoto, Japan). Particle size distribution was characterized using the hydrometer method with readings at 0.5, 1, 90 and 1440 minutes for

the < 0.05 mm fraction (i.e. silt + clay) with sand fraction characterized by dry sieving (Gee and Or, 2002). The mineralogical composition of the soils was characterized by X-ray diffraction analysis (Whittig and Allardice, 1986) and X-ray fluorescence spectroscopy analysis (Jenkins, 1999). Bulk soil and phyllosilicate weight percent mineralogy was also quantified by X-ray diffraction using glycol-solvated method on request by the US Army Corps of Engineers, Engineer Research and Development Center, Vicksburg, MS. Results for bulk soil mineralogical analyses on mass basis and relative percentage of phyllosilicate fraction are presented in Figures 3.1 and 3.2 (All figures for this Chapter are located in Appendix D). Soil specific surface was determined by gas absorption (Quantachrome NOVA-1000 gas sorption analyzer, using N_2 gas), based on the BET equation for multilayer absorption (Pennell, 2002). Dry bulk density was calculated following Blake and Hartge (1986b). Basic soil exchange phase chemical analysis was performed on request by the University of Tennessee Soil and Forage Testing Laboratory, Nashville, TN (Appendix C). The wilting point water content (water content held at a potential of -1500 kPa) on a gravimetric basis was estimated using a WP4 Dew Point PotentiaMeter (Decagon devices, Inc., Pullman, WA) as described by Scanlon et al. (2002). Soil chemical properties and X-ray diffraction plots are presented in Appendix C. Saturated hydraulic conductivity was determined using a falling head method (Reynolds and Elrick, 2002).

$$K_{sat} = (L/t) \ln (h_0/h_t) \qquad [3.1]$$

where: K_{sat} = saturated hydraulic conductivity (cm s^{-1}), L = soil length (cm), t = time (s), h_0 = height of water above sample at time t = 0, and h_t is the height of water above the sample at time = t.

Experimental Design

The experimental design was a factorial with three soils (Clay, Silty Clay Loam and Sandy Loam); two disturbance treatments (disturbed and undisturbed); and five solute levels: two $CaCl_2$ concentrations, two KCl concentrations and distilled-deionized water as a control; and two replications. Thus the factorial design consisted of 3 x 2 x 5 x 2 = 60 samples.

Laboratory Equipment

The Hydra Probe (Seyfried and Murdock, 2004) (Stevens Water Monitoring Systems, Inc., Portland OR) was employed to measure both components of the soil dielectric permittivity, i.e. real and imaginary permittivity, in addition to temperature. Decagon T5 miniature pressure transducer tensiometers (hereafter refer to as mini-tensiometers) (UMS, 2001) were used to measure the water potential in the wet range of the water retention curve (i.e. suctions $\leq$ 10 kPa). Load cells were used to measure the weight change of the samples during the experiments (Transducer Techniques, model LSP-1). The Hydra Probe and the mini-tensiometers were connected to VITEL VX110 datalogger (Stevens Water Monitoring Systems, Inc., Portland OR) while the load cells were connected to the Campbell 21X (Campbell Scientific, Inc., discontinued) datalogger. Pictures of the devices used are presented in Appendix A.

Experimental Procedures

In the laboratory, the disturbed and undisturbed replicate samples were saturated with saline solutions at five concentrations, namely distilled-deionized water (0 Mol L^{-1} or control), KCl at 0.01 and 0.02 Mol L^{-1} and $CaCl_2$ at 0.01 and 0.02 Mol L^{-1} for three days (Details of the procedure for selecting the salt concentrations are presented in Chapter IV). All soil samples were flushed with approximately two pore-volumes of the designated solution after saturation (The saturated hydraulic conductivity being measured in the process). The samples were then weighed on an electronic balance and Hydra Probe sensors were inserted at one end and mini-tensiometers at the other. The saturated samples containing the Hydra Probes and mini-tensiometers were placed horizontally on load cells (Transducer Techniques, model LSP-1). A schematic description of the setup and pictures of the equipment are presented in Appendix A. The Hydra Probes, mini-tensiometers and the load cells were connected to dataloggers (VITEL VX1100 and Campbell 21X micrologger). The soil electrical properties and water potential were measured by the Hydra Probes and T5 mini-tensiometers, respectively, and recorded by the Vitel datalogger, while the change in weight of the samples in time, due to air drying, was measured

by the load cells and recorded by the Campbell datalogger. All measurements were recorded in five minute intervals. After approximately five days, when the decrease in sample weight with time was negligible, the probes were removed from the soil samples. The samples were then weighed on an electronic balance, oven dried at 105°C and then reweighed for determining water content during the drying cycle and dry bulk density. The average air temperature in the lab during the drying cycles was 21.5°C (CV = 5.24%). The data sets usually consisted of over 1100 observations for each sample. The observations consisted of soil temperature (T, °C), real dielectric permittivity (ε_r), imaginary dielectric permittivity (ε_i), volumetric water content (θ_v, $cm^3\ cm^{-3}$), conductivity ($S\ m^{-1}$), water potential (|kPa|), and load cell signal ($mV\ V^{-1}$). The load cell signal was converted to mass by linear calibration equations in the form of Eq.[3.2].

$$M = a_1 S + b_1 \qquad [3.2]$$

where: M = mass (g), *a1* = slope, S = signal ($mV\ V^{-1}$), *b1* = intercept.

Load Cell Calibration

The design of the load cell system used to record the change in soil weight during the drying experiments is presented in Figure 3.3. Four Transducer Techniques load cells were used to record the change in signal with decrease in soil water content. The signal was then converted to mass loss using specific calibration equations for each load cell (Eq.[3.2]). The calibration equations for each of the four load cells are presented in Figure 3.4. Standard weights, with masses varying from one to 200 g were used in the calibration procedures. To validate the calibration equations, the volumetric water contents of cores packed with homogeneous sand sized material were estimated using the load cells data and a standard Mettler Toledo laboratory scale (Model B2002-S College). The comparisons of water contents estimated using load cells and scale is presented in Figures 3.5, 3.6, 3.7 and 3.8 for each of the load cells. Results show a very good agreement between results from load cells and scale. The coefficient of determination (R^2) was > 0.9990 for all four load cells.

Experiments with Glass Beads

The air drying experiments described for the soil samples were also performed using samples packed with glass beads. The objective of the glass bead experiments was to investigate the interactions between physical and hydraulic properties in a chemically and electrostatically inert media of known porosity and particle size distribution. The data were also used to evaluate the calibration equations developed for the Hydra Probe. The glass beads had average diameters of 2.0, 1.0, 0.5, 0.25, 0.125 and 0.0625 mm and a particle density of 2.5 g cm^{-3} (Mo-Sci Corp., Rolla, MS). Repacked samples were made up by mixing the glass bead fractions in different proportions: 44, 25, 15, 8, 5 and 3% (sample D2.2); 30, 23, 17, 13, 10 and 7% (sample D2.6); 23, 20, 17, 15, 13 and 12% (sample D2.8), 20, 18, 17, 16, 15 and 14% (sample D2.9), and 18, 17.5, 17, 16.5, 16, and 15% (sample D2.95) respectively, with two replicates. The average and standard deviation (in parentheses) of the bulk density values for the glass bead core pairs were: 1.76(0.01), 1.85(0.04), 1.84(0.01), 1.81(0.02) and 1.79(0.01) g cm^{-3} for the distributions described above, respectively.

Numerical Modeling of Air Drying Experiments

In order to evaluate potential heterogeneities in the water content distribution within the core during drying, numerical modeling experiments were performed in Hydrus 2D (Rassam et al., 2003) and compared to observed data. The air drying simulations were performed for each soil texture and disturbance scenario following Rassam et al. (2003). The domain of the horizontal drying experiment is presented in Fig. 3.9; both the left and right ends were open to the atmosphere and the upper and lower ends were no-flow boundaries. In the numerical modeling process, at time = 0 the soil cores were fully saturated with water. As time increased in steps, varying from 0.01 h for the minimum time step, 0.1 h for the initial time step and 1 h for the maximum time step, the water potential at the left and right boundary conditions (atmospheric boundary conditions) decreased until reaching the critical water suction value for each soil, i.e. 1500 kPa for Clay and Silty Clay Loam and 500 kPa for Sandy Loam (Rassam et

al., 2003). This causes the water content inside the sample to decrease, until reaching a condition where the water content does not change significantly with time. In addition to the critical water potential at the boundary conditions, the maximum evaporation rate (cm h^{-1}) and soil bulk density (g cm^{-3}) are parameters that can be varied in the Hydrus 2D numerical model. These parameters were varied in order to match the numerical model data to the observed data from the air drying experiments. The data were matched by time, and the model mass balance (numerical domain average) was compared to the observed data. The forward predictions were performed in a semi-empirical iterative fashion, as the input parameters for the forward predictions in Hydrus 2D were "manually" modified until a best fit could be achieved in relation to the observed drying data.

CHAPTER IV. SOIL CHARACTERIZATION AND PRELIMINARY RESULTS

Salt Concentrations

As described in Chapter III, in addition to distilled-deionized water, two salts ($CaCl_2$ and KCl) at two concentrations were used in the experiments. The salt concentration has a major influence on the soil imaginary dielectric permittivity (ε_i) and electrical conductivity. To determine the salt concentrations to be used in the experiments, the dielectric response of the Hydra Probe was investigated using KCl solutions at 0.005; 0.01; 0.02 and 0.05 Mol L^{-1} and $CaCl_2$ solutions at 0.001; 0.005; 0.01; 0.02 and 0.05 Mol L^{-1} concentrations (no soil). According to the Hydra Probe manual, when the imaginary dielectric constant exceeds the real dielectric constant by a factor of two or greater, the accuracy of the real dielectric constant is degraded. Based on data presented in Figures 4.1 and 4.2, concentrations of 0.01 and 0.02 Mol L^{-1} were chosen for both salts (All figures for this Chapter are located in Appendix F). In both cases, the 0.01 Mol L^{-1} concentration was enough to discriminate the electrical response from that of pure water, because at 50 MHz, the imaginary part of the complex dielectric response of pure water is very small (<5). For $CaCl_2$, the 0.02 Mol L^{-1} concentration provides imaginary dielectric permittivity values that are about twice the real permittivity (Figure 4.2). However, as shown in subsequent chapters, because of the attenuation from soil components, the imaginary response is usually lower than the real permittivity in soil samples saturated with $CaCl_2$ 0.02 Mol L^{-1}.

Soil Physicochemical Properties

Soil physicochemical properties are presented in Table 4.1 (All tables for this Chapter are located in Appendix E). Clay content varied from 6.27 to 45.59% while sand content ranged from 13.03 to 74.41%. Total carbon was greater in the Silty Clay Loam soil, which might be related to the fact that this soil profile was under grass, with a denser root system than in the

other soils, located under pines (Clay) and short grass (Sandy Loam). Specific surface area was positively correlated to clay content, ranging from about 2.12 to 34.68 $m^2\ g^{-1}$.

Bulk density values were significantly higher in the Sandy Loam soil, including the disturbed samples, but virtually the same for the Clay and Silty Clay Loam soils. Analysis of variance (ANOVA) for soil bulk density was significant at $P > F < 0.0001$. The effects soil texture, disturbance and their interactions were significant at $P = 0.01$. As expected, the saline solution saturation did not have any influence on bulk density. The bulk density values were higher in the Sandy Loam soil, and for any soil texture, the undisturbed samples had higher bulk densities (Figure 4.3). This is related by the packing procedure, which was not effective in producing bulk density values close to the original values in undisturbed samples. The bulk density values for Clay and Silty Clay Loam soils were not statistically different (Figure 4.3) indicating similar values of total porosity for these soil samples.

Geometric means for saturated hydraulic conductivity were in the order of 10^{-3} cm s^{-1}, except in the undisturbed Clay and Sandy Loam soils, where the magnitudes were about 10^{-5} and 10^{-4} cm s^{-1}, respectively. The ANOVA for the logarithm of the saturated hydraulic conductivity (log K_{sat}) data as a dependent variable and soil texture, disturbance and salt treatment as independent factors was significant at $p > F < 0.0001$. The factors of soil texture, disturbance and the interaction of soil texture x disturbance were also significant at that same probability level. A plot of the averages of log K_{sat} for each soil texture and disturbance is presented in Figure 4.4. The greatest differences in log K_{sat} were for the undisturbed samples; the lowest conductivities were found in the Clay soil, followed by the Sandy Loam and the Silty Clay Loam. For the repacked samples, the Silty Clay Loam soil had the lowest conductivities (Figure 4.4). The Clay soil was expected to have lower conductivities, since it was located in an uncultivated area. The similar conductivities for the repacked samples can be explained by the homogenization process of repacking the soil cores with air dried and sieved soil. The absence of a salt effect in the saturated hydraulic conductivity ($P > F = 0.53$) indicates that the soils were not subjected to significant swelling during saturation with the different solutions, which could potentially change structural properties and hence hydraulic conductivity.

Soil Water Desorption Curves

Clay Samples

The water desorption data for the undisturbed Clay soil samples are presented in Figure 4.5. The data are similar to a traditional water retention curve, where the volumetric water content is plotted as a function of the water potential. The main differences are that the water potential data were collected using a mini-tensiometer and the sample was subjected to air drying instead of being placed on a pressure plate. The water potential data measured by the mini-tensiometers were generally satisfactory. In only three cases the mini-tensiometers lost hydraulic contact at suctions lower than 80 kPa.

Water desorption data for the disturbed (repacked) Clay samples are presented in Figure 4.6. The curves follow the same exponential decay form as in the undisturbed samples. The main differences between the disturbed and the undisturbed samples are the saturated water contents, which were higher in the disturbed samples, and the fact that for one of the water treatments the mini-tensiometer held the water column up to a water potential of 250 |kPa| (Figure 4.6). This phenomenon could be an instrumentation reading error however, since the maximum water potential value for a tensiometer is usually about 80 |kPa|. As in the case of the undisturbed samples, any differences in water retention data among treatments should be predominantly related to soil structural effects since the tensiometer does not discriminate osmotic effects between salt treatments (Hillel, 1998).

Silty Clay Loam Samples

There was a large variability in the water desorption curves for the undisturbed Silty Clay Loam samples (Figure 4.7). As an illustration, the water contents at a potential of 60 |kPa| vary from about 0.21 $cm^3\ cm^{-3}$ to about 0.35 $cm^3\ cm^{-3}$. This variability can be justified by the higher structural variability in the undisturbed Silty Clay Loam than in its counterparts. The standard deviation (stdev) of the bulk density in the undisturbed samples was higher than any of the other soils (stdev = 0.03 $cm^3\ cm^{-3}$).

The variability in water desorption data was much lower in the Silty Clay Loam disturbed samples (Figure 4.8). As mentioned earlier this can be related to the homogenization process during soil repacking. The lower variability in the data is also reflected by the smaller standard deviations for the bulk densities in relation to the disturbed samples (stdev = 0.01 cm^3 cm^{-3}). Another difference between disturbed and undisturbed samples is that the water continuity in the tensiometers breaks at a lower water potential (i.e. absolute value) in the disturbed samples. This might be related to the poorer contact between soil and the tensiometer cup in the less dense and less structured repacked samples.

Sandy Loam Samples

Water desorption curves for the undisturbed Sandy Loam samples follow a standard shape for coarse materials (Figure 4.9). In particular, there is evidence of a pronounced air entry value. The only discrepancy is in the sample treated with $CaCl_2$ 0.01 Mol L^{-1} replication b, which has a higher initial porosity (and therefore saturation) than the other samples.

As expected, there was less variability in the water desorption curves for the disturbed Sandy Loam soil (Figure 4.10). The range of water potentials was about the same as for undisturbed samples, from about 0 to 60 |kPa|. Although there was some variability in bulk density values in the disturbed sand samples (stdev = 0.02 g cm^{-3}) this variability did not cause major differences among samples in the water desorption data.

Statistical Analysis

Statistical analysis was performed by fitting the soil water desorption data for each sample to the van Genuchten water retention model (van Genuchten, 1980):

$$\theta_v = \theta_r + (\theta_s - \theta_r) / [1 + (\alpha \psi)^n]^{1- 1/n} \qquad [4.1]$$

where: θ_v = measured volumetric water content (cm^3 cm^{-3}), θ_r = residual water content (cm^3 cm^{-3}), θ_s = saturated water content (cm^3 cm^{-3}), α = inverse of air entry suction (kPa^{-1}), ψ = water suction (kPa), n = fitting parameter (dimensionless). In order to fit Eq.[4.1] the parameters θ_r and θ_s were determined experimentally, while α and n were fitted by using nonlinear regression in

the SAS® software package. The residual water content θ_r was calculated from the dry range water retention data measured using the WP4 PotentiaMeter (Scanlon et al., 2002). The measured gravimetric water content for each soil at a suction of 1500 kPa (i.e. wilting point water content) was assumed to represent the residual water content and converted to a volumetric residual water content by using the bulk density from each sample. The saturated water content, θ_s, was assumed to be equal to the total porosity, calculated as $\phi = \theta_s = 1 - D_s/D_b$, where ϕ = total porosity, D_s and D_b are the solid and bulk densities (g cm^{-3}), respectively. These assumptions were adopted because the nonlinear regression failed to converge for several samples when using θ_s and θ_r as fitting parameters, probably due to overparameterization and nonuniqueness in the fitting procedures. The average (and standard deviation in parentheses) of the sum of squared errors of the nonlinear regression fitting was 0.0318(0.0412) cm^3 cm^{-3}. The average α (and standard deviation) was 2.25(9.20) kPa^{-1} and the average (and standard deviation) n was 1.39(0.28), from a population of 59 samples (ψ data for one of the Sandy Loam undisturbed samples were lost and treated as missing values).

The ANOVA's were performed with θ_s, θ_r, α and n as independent variables in a model where soil texture, disturbance and salt treatments and their interactions were the factors evaluated. The overall ANOVA for α was not significant ($P > F = 0.48$) while the ANOVA's for θ_s, θ_r and n were all highly significant ($P > F < 0.0001$). The effects of soil texture, disturbance and their interaction were significant at $P = 0.01$ for θ_s and θ_r, while the salt treatment effect and their interactions were not significant. Results for the averages of θ_s and θ_r are presented in Figures 4.11 and 4.12. For both disturbed and undisturbed treatments the Clay and Silty Clay Loam soils had higher saturated water contents (Figure 4.11). This can be explained by the fact that sandy soils usually have lower total porosity and higher bulk density, resulting in less pore space available for saturation with water. The Clay soil had the highest values of θ_r, followed by the Silty Clay Loam soil, while the Sandy Loam soil residual water content value was significantly less than the other soils (Figure 4.12). The dry range water retention is controlled by textural factors (Nimmo, 1997) in other words, the higher the content of clay, especially active type clays, the greater the water retained at large water suctions.

For the n parameter, soil texture, disturbance, soil texture x disturbance and salt treatment effects were all significant at $P = 0.01$. The average n for each salt treatment is presented in Figure 4.13. Overall, there was a small trend of decreasing of n with increasing in salt concentration (Figure 4.13). Although this could be an experimental artifact, it is also possible that the addition of salts has changed water properties (i.e. density, viscosity, surface tension etc.) to a point where the shape of the water retention curve is altered. The n parameter is an increasing function of the slope of the water retention curve (van Genuchten, 1980). In other words, the steeper the slope of the curve, the higher the value of n. The addition of salt causes n to decrease, indicating a decrease in the slope of the curve. Another hypothesis is that the addition of salt might be altering the mesoporosity of the sample and thus the slope of the curves, by changing the structural properties due to different levels of swelling or shrinkage (as the soil is air dried) due to the interactions of salts and the mineral grains and clays.

With respect to the soil texture and disturbance effect, n was higher in coarser, undisturbed material, indicating a steeper slope of the water retention functions in these materials, related to the predominance of coarser and medium sized pores, which drain relatively quickly with the increase in tension (Figure 4.14).

Soil Electrical Properties

Clay Samples

The electrical properties measured during the drying experiments performed on undisturbed samples of the Clay soil are presented in Figures 4.15, 4.16, and 4.17. The soil real dielectric permittivity (ε_r) was highly responsive to the increase in volumetric water content. However, there is no clear distinction in ε_r curves among treatments (Figure 4.15). The imaginary permittivity response provides a better discrimination among treatments (Figure 4.16). The higher $CaCl_2$ concentrations, in particular, are distinguishable from the other treatments, with a steeper response. The distilled-deionized water curves (control) show a muted response relative to the other treatments. The distinction among KCl 0.01 Mol L^{-1}, KCl 0.02 Mol L^{-1} and

$CaCl_2$ 0.01 Mol L^{-1} responses is not very clear, especially at lower water contents. This could be related to variations in soil physical properties. For example, sample KCl 0.02 Mol L^{-1} (replicate b) had a consistently lower ε_i value than its duplicate (a). However, its bulk density was slightly higher, which leads to less total porosity and lower space available for saturation with the salt solution. Soil electrical conductivity basically represents a rescaling of the ε_i data (Figure 4.17). The conductivity measured by the probe is not presented, since the resolution (0.01 S m^{-1}) is too coarse for any reasonable interpretation of the data. The conductivity plots presented in Figure 4.17 were calculated from the ε_i data using Eq.[2.13] (Campbell, 1990; Seyfried et al., 2005).

Results for the disturbed Clay soil samples were somewhat similar to the undisturbed samples (Figures 4.18, 4.19 and 4.20). The only difference seems to be that the relationships are more linear in the disturbed samples. This is to be expected since the process of packing reduces spatial heterogeneity within the samples. There was not a great differentiation among treatments for ε_r as a function of volumetric water content (Figure 4.18). In any case it is very likely that treatment distinction from the ε_r data is not possible. The real component of soil permittivity is not strongly influenced by ion concentration at the frequency of operation of the Hydra Probe. In other words, the increase in salt concentration causes loss of energy due to the increase in ionic conductivity. This loss is quantified by the ε_i component of the dielectric permittivity (Robinson et al., 2003). The ε_i plots in the disturbed samples (Figure 4.19) provide a better distinction of treatments than in the undisturbed soils (Figure 4.16). Here the process of homogenization during repacking also shows its effects. At intermediate to high water contents ($\theta_v > 0.30$ cm^3 cm^{-3}) there is a very clear distinction among the $CaCl_2$ 0.02 Mol L^{-1}, KCl 0.01 Mol L^{-1} and distilled-deionized water treatments, however data for KCl 0.02 Mol L^{-1} and $CaCl_2$ 0.01 Mol L^{-1} are not readily distinguishable, which might be due to the fact that the effective ionic strengths of these two salt concentrations are similar in the disturbed Clay samples. As discussed earlier, the conductivities are simply a transformation of ε_i data by using Eq.[2.13] (Figure 4.20) and will be addressed in depth in Chapter VI.

Silty Clay Loam Samples

Electrical properties data for undisturbed Silty Clay Loam samples are presented in Figures 4.21, 4.22 and 4.23. The most striking characteristic of the silty samples is that the ε_r vs. θ_v curves increase in a slightly sigmoidal fashion (Figure 4.21). The reasons behind this behavior are unclear, although it might be related to the pore size distribution of the silty samples. As with the clay soil, there is no clear distinction among treatments. For ε_i data the same is true for θ_v values < 0.35 cm^3 cm^{-3} (Figure 4.22). However, for θ_v values > 0.35 cm^3 cm^{-3} there is a reasonable distinction among the treatments and the control (Figure 4.22). At any water content above 0.35 cm^3 cm^{-3} the slope of the ε_i vs. θ_v relationships decreases among treatments in the order $CaCl_2$ 0.02 Mol L^{-1} > $CaCl_2$ 0.01 Mol L^{-1} > KCl 0.02 Mol L^{-1} > KCl 0.01 Mol L^{-1} > control (Figure 4.22). This order of decrease is what was intended when the experiments were designed. The fact that the expected behavior is only noticeable at water contents close to saturation might be due to the fact that at lower water contents, matrix and air might be somehow damping the solution effect on the ε_i measurements.

Data for Silty Clay Loam disturbed soil samples are presented in Figures 4.24, 4.25 and 4.26. As for disturbed Clay samples, the ε_r response is much more linear than in the undisturbed case. For the disturbed samples, the distinction of treatments by using ε_i data is better than in the undisturbed samples. For the control and the KCl 0.01 Mol L^{-1} treatments, the distinction is visible at relatively low water contents (~0.20 cm^3 cm^{-3}). The distinction between KCl 0.02 Mol L^{-1} and $CaCl_2$ 0.01 Mol L^{-1} is less prominent, but still noticeable at θ_v > 0.30 cm^3 cm^{-3}. An interesting feature of the ε_i vs. θ_v disturbed data is that the order of decrease in ε_i in treatments for higher water contents changed to $CaCl_2$ 0.02 Mol L^{-1} > KCl 0.02 Mol L^{-1} > $CaCl_2$ 0.01 Mol L^{-1} > KCl 0.01 Mol L^{-1} > control. This inversion in the order of KCl 0.02 Mol L^{-1} and $CaCl_2$ 0.01 Mol L^{-1} might be due to subtle differences in the interactions between salt solutions and soil physicochemical elements in disturbed samples (Figure 4.25).

Sandy Loam Samples

The electrical properties data for the undisturbed Sandy Loam soil are presented in Figures 4.27, 4.28 and 4.29. The ε_r vs. θ_v data are very similar to the other soil and disturbance

treatments. The only difference among the soils and disturbances is in the range of values and slopes. A more in depth analysis of models for the relationship between θ_v vs. ε_r is presented in Chapter V. The ε_i vs. θ_v relationship is much more distinguishable among treatments in the undisturbed sandy soil than in any other undisturbed soil treatment (Figure 4.28). The predominance of coarse grain particles, mainly sand and silt in the Sandy Loam soil might account for this observation. Coarser grain particles are less electrostactically active, have less surface area, and are able to capture less exchangeable ions in relation to finer grain particles (mainly clay). Therefore the change in ε_i is accounted for mainly by the salt treatments and their interaction with decreasing water content in the sandy material, and not by electrostatic processes between active clay sized particles and salt solutions (Figure 4.28).

Regarding the Sandy Loam disturbed samples (Figures 4.30, 4.31 and 4.32), as with the other disturbed samples, there is no distinction among treatments and control in the ε_r vs. θ_v plots (Figure 4.30). The most striking feature in the Sandy Loam data is that the distinction among the KCl 0.02 Mol L^{-1} and $CaCl_2$ 0.01 Mol L^{-1} salt treatments is actually less clear in the disturbed samples, which contrasts to previous soils results. The relationship between ε_r or ε_i and θ_v for the control treatment has a very small slope, corroborating the hypothesis of less interaction between solution and soil physicochemical components in coarse grained materials (Figures 4.30 and 4.31).

Glass Beads

Results for samples packed with glass beads are presented in Figures 4.33, 4.34, 4.35 and 4.36. There was very little distinction among samples for the real and imaginary dielectric permittivity measurements versus water content data (Figures 4.33 and 4.34). Unlike the soil experiments, all the glass beads samples were saturated with distilled-deionized water, and therefore the imaginary permittivity and the electrical conductivity of the samples were not expected to vary much among the samples (Figures 4.34 and 4.35). The imaginary permittivity values are very low ($\varepsilon_i < 3.5$) resulting in low bulk conductivity values ($\sigma_a < 0.01$ S m^{-1}). There is abnormal behavior in measurements of ε_r, ε_i and conductivity for samples (D2.6 b and D2.9 b) at water contents lower than 0.1 cm^3 cm^{-3}, likely resulting from instrument errors, and these data

were not used in further analyses (Figures 4.33, 4.34 and 4.35). The range of water retention data is small, with water potentials varying from 0 to about 15 (|kPa|) (Figure 4.36). This is a result of the samples being composed of relatively coarse material (> 0.0625 mm) resulting in the absence of fine and very fine porosity which retains water at higher tensions. Overall, the shapes of the water desorption curves are very similar, except for sample D2.2 composed of coarser material, which behaves more a like a pure sand material (Figure 4.36). The water desorption data for the glass beads was not part of the overall experimental design and therefore was not included in the ANOVA's discussed in previous sections.

Numerical Modeling Results

A summary of the specified and "best-fit" parameters used in the Hydrus 2D simulations is presented in Table 4.2. The bulk density was kept as close as possible to the measured average bulk density for each soil/disturbance combination while the maximum evaporation rate and critical water potential at the evaporation boundary were kept as close as possible to the values recommended by Rassam et al. (2003) as the true values at laboratory conditions were unknown. The R^2 values between predicted and estimated volumetric water contents were 0.98 for Clay disturbed, 0.93 for Clay undisturbed, 0.95 for Silty Clay Loam disturbed, 0.85 for Silty Clay Loam undisturbed, 0.98 for Sandy Loam disturbed, and 0.90 for Sandy Loam undisturbed data. The predicted versus observed data for all soil and disturbance treatments is presented in Figure 4.37. Overall, there was a good agreement among the observed and predicted data for the initial half of the experiments. In other words the data were relatively close to the 1:1 line (Figure 4.37). At low water contents (longer drying times) the numerical model predictions tend to go to the residual water content defined by the critical water potential for each soil, deviating from what was observed under laboratory conditions, where the air drying process and air relative humidity likely prevented the soil water content from approaching the residual values.

The variation among observation nodes in time and space is presented in Figure 4.38 for a typical numerical modeling simulation (Silty Clay Loam disturbed). Overall there were not any

major differences in the results among any of the soils, and thus only one example is shown. The range of predictions was small among the observation nodes, indicating relatively low heterogeneity of water content distribution inside the cores relative to the wide range of water content variations over time. The deviation of the predicted data might be related to the shape of the predictive model [van Genuchten - Mualem model (Rassam et al., 2003)] as it approaches a limiting value, rather than the nature of the drying process itself. In any case, the variation in space within the cores is much less than the variation over time, indicating a relatively low water content gradient within the cores at any instant in time (Figure 4.38). Also, the variation in θ_v is averaged by both the gravimetric water content and complex dielectric permittivity estimations in the measurements. Based on these results, the variation in water content distribution within the samples was assumed to be negligible when developing the models and analyses presented in the next chapters.

CHAPTER V. EFFECTS OF TEXTURE, DISTURBANCE AND SALINITY ON THE ESTIMATION OF SOIL WATER CONTENT USING A 50 MHZ IMPEDANCE SENSOR

This chapter is a lightly revised version of a paper by the same name to be submitted for publication in the journal *Transactions of the American Association of Agricultural and Biological Engineers* in 2009 by Tairone Paiva Leao, Edmund Perfect and John S. Tyner:

Leao, T.P., E. Perfect, and J.S. Tyner. 2009. Effects of texture, disturbance and salinity on the estimation of soil water content using a 50 MHz impedance sensor. To be submitted to *Transactions of ASABE*.

My use of "we" in this chapter refers to my co-authors and myself. My primary contributions to this paper include (1) Most of the writing (2) Most of the field and laboratory work, and (3) Most of the statistical and mathematical analyses.

Abstract

The Hydra Probe (HP) is an electrical impedance sensor that operates at a fixed frequency of 50 MHz. It is not clear if soil water content estimations from the HP are texture, disturbance or salinity independent. The main objective of this research was to investigate the mixed effects of texture, disturbance and salinity on the estimation of soil water content as measured with the HP. Disturbed and undisturbed duplicate samples from a range of soil textures (Clay, Silty Clay Loam, and Sandy Loam) were saturated with distilled-deionized water and saline solutions at four concentrations: KCl and $CaCl_2$ at 0.01 and 0.02 Mol L^{-1} for three days and then air dried under laboratory conditions, generating monotonic drying curves. Real and imaginary components of the dielectric permittivity were measured every 5 minutes by the HP and logged. Load cells recording changes in sample weight over time, which were later converted into volumetric water content, were also logged. Regression analysis and analysis of variance

(ANOVA) were conducted to determine if soil texture, disturbance and salinity significantly influenced the estimations of volumetric water content from real dielectric permittivity. Our main conclusions were that there was no benefit in including the imaginary dielectric permittivity, or a correction for the loss tangent, in models for estimating water content at 50 MHz. Based on our results, Clay soils should be assessed independently when developing calibration equations for the Hydra Probe. Furthermore, the sensor's water content estimations are sensitive to soil disturbance.
Keywords: Hydra Probe, Impedance, TDR, Water Content Estimation, Dielectric, Complex Permittivity

Introduction

The determination of volumetric water content from soil electrical properties has been the subject of much research since the early investigations on time domain reflectometry (TDR) in the late 1970s and 80s. It is evident from electromagnetic theory that the complex dielectric permittivity of a porous medium has two components (i.e. Kraus, 1992; Raju, 2003):

$$\varepsilon^* = \varepsilon_r - j\,\varepsilon_i \qquad [5.1]$$

where ε^* = complex dielectric permittivity = $\varepsilon/\varepsilon_0$ (-), ε = permittivity of the media (F m^{-1}), ε_0 = permittivity of free space (8.854 x 10^{-12} F m^{-1}), j = imaginary number, $\sqrt{-1}$, ε_r = real component of ε^* and ε_i = imaginary component of ε^*. The imaginary component of ε^* is related to the loss of energy caused mainly by two factors, molecular relaxation and DC conductivity (Seyfried et al., 2005):

$$\varepsilon_i = \varepsilon_{i,mr} + (\sigma/2\pi f\varepsilon_0) \qquad [5.2]$$

where $\varepsilon_{i,mr}$ = relative permittivity due to molecular relaxation (-), σ = low frequency conductivity (DC) (S m^{-1}) and f = measured frequency (Hz). The magnitude of the energy dissipation in the medium can be evaluated using the loss tangent (Seyfried and Murdock, 2004; Seyfried et al., 2005):

$$\tan\delta = \varepsilon_{i/}\varepsilon_r \qquad [5.3]$$

In their early research, Topp et al. (1980) concluded that the contribution of the imaginary part to ε* was negligible at the operating frequencies of TDR (around 20 kHz to 1.5 GHz) (Davis and Annan, 1977; Topp et al., 1980) and thus water content could be determined from ε_r alone. Although the contribution of ε_i has been found to be negligible at the range of frequencies of the TDR there is, so far, not enough evidence that this assumption holds for sensors which operate at fixed, lower frequencies, such as the Hydra Probe. Nevertheless, the assumption that $\varepsilon^* \approx \varepsilon_r$ has been implied in much of the research using the 50 MHz Hydra Probe (Stevens Water Monitoring System Inc., 2007; Bosch, 2004). A calibration equation including a linear correction term for the loss tangent has been published for the Hydra Probe sensor (Seyfried et al., 2005). The effects of salinity on water content estimations in soils were recently investigated for the EnvironScan capacitance probe (Thompson et al., 2006), but no such equivalent study has been conducted for the Hydra Probe impedance device.

Calibration equations for different textural classes have been provided for the Hydra Probe, implying that there is a textural effect on the water content estimations (Bosch, 2004; Seyfried and Murdock, 2004; Seyfried et al., 2005). However, the authors are unaware of any study that tested the textural effects by using statistical methods. The effect of soil structure in the estimations is often neglected. Most studies were conducted using disturbed samples that had been oven dried, sieved and repacked in more or less uniform samples (Seyfried and Murdock 2004; Seyfried et al., 2005).

The main objective of this research was to investigate the mixed effects of texture, disturbance, and saline solution saturation on the estimation of soil water content at 50 MHz using the Hydra Probe. Specifically we investigated the impact of these factors on the complex permittivity (ε_r and ε_i). The hypotheses were: i) a model for determination of volumetric water content including the imaginary component of the complex dielectric response can increase the accuracy and precision of the estimates, and ii) the water content estimations are texture, disturbance and salinity independent.

Materials and Methods

This study is a continuation of the research reported by Leao and Perfect (2007). Briefly, thirty undisturbed and three disturbed bulk soil samples were collected on June 10, 2005 at the Plant Sciences experimental farm at the University of Tennessee, Knoxville. The sampling was performed in areas encompassing three soil series, covering three contrasting soil textural classes, according to the USDA system: Clay (fine-loamy, siliceous, semiactive, thermic Typic Paleudult) Sandy Loam (fine-loamy, siliceous, semiactive, thermic Humic Hapludult) and Silty Clay Loam (fine-silty, mixed, active, mesic Fluvaquentic Eutrudept) (Table 5.1) (All tables for this Chapter are located in Appendix G).

The undisturbed samples were collected using a Uhland core sampler, with cores having the dimensions of 5.37 cm inner diameter by 6 cm long. The bulk disturbed samples were collected using a shovel and approximately 5 kg of soil was obtained for each soil series. All samples were collected at a depth of 20 to 25 cm, which was beneath the main root mass. The disturbed soil samples were air dried, broken apart by hand, sieved using a 2 mm sieve, and repacked into ten disturbed cores for each soil. The repacked cores and the undisturbed samples were of the same dimensions. Average bulk densities of the disturbed and undisturbed soil samples are presented in Table 5.1.

Disturbed and undisturbed duplicate samples were saturated from the bottom up, with saline solutions at five concentrations, namely distilled-deionized water (0 or control), KCl at 0.01 and 0.02 Mol L^{-1} and $CaCl_2$ at 0.01 and 0.02 Mol L^{-1} for three days. All soil samples were flushed by gravity driven flow from the top to the bottom, with approximately two pore-volumes of the designated solution after saturation. The samples were then weighed on an electronic balance and Hydra Probe sensors (Stevens Water Monitoring System Inc., 2007) were inserted at one end and UMS T5 miniature pressure transducer tensiometers (UMS, 2001) at the other. The saturated samples containing the Hydra Probes and mini-tensiometers were placed horizontally on load cells (Transducer Techniques, model LSP-1). Hydra Probes, mini-tensiometers and the load cells were connected to dataloggers (VITEL VX1100 and Campbell 21X micrologger). The soil complex permittivity (ε_r and ε_i) was measured by the Hydra Probes and recorded by the Vitel datalogger, while the change in weight of the samples over time, due to air drying, was measured

by the load cells and recorded by the Campbell datalogger. The mini-tensiometers were used to record the soil water potential, which was used to fit the water retention curves, as described in Chapter IV. All measurements were recorded in five minute intervals. After approximately five days, the probes were removed from the soil samples. The samples were weighed on an electronic balance, oven dried at 105°C, and then reweighed to calculate the remaining water content after air drying and the dry bulk density. The average air temperature in the lab during the drying cycles was 21.5°C (CV = 5.24%).

The data sets usually consisted of over 1100 observations for each sample. The observations consisted of soil complex permittivity variables (ε_r and ε_i), volumetric water content (θ_v, cm^3 cm^{-3}) and soil water potential (ψ, kPa). Data reduction and identification of outliers were performed by analysis of the studentized residuals (Pedhazur, 1997; Heuscher et al., 2005). A cutoff criterion for the studentized residuals of |2.5| was adopted for our data. The same criterion has been successfully applied in other types of research (Hao and Kravchenko, 2007). Simple and multiple linear regression analyses were also performed to evaluate the possible contribution of each variable in the overall model and to determine regression coefficients. The dependent variable in the regression model was measured volumetric water content and the independent variables were ε_r, ε_i, and the loss tangent: $\tan \delta = \varepsilon_i / \varepsilon_r$. All statistical analyses were performed using SAS® software v9.13. Based on the recommendations of Seyfried and Murdock (2004) and Seyfried et al. (2005) sensor specific calibrations were not explored in this research. Our results were compared to models in the literature, including those proposed by Topp et al. (1980) and Seyfried et al. (2005) as well as with the Hydra Probe manufacturer equation for sand (Bosch, 2004; Leao and Perfect, 2007). Evaluation of new and existing models was also performed using an independent dataset collected in the same manner as described previously, but with glass beads instead of soil. The glass beads had average diameters of 2.0, 1.0, 0.5, 0.25, 0.125 and 0.0625 mm and a particle density of 2.5 g cm^{-3} (Mo-Sci Corp., Rolla, MS). Disturbed samples were made up by mixing the glass bead fractions in different proportions: 44, 25, 15, 8, 5 and 3% (one sample); 30, 23, 17, 13, 10 and 7% (two samples); 23, 20, 17, 15, 13 and 12% (one sample), and 20, 18, 17, 16, 15 and 14% (one sample), respectively. The bulk densities for the glass bead cores were: 1.78, 1.85, 1.80, 1.81 and 1.82 g cm^{-3} for the distributions/samples described above, respectively.

In order to assess potential heterogeneities in the water content distribution within the core during drying, numerical modeling experiments were performed in Hydrus 2D and compared to observed data. The air drying simulations were performed for each soil texture and disturbance scenario following Rassam et al. (2003). The horizontal drying experiment model domain is presented in Fig. 5.1a (All figures for this Chapter are located in Appendix H). The left and right ends are open to atmosphere while the upper and lower ends are no-flow boundaries. The forward predictions were performed in a semi-empirical iterative fashion. Nodes 1 and 10 corresponded to the boundary conditions and thus were not used in the comparison. The input parameters (maximum evaporation rate and critical water potential at the evaporation boundaries) for the forward predictions in Hydrus 2D were "manually" changed until a best fit was achieved in relation to the observed drying data. This procedure was necessary because these parameters were unknown. The resulting critical water potentials were -500 kPa for the Sandy Loam soil and -1500 kPa for the Clay and Silty Clay Loam soils. The maximum evaporation rates varied from 0.012 to 0.02 cm h^{-1}.

Results

Numerical modeling of drying experiments

A typical drying experiment data along with results from the numerical simulation for a Sandy Loam soil are presented in Fig. 5.1b. The greatest difference in water content in time for all soils/disturbances in the numerical models corresponded to the nodes 6 and 9 (Fig. 5.1). These maximum and average maximum differences data, calculated from nodes 6 and 9 are presented in Table 5.2 along with the R^2 values between the model mass balance (numerical domain average) and observed water contents for the whole experiment over time. The maximum error was about 0.03 cm^3 cm^{-3} and the average maximum difference varied between 0.013 to 0.018 cm^3 cm^{-3} for all soils/disturbances. The peak time, when the maximum error occurred, is also presented. Overall the error was small and fairly constant up to peak time and then decreased again. Given the relatively small magnitude of these errors, the effect of spatial

gradients in the water content and electrical properties were ignored, and the Hydra Probe measurements were used without any corrections as described in the next sections.

Regression Modeling

The validity of including both $\sqrt{\varepsilon_r}$ and $\sqrt{\varepsilon_i}$ in a multiple regression model for estimating θ_v was assessed through regression diagnosis tools, i.e.

$$\theta_v = \beta_0 + \beta_1 \sqrt{\varepsilon_r} + \beta_2 \sqrt{\varepsilon_i} \quad [5.4]$$

The Variance Inflation Factor (VIF) and the multiple correlation among the partial slopes β_1 and β_2 were evaluated (Neter et al., 1990). For the entire data set (N = 60 samples), the average VIF was 276.7 with a standard deviation of 180.4; in only one sample was the VIF < 10, the critical threshold for multicollinearity (Neter et al., 1990). In all samples the correlation of β_1 and β_2 estimates was < -0.94 (i.e. the two parameters were strongly negatively correlated). The increase in regression ANOVA's root mean square error (ARMSE) obtained by removing $\sqrt{\varepsilon_i}$ was only 0.0003 cm^3 cm^{-3}. The average ARMSE with two independent variables was not significantly different from the average ARMSE with only one independent variable ($p > |t| = 0.43$). Based on these indicators, we decided not to develop regression models including both $\sqrt{\varepsilon_r}$ and $\sqrt{\varepsilon_i}$ simultaneously. The inclusion of a correction term for dielectric loss in the water content estimation model will be addressed later in the chapter.

All subsequent analyses within this chapter are based on a simple regression model for the water content as a function of $\sqrt{\varepsilon_r}$:

$$\theta_v = \beta_0 + \beta_1 \sqrt{\varepsilon_r} \quad [5.5]$$

Fitting Eq.[5.5] to the raw data resulted in average, minimum and maximum R^2 values of 0.99, 0.98 and 0.99, respectively with $p < 0.0001$ in all cases. A data set composed of 60 slopes (β_1) and intercepts (β_0) was then assessed for differences among treatments. These coefficients were strongly negatively correlated (r = -0.92, $p < 0.0001$) indicating that an increase in the slope caused a decrease in the intercept and vice-versa.

The set of slopes and intercepts was evaluated by ANOVA with Duncan's Multiple Range Test (DMR) used to compare the several combinations of treatments (James, 1964; Griffin et al., 2003). The ANOVA model was composed of the regression coefficients as

independent factors and soil texture, disturbance, salt and their interactions as classification factors. The overall ANOVA for the intercepts was not significant (p = 0.62). However, a hierarchical removal of factors/interactions with highest $p > F$ values resulted in a significant ANOVA (p = 0.012) with both soil and disturbance classification factors being independently significant at p = 0.05. Results for the intercept means comparison by DMR for soil texture and disturbance are presented in Tables 5.3 and 5.4, respectively. The same process was repeated for the slope coefficient. The overall ANOVA was not significant (p = 0.30) and the hierarchical removal of factors/interactions showed same results as the intercept coefficient. For slopes, the ANOVA was significant at p = 0.0011 with the soil and disturbance classification factors significant at $p < 0.01$. DMR means comparison for slopes are also presented in Tables 5.3 and 5.4.

Based on the ANOVA results for the regression coefficients of $\theta_v = f(\sqrt{\varepsilon_r})$ we recommend that, when developing calibration equations for the Hydra Probe, clay soils should be assessed independently. Since there was no distinction among the Sandy Loam and Silty Clay Loam soils, a combined model was developed for these two soils (referred to from now on as Loam). The disturbance factor was also significant and therefore it was necessary to develop separate equations for disturbed and undisturbed conditions within each soil and/or soil group. The individual coefficients for soil texture and disturbances are presented in Table 5.5.

The data corresponding to the regression parameters in Table 5.5 are presented in Figs. 5.2, 5.3, 5.4 and 5.5. The data for the Clay soil are presented in Figs. 5.2 and 5.3 for disturbed and undisturbed samples, respectively. The data for the combined samples of Sandy Loam and Silty Clay Loam (Loam) soils are presented in Figs. 5.4 and 5.5 for disturbed and undisturbed samples, respectively. Comparing Fig. 5.4 to the other graphs, and from the results in Table 5.5, it is noticeable that the Loam disturbed samples provided the overall best fit to the square root linear regression equation. Based on the R^2 and ARMSE values, the greatest dispersions around the best fit models were found in the Clay undisturbed and Loam undisturbed datasets (Table 5.5 and Figs. 5.3 and 5.5).

Relationships with Loss Tangent and Bulk Density

Following the approach of Seyfried et al. (2005) we attempted to include a correction factor for the loss tangent in our regression models, i.e.

$$\theta_v = A_{lc} \sqrt{\varepsilon_r} + B \qquad [5.6]$$

where:

$$A_{lc} = A_0 + A_1 \tan \delta_s \qquad [5.6a]$$

and A_{lc} = loss corrected slope coefficient, A_0, A_1 and B = fitting coefficients, and tan δ_s = loss tangent (tan $\delta = \varepsilon_i/\varepsilon_r$) measured at complete saturation. We found no significant correlation among the loss tangent values for saturated soil (tan δ_s) and either the β_0 or β_1 coefficients from Eq.[5.5] (tan δ_s versus β_0: r = 0.12, p = 0.34; and tan δ_s versus β_1: r = -0.18, p = 0.18). Seyfried et al. (2005) found a relationship between β_1 and tan δ_s (R^2 = 0.53; significance not provided) and were able to predict β_1 from tan δ_s using linear regression. The non-reproducibility of their results might be partially explained by the fact that we had relatively low values of tan δ_s. The tan δ_s was always less 1.18 (average 0.48±0.20), well below the 1.45 value which, when exceeded, is reported to cause deterioration in the accuracy of ε_r estimations (Seyfried et al., 2005).

Since we had a continuous range of loss tangent values (i.e. tan $\delta = \varepsilon_i/\varepsilon_r$ for all observed volumetric water contents) we also attempted to include the loss tangent as an additional variable in multiple regression models. The average R^2 for the 60 samples was 0.99 in both cases (i.e. with or without tan δ), and the RMSE only decreased by 0.0003 cm^3 cm^{-3} when $\theta_v = f(\sqrt{\varepsilon_r}, \tan \delta)$ in comparison to $\theta_v = f(\sqrt{\varepsilon_r})$ only. The VIF was greater than or equal to 10 in over 50% of the samples, indicating some degree of collinearity among the $\sqrt{\varepsilon_r}$ and tan δ coefficients. Based on this information, the second main result of this research is that, for our dataset, there was no benefit in attempting to correct the models for the loss tangent.

In contrast with the range of data available for fitting the function $\theta_v = f(\sqrt{\varepsilon_r})$, structural parameters [dry bulk density (D_b), logarithm of the saturated hydraulic conductivity (log K_{sat}) and the coefficients α and n from the van Genuchten equation (van Genuchten, 1980) obtained as described in Chapter IV] could not be included as independent variables in the multiple regression models, since there was only one value associated with each sample. However, it was

possible to correlate these parameters with the β_0 and β_1 coefficients fitted to Eq.[5.5]. Linear regression analyses for either β_0 or β_1 versus D_b resulted in models with adjusted R^2 values < 0.08 (regression significant at $p = 0.05$). The coefficients β_0 and β_1 were also correlated with logarithm of the saturated hydraulic conductivity ($\log K_{sat}$) and α and n. The correlation was only significant between β_0 and β_1 and the α parameter ($p = 0.05$). Regression analysis of either β_0 or β_1 as a function of α resulted in R^2 values < 0.09 (regression significant at $p = 0.05$). Based on these analyses we concluded that none of the soil structural parameters investigated were strongly related to the β_0 and β_1 coefficients.

Following the approach of Leao and Perfect (2007) setting $\theta_v = 0$ in Eq.[5.5] it is possible to estimate the permittivity of the solid phase as $\varepsilon_s = (-\beta_0/\beta_1)^2$. The average ε_s calculated using this procedure was 3.38±0.56. Contrary to what was suggested by Regalado (2004), we found no significant correlation between D_b and ε_s (r = -0.21; $p = 0.1138$).

Comparison with other models

A comparison of the models developed in this research with those of Seyfried et al. (2005), Topp et al. (1980) and the manufacturer's equation for sand (Bosch, 2004; Leao and Perfect, 2007) is presented in Figs. 5.2, 5.3, 5.4 and 5.5. A statistical comparison was performed by evaluating the root mean square error (RMSE) between the volumetric water content from observed (θ_{obs}) data and the volumetric water content predicted by a particular model (θ_{est}) (Huisman et al., 2001):

$$\mathrm{RMSE} = \sqrt{\frac{\sum_{i=1}^{N} (\theta_{obs(i)} - \theta_{est(i)})^2}{N}} \qquad [5.7]$$

where N = number of observations. The RMSE values for the data in Figs. 5.2 to 5.5 are shown in Table 5.6. Best fit models for each soil and disturbance were compared to the Seyfried, manufacturer's sand (hereafter referred to as Sand for simplification) and the Topp equations. For the Clay disturbed data, the performance of our new model was superior to the literature models. For the Clay undisturbed data the situation is quite distinct; our new model, the Seyfried and Sand models all had RMSE values within 0.0007 $cm^3\ cm^{-3}$ of each other, while the Topp

model had a substantially higher RMSE than the other models. For the Loam disturbed and undisturbed data, our model had a RMSE very close to that of the Sand model, followed closely by the Seyfried model. We expected that our models would out perform the literature models since they were specifically developed for these soils/disturbances. As discussed by Seyfried et al. (2005) a calibration equation developed for a specific dataset will always out perform general equations developed from different datasets. Therefore, one important feature of Table 5.6 is to evaluate the quality of previous models as universal predictors. Among the literature models evaluated, the Hydra Probe manufacturer's sand equation had the best performance for predicting volumetric water content from ε_r. Results acquired from a larger data set in this study validate our previous recommendation that for the Hydra Probe, in the absence of soil specific calibration equations, the manufacturer's sand equation should be employed as an all purpose model (Leao and Perfect, 2007).

Regarding the square root linear model, the average slope (β_1) in this research was 0.119 and the average intercept (β_0) was -0.219 (N = 60 samples). While the average β_1 was slightly higher than that of Seyfried et al. (2005) (β_1 = 0.110), the average β_0 was lower than that of Seyfried et al. (2005) (β_0 = -0.180). Topp and Ferre (2002) report that for a square root linear model developed for TDR data β_1 = 0.115 and β_0 = -0.176 which are close to the values reported for the 50 MHz sensor. Calculating ε_s from the coefficients above, we get ε_s = 2.68 for the Seyfried et al. (2005) model, ε_s = 2.34 for the TDR model and ε_s = 3.40 for our average model. The value of ε_s estimated with the coefficients from this research is closer to values reported in the literature for common soil minerals (Robinson, 2004).

Error Analysis

The Mean Absolute Error (MAE) (Legates and McCabe, 1999; Brouder et al., 2005) was used to investigate the increase in accuracy obtained by including disturbance and soil texture factors in our regression models. The MAE is defined as:

$$MAE = \frac{1}{N}\sum_{i=1}^{N} | \theta_{obs(i)} - \theta_{est(i)} | \qquad [5.8]$$

Mean absolute errors were calculated for each scenario, i.e., a single regression model for the whole dataset (general model), a model for each soil (Clay, Sandy Loam, and Silty Clay Loam), a model for each disturbance treatment (disturbed and undisturbed), and a model for each soil texture / disturbance combination (3 textures x 2 disturbances = 6 models). Ignoring the effects of both soil texture and disturbance (i.e. the general model) resulted in a MAE of 0.0177 cm^3 cm^{-3}. Accounting for soil texture, but ignoring disturbance, resulted in an average reduction in the MAE of 3.91%. Similarly, accounting for disturbance, but ignoring soil texture, reduced the MAE by an average of 2.55%. When both soil texture and disturbance were taken into account the average reduction in MAE relative to the general model was 8.45%. These results clearly illustrate the value of including both soil texture and disturbance effects in the development of calibration equations for the HP.

Model evaluation with glass beads

A plot of models developed and/or evaluated in this research versus experimental data from glass beads is presented in Fig. 5.6. Glass beads were chosen because, as with purified sand (Malicki and Walczak, 1999), such standard materials are widely used in experiments with artificially packed samples (Topp et al., 1980; Friedman, 1998) and offer the advantages of easily replicable texture and negligible cation exchange capacity. The model developed for the combined Loam disturbed data was chosen for evaluation, along with the Topp, Seyfried and Sand (manufacturer's sand model) models, because it should provide a better prediction of volumetric water content for the silt and sand sized repacked glass beads samples. The RMSE's for the predicted water content from each model and the observed data in the glass beads samples are presented in Table 5.7. The Loam disturbed model had the best overall performance followed very closely by the Sand model. Both of these models tended to over-predict θ_v at low values of ε_r. The Seyfried model generally had higher water content estimations than the Sand and Loam disturbed models. The Topp equation provided estimations of θ_v substantially higher and outside the range of measured values of volumetric water content over the entire range of ε_r (Fig. 5.6).

Discussion

For our soils, there was no benefit in including the imaginary permittivity as an additional variable in the regression models or in attempting to correct a simple linear model of $\theta_v = f(\sqrt{\varepsilon_r})$ for the loss tangent ($\tan \delta = \varepsilon_i/\varepsilon_r$). This provides a confirmation that $\varepsilon^* \approx \varepsilon_r$ for the estimation of volumetric water content in the frequency of operation of the Hydra Probe. This assumption has been stated to hold true for the range of frequencies of TDR (Topp et al., 1980; Topp and Ferre, 2002). At the frequency of operation of the Hydra Probe, 5 x 10^7 Hz, the real permittivity of water at 20°C is much greater than the imaginary value $\varepsilon_r \approx 80$ and $\varepsilon_i \approx 2$ (Raju, 2003). The addition of salt to distilled-deionized water does not seem to have altered this behavior significantly. It was therefore possible to use the salt treatments as replications for the soil and disturbance treatments. The loss tangent exceeded one (i.e. $\varepsilon_i > \varepsilon_r$) in only 10% of the samples tested. In the presence of salt solutions, the loss tangent generally increased to a maximum when the water content was near saturation. The highest loss tangents were associated with the highest $CaCl_2$ concentration (0.02 Mol L^{-1}). None of the samples had $\tan \delta > 1.45$, and therefore it is likely that the losses represented by ε_i did not noticeably affect the quality of the estimations of θ_v from ε_r.

The slopes and intercepts of $\theta_v = f(\sqrt{\varepsilon_r})$ were dependent on soil texture and disturbance, but not on salinity. According to Eq.[5.2] conductivity and molecular relaxation losses will affect ε_i, but not ε_r, and therefore the latter is unaffected by the inclusion of salinity which will mainly increase the conductive losses. Our results here differ from those of Leao and Perfect (2007) who found that the estimation of water content was independent of texture and disturbance. However, that research was performed on only a subset of the data presented here (12 samples) and therefore, the new estimations with the full dataset (60 samples) are expected to be more reliable than the preliminary results.

The absence of significant correlations between structural parameters (D_b, log K_{sat}, α and n) and the linear regression parameters is somewhat surprising. We expected that the differences in slopes and intercepts would be correlated to structural characteristics of the soil, reflected by bulk density, saturated hydraulic conductivity and water retention parameters. This result

suggests that other unknown factors, not measured in this study, are contributing to the heterogeneity in the model parameters. The absence of a correlation between D_b and ε_s is also surprising since the increase in solid particles within a fixed volume should reduce the damping effect of air and thus increase ε_s. One explanation for this observation is that the dielectric permittivity of solids ($\varepsilon_s \approx 3.4$) is not much larger than the dielectric permittivity of air ($\varepsilon_{air} \approx 1$) so that the contrast is too small to cause significant changes as the bulk density increases.

As quantified by the MAE, the overall accuracy of the HP in this study, without accounting for texture and disturbance, was 0.0177 cm^3 cm^{-3}. Accounting for both soil texture and disturbance resulted in an average reduction in the MAE of 8.45%. If it is not possible to include both effects when developing calibration equations, we recommend accounting for soil texture since this effect resulted in a greater reduction in MAE (3.91%) than differentiating between undisturbed and disturbed conditions (2.55%).

The glass beads data set provided an independent means of evaluating the models developed in this research. Our model for the Loam disturbed datasets provided the best forward prediction of the glass beads volumetric water content according to the RMSE (Table 5.7) and visual inspection of the data (Fig. 5.6). The manufacturer's sand model once again proved its robustness for estimating soil water content from ε_r in different materials under variable disturbance conditions.

Conclusions

We found no benefit in including the imaginary dielectric permittivity or a correction for the loss tangent in models for estimating water content at 50 MHz using the Hydra Probe. Clay soils should be assessed independently when developing calibration equations for the Hydra Probe. The sensor's water content estimations are disturbance dependent. However, there were only weak correlations among the linear regression coefficients of $\theta_v = f(\sqrt{\varepsilon_r})$ and independently measured soil structural parameters. This result implies that additional measurements accounting for structural disturbance in the models should be sought in further research.

Acknowledgements

We would like to acknowledge (in alphabetical order): Dr. John Curtis, formerly of USACE/ERDC for suggestions and soil mineralogical analyses, Dr. Paul Denton of University of Tennessee Plant Sciences Department for the help with soil sampling, Mr. Mike Newman of University of Tennessee for statistical consulting, Dr. Alvaro Pires da Silva of ESALQ-University of Sao Paulo, Brazil for soil analysis and suggestions and Mr. Wesley Wright of University of Tennessee Biosystems Engineering Department for help with instrumentation setup. Without the help of these individuals this research would not be possible. This research was funded by the US Army Corps of Engineering – Engineering Research and Development Center, contract: BR05-0001C, UT – USACE/ERDC.

CHAPTER VI. NEW SEMI-EMPIRICAL FORMULAE FOR PREDICTING SOIL SOLUTION CONDUCTIVITY FROM DIELECTRIC PROPERTIES AT 50 MHz

This chapter is a lightly revised version of a paper by the same name to be submitted for publication:

Leao, T.P., E. Perfect, and J.S. Tyner. 2009. New semi-empirical formulae for predicting soil solution conductivity from dielectric properties at 50 MHz. Journal to be determined.

My use of "we" in this chapter refers to my co-authors and myself. My primary contributions to this paper include (1) Most of the writing (2) Most of the field and laboratory work, and (3) Most of the statistical and mathematical analysis.

Abstract

The electrical conductivity of the pore solution is an important measurement in agricultural and environmental soil applications. It can be used to calculate the concentration of salts in the soil solution and to trace and monitor the transport of ionic solutes. Most models for predicting the soil pore solution conductivity rely on measurements of soil volumetric water content to provide accurate predictions. However, because these measurements are not always available and because of the complex interactions between soil and water, this can be a complicating factor. Electromagnetic sensors offer an alternative approach because estimations of pore water conductivity can be obtained without direct knowledge of the volumetric water content. The objective of this research was to develop and test two new semi-empirical formulae for predicting the pore solution electrical conductivity that are mathematically independent of water content. The resulting models are dielectric equivalents of Rhoades type two-pathway models based on linear and power law solutions for the transmission coefficient. The models were fitted by nonlinear regression to a data set from samples of different soil textures and disturbance

treatments, saturated with solutions of varying electrical conductivities (~0, 1.23, 2.41, 2.02 and 3.96 dS m^{-1}) and then used to forward predict the soil solution electrical conductivity. Overall the average soil solution conductivity predicted by the new models compared well to the known saturating solution conductivities (average R^2 = 0.82 and average root mean square error of 0.80 dS m^{-1}).
Keywords: Electrical conductivity, TDR, pore solution, semi-empirical model, water content, Hydra Probe.

Introduction

The complex dielectric permittivity of a porous medium is partitioned into two components (i.e. Kraus, 1992; Raju, 2003):

$$\varepsilon^* = \varepsilon_r - j\,\varepsilon_i \qquad [6.1]$$

where ε^* = complex dielectric permittivity = $\varepsilon/\varepsilon_0$ (-), ε = permittivity of the porous medium (F m^{-1}), ε_0 = permittivity of free space (8.854 x 10^{-12} F m^{-1}), j = imaginary number, $\sqrt{-1}$, ε_r = real component of ε^* and ε_i = imaginary component of ε^*. The imaginary component of ε^* is related to the loss of energy caused mainly by two factors, molecular relaxation and DC conductivity (Seyfried et al., 2005):

$$\varepsilon_i = \varepsilon_{i,mr} + (\sigma/2\pi f\varepsilon_0) \qquad [6.2]$$

where $\varepsilon_{i,mr}$ = relative permittivity due to molecular relaxation (-), σ = low frequency conductivity (DC) (S m^{-1}) and f = measured frequency (Hz).

The Hydra Probe (HP) is an electrical impedance sensor that operates at a fixed frequency of 50 MHz (Stevens Water Monitoring System Inc., 2007). It is most commonly used to estimate soil volumetric water content from ε_r by using empirical calibration equations (see Chapter V). One of the difficulties with the design of the Hydra Probe is that the effects identified in Eq.[6.2], i.e. molecular relaxation and low frequency conductivity, cannot be decoupled. It is often assumed that the contribution of $\varepsilon_{i,mr}$ to ε_i is very small. The conductivity in the Hydra Probe can then be calculated directly from the imaginary permittivity, i.e. by rearranging and neglecting $\varepsilon_{i,mr}$ in Eq.[6.2] we get (Campbell, 1990; Seyfried et al., 2005):

$$\sigma_d = (\varepsilon_i \, 2\pi \, f \, \varepsilon_0) \quad [6.3]$$

where σ_d = dielectric conductivity (S m^{-1}).

Equation [6.3] is the default way of calculating conductivity with the Hydra Probe (Stevens Water Monitoring System Inc., 2007). The dielectric conductivity (σ_d) in Eq.[6.3] has been found to be equivalent to the soil electrical conductivity (i.e. from Eq.[6.2]) over the range of interest in most soils (Seyfried and Murdock, 2004; Seyfried and Grant, 2007). Thus, here we will assume that the dielectric conductivity (σ_d) is equivalent to the soil apparent bulk electrical conductivity (σ_a).

The apparent bulk electrical conductivity of soil can be broken-down into two components (Mualem and Friedman, 1991):

$$\sigma_a = \chi \, \sigma_w + \sigma_s \quad [6.4]$$

where: χ = a geometric factor, accounting for the irregular distribution of water in soil pores, σ_w = soil pore solution electrical conductivity (S m^{-1}) and σ_s = soil solid phase surface electrical conductivity (S m^{-1}).

Equation [6.4] can be expressed in a suitable form for unsaturated soil conditions, as a two-pathway model (Rhoades et al., 1976; Amente et al., 2000):

$$\sigma_a = \theta_v \, T(\theta_v) \, \sigma_w + \sigma_s \quad [6.5]$$

where: θ_v = soil volumetric water content (cm^3 cm^{-3}), and $T(\theta_v)$ = a transmission coefficient (also known as tortuosity, and geometric or formation factor) as a function of θ_v. The transmission coefficient has been described either as a linear function of volumetric water content (Rhoades et al., 1976; Amente et al., 2000) or as a power function of volumetric water content (Amente et al., 2000).

In most electromagnetic methods, σ_a and θ_v can easily be estimated once the particular sensor has been calibrated for specific soils and conditions; see for example Topp et al. (1980) and Hamed et al. (2003) for time domain reflectometry (TDR) and Chapter V for the Hydra Probe (HP). The 50 MHz Hydra Probe estimates volumetric water content from the real component of dielectric permittivity, ε_r, and apparent bulk electrical conductivity from the imaginary component of dielectric permittivity, ε_i, by using Eq.[6.3]. Although values for σ_a can be routinely obtained from the ε_i readings, there is a need for more research on how to estimate

the pore water conductivity (σ_w). In theory, the pore water conductivity is the best index of soil salinity, because it is the salinity actually experienced by the plant root (Corwin and Lesch, 2005) and consequently plant response is much more related to salt concentration in the soil solution than the total salt content of the soil (Rhoades et al., 1989). In addition, the actual salt concentration in the pore solution can be calculated once the pore water conductivity is know, with direct applications to modeling and monitoring the transport of contaminants and other relevant solutes in porous media.

Field extraction of soil solution samples for direct measurement of σ_w is often impractical and subject to instrumental and sampling error. Furthermore, the soil solution composition often varies temporally and spatially (Corwin and Lesch, 2005). Thus it is desirable to estimate σ_w based on more easily performed indirect measurements. Electromagnetic sensors are an attractive alternative for such a purpose, mainly because they can, theoretically, provide in-situ, minimum disturbance, real-time estimates of σ_w that are independent of soil water content. Two examples of such models for the determination of σ_w from electromagnetic properties are those of Hilhorst (2000) for the 30 MHz Sigma Probe sensor and Malicki and Walczak (1999) for TDR. No such equivalent has been derived for the 50 MHz Hydra Probe. Thus, we shall, over the next few steps, develop two new models for predicting σ_w using the Hydra Probe.

Theory

Model I

There is experimental evidence that soil volumetric water content can be estimated with the 50 MHz Hydra Probe using a square-root linear model (Seyfried et al. 2005):

$$\theta_v = A \sqrt{\varepsilon_r} + B \qquad [6.6]$$

where A and B are empirical fitting coefficients. Recalling Eq.[6.5], the transmission coefficient is a function of water content $T(\theta_v)$. Since water content is estimated from ε_r, T must also be a function of ε_r. Employing the well known linear form for T we have (Rhoades et al., 1976):

$$T = a\,\theta_v + b \qquad [6.7]$$

where a and b are empirical fitting coefficients. Inserting Eq.[6.6] into Eq.[6.7] we obtain:

$$T = C \sqrt{\varepsilon_r} + D \quad [6.8]$$

where C = aA and D = (aB + b).

Now, substituting Eqs.[6.6] and [6.8] into Eq.[6.5] and combining the empirical coefficients we obtain:

$$\sigma_a = (\alpha \sqrt{\varepsilon_r} + \beta \varepsilon_r + \gamma) \sigma_w + \sigma_s \quad [6.9]$$

where $\alpha = (AB + BC)$, $\beta = AC$ and $\gamma = BD$.

Equation [6.9] is a dielectric equivalent to Eqs.[6.4] and [6.5]. In Eq.[6.9] the transmission coefficient now assumes the form of a dielectric relationship, accounting for the changes in electrical properties of the porous medium as its geometric-dielectric relations change with the tortuosity of the conductivity paths defined by the soil solution distribution, soil texture and structure, i.e.

$$T_d = \alpha \sqrt{\varepsilon_r} + \beta \varepsilon_r + \gamma \quad [6.10]$$

with T_d somewhat arbitrarily defined as the dielectric transmission coefficient.

Rearranging Eq.[6.9] and inserting Eq.[6.3] we can now predict σ_w from ε_r and ε_i once the model has been parameterized:

$$\sigma_w = (\varepsilon_i 2\pi f \varepsilon_0 - \sigma_s)/(\alpha \sqrt{\varepsilon_r} + \beta \varepsilon_r + \gamma) \quad [6.11]$$

This new pore water conductivity model is mathematically simple, valid for any value of $\varepsilon_r \geq \varepsilon_s$ (i.e. ε_s = real permittivity of soil solid particles). Since in theory the apparent conductivity will always be equal to or greater than the solid phase conductivity the model is constrained to $(\varepsilon_i 2\pi f \varepsilon_0 - \sigma_s) \geq 0$. Mathematically, the denominator in Eq.[6.11] cannot be zero and therefore $(\alpha \sqrt{\varepsilon_r} + \beta \varepsilon_r + \gamma) > 0$, since negative values would generate negative σ_w predictions, which are not physically meaningful.

Model II

In a study evaluating models for predicting soil solution conductivity from bulk conductivity using semi-empirical and hydraulic property-based models, Amente et al. (2000) found that a simple power law function for the transmission coefficient provided the best predictions among many other more complex expressions. If we use the power function

presented by Amente et al. (2000), then the transmission factor in Eq.[6.5] takes the following form:

$$T = \theta_v^{\lambda} \quad [6.12]$$

where λ is an empirical fitting coefficient. Now if we insert Eq.[6.12] into Eq.[6.5] we get:

$$\sigma_a = \theta_v^{\lambda + 1} \sigma_w + \sigma_s \quad [6.13]$$

Substituting Eq.[6.6] into Eq.[6.13] yields:

$$\sigma_a = (A \sqrt{\varepsilon_r} + B)^{\lambda + 1} \sigma_w + \sigma_s \quad [6.14]$$

where the dielectric transmission coefficient now assumes the form:

$$T_d = (A \sqrt{\varepsilon_r} + B)^{\lambda + 1} \quad [6.15]$$

Inserting Eq.[6.3] into Eq.[6.14] and solving for σ_w a new pore solution conductivity model is obtained in terms of ε_r and ε_i:

$$\sigma_w = (\varepsilon_i 2\pi f \varepsilon_0 - \sigma_s) / (A \sqrt{\varepsilon_r} + B)^{\lambda + 1} \quad [6.16]$$

Eq. [6.16] is valid for any value of $\varepsilon_r \geq \varepsilon_s$, $(\varepsilon_i 2\pi f \varepsilon_0 - \sigma_s) \geq 0$ and $(A \sqrt{\varepsilon_r} + B)^{\lambda + 1} > 0$.

Two important theoretical considerations can be immediately drawn from Eqs.[6.14] and [6.16]. First, if the coefficients A and B assume the same values as when they are used to calibrate the volumetric water content dielectric permittivity relationship of Eq.[6.6], then the pore water conductivity function can be obtained for the Hydra Probe by inversely estimating the λ coefficient only. This parameter is theoretically related to the gas diffusion/permeability and thus can be obtained independently (Amente et al. 2000). Second, if λ is measured by an independent method, then in theory a volumetric water content predictive function could be obtained by inversely estimating A and B in Eq.[6.16] independently of knowledge of water content. In other words, a predictive model for water content could be developed from electrical properties alone, without knowledge of soil water content for the calibration process.

Our specific goals with this research are to:

i. Parameterize Eqs.[6.11] and [6.16] for different textured soils and disturbance conditions using nonlinear regression techniques.

ii. Generate inverse predictions of soil solution conductivity using the parameterized forms of Eqs.[6.11] and [6.16].

iii. Compare our model predictions with the Malicki and Walczak (1999), and Hilhorst (2000) model predictions.

Materials and Methods

Thirty undisturbed cores and three disturbed bulk soil samples were collected on June 10, 2005 at the Plant Sciences experimental farm at the University of Tennessee, Knoxville. The sampling was performed in areas encompassing three soil series, covering three contrasting soil textural classes, according to the USDA system: Clay (fine-loamy, siliceous, semiactive, thermic Typic Paleudult) Sandy Loam (fine-loamy, siliceous, semiactive, thermic Humic Hapludult) and Silty Clay Loam (fine-silty, mixed, active, mesic Fluvaquentic Eutrudept) (Table 6.1) (All tables for this Chapter are located in Appendix I).

The undisturbed cores were collected using a Uhland core sampler, with samples having the dimensions of 5.37 cm inner diameter by 6 cm height. The bulk disturbed samples were collected using a shovel; approximately 5 kg of soil was obtained for each soil type. All samples were collected at a depth of 20 to 25 cm, which was beneath the main root mass. The disturbed soil samples were air dried, broken apart by hand, sieved using a 2 mm mesh sieve and used to pack ten disturbed cores for each soil. The cores used for the repacked samples had the same dimensions as the cores used for the undisturbed samples. The average bulk densities of the disturbed and undisturbed soil samples are presented in Table 6.1.

Disturbed and undisturbed duplicate samples were saturated from the bottom up, with saline solutions at five concentrations, namely distilled-deionized water (~0 or control), KCl at 0.01 and 0.02 Mol L^{-1} and $CaCl_2$ at 0.01 and 0.02 Mol L^{-1} for three days. All soil samples were flushed by gravity driven flow from the top to the bottom, with approximately two pore-volumes of the designated solution after saturation. The samples were then weighed on an electronic balance and Hydra Probe sensors (Stevens Water Monitoring System Inc., 2007) were inserted at one end. The saturated samples containing the Hydra Probes were placed horizontally on load cells (Transducer Techniques, model LSP-1). Hydra Probes and the load cells were connected to dataloggers (VITEL VX1100 and Campbell 21X micrologger). The soil complex permittivity (ε_r

and ε_i) was measured by the Hydra Probes and recorded by the Vitel datalogger, while the change in weight of the samples over time, due to air drying, was measured by the load cells and recorded by the Campbell datalogger. All measurements were recorded in five minute intervals. After approximately five days, the probes were removed from the soil samples. The samples were weighed on an electronic balance, oven dried at 105°C, and then reweighed to calculate the remaining water content after air drying and the dry bulk density. The average air temperature in the laboratory during the drying cycles was 21.5°C (CV = 5.24%). All measurements were temperature corrected (Stevens Water Monitoring System Inc., 2007).

The data sets usually consisted of over 1100 observations for each sample. The observations consisted of soil complex permittivity variables (ε_r and ε_i) and volumetric water content (θ_v, cm^3 cm^{-3}). Apparent soil conductivity (σ_a) was calculated from Eq.[6.3]. The saturating solution conductivity (σ_w) was calculated based on measured imaginary permittivity values of the salt solutions and Eq.[6.3]. The salt solutions generated five distinct conductivity values: σ_w = 0, 1.23, 2.41, 2.02 and 3.96 dS m^{-1} for distilled-deionized water, KCl 0.01 Mol L^{-1}, KCl 0.02 Mol L^{-1}, $CaCl_2$ 0.01 Mol L^{-1} and $CaCl_2$ 0.02 Mol L^{-1}, respectively. For the calculations, the conductivity of distilled-deionized water was assumed to be 0.0545 x 10^{-5} dS m^{-1} which is the standard for this solution (Pashley et al., 2005). The soil solid phase surface electrical conductivity (σ_s) was estimated for each soil from the measured soil imaginary permittivity using Eq.[6.3]. Measurements were acquired by inserting the Hydra Probe to air dried unpacked sieved samples of each soil, recording the readings for about 30 minutes and averaging them. The mean values and associated standard deviations (in parenthesis) of σ_s were 0.014(0.0013) dS m^{-1} for clay, 0(0.0014) dS m^{-1} for sandy loam and 0.009(0.0010) dS m^{-1} for silty clay loam. Equations [6.9] and [6.14] were parameterized using nonlinear regression and then solved for the pore solution conductivity (σ_w) generating two inverse predictive functions (Eqs.[6.11] and [6.16]). All statistical analyses were performed using SAS® software v9.13.

The semi-empirical models developed in this research were compared to two water content independent models found in the literature, one developed for TDR (Malicki and Walczak, 1999):

$$\sigma_w = (\sigma_a - 0.08) / (\varepsilon_a - 6.2) (0.0057 + 0.000071\ S) \qquad [6.17]$$

where S = sand content (%), and the other for a 30 MHz sensor (Hilhorst, 2000):

$$\sigma_w = \varepsilon_w \sigma_a / (\varepsilon_a - \varepsilon_h) \quad [6.18]$$

where ε_w = dielectric permittivity of the soil solution and ε_h is the "offset", the value of dielectric permittivity where the soil apparent conductivity is zero. Hilhorst (2000) suggested a "universal" value of $\varepsilon_h = 4.1$, and this value was used in our calculations involving Eq.[6.18]. For the 30 MHz model the apparent soil conductivity (ε_a) is represented by the real component of dielectric permittivity (ε_r) and ε_w is the ε_r value measured in the saturating solutions (Hamed et al., 2003). For the TDR model we assumed that the real component of dielectric permittivity (ε_r) is a good approximation of the apparent permittivity (ε_a) (Topp et al., 1980).

Model comparisons were performed using the coefficient of determination (R^2) and root mean square error (RMSE) among average pore solution conductivity predictions for each of the equations and the initial saturating solution conductivity values (Huisman et al., 2001):

$$\text{RMSE} = \sqrt{\frac{\sum_{i=1}^{N} (\sigma_{w*} - \sigma_w)^2}{N}} \quad [6.19]$$

where N = number of observations, σ_{w*} is the predicted pore solution conductivity from the different models and σ_w is the measured solution conductivity, both in dS m^{-1}.

Results and Discussion

Model Fitting

Equations [6.9] and [6.14] were fitted to data on a by soil and disturbance basis, and also as a general model, including all treatments, using nonlinear regression in SAS® statistical analysis software. Equation [6.14] was fitted following two procedures. In the first, all three parameters (i.e. A, B and λ) were fitted by nonlinear regression (case I) and in the second the parameters A and B were previously estimated using Eq.[6.6] (see Chapter V) (case II). The linear regression general fit of Eq.[6.6] resulted in A = 0.1188 and B = -0.2190. All of the fits were highly significant ($p < 0.0001$). For the soil and disturbance fittings, the average R^2 was 0.91 for Eq.[6.9] and Eq.[6.14] case I, and 0.94 for Eq.[6.14] case II. The general fittings resulted in an R^2 of 0.82 for Eq.[6.9] and Eq.[6.14] case I, and an R^2 of 0.84 for Eq.[6.14] case II. The

nonlinear regression including all treatments includes more variability in the dataset, resulting in a decrease in the R^2 values for the fits. The parameter estimates for the best fit nonlinear regression analyses of Eqs. [6.9] and [6.14] cases I and II are presented in Figs. 6.1, 6.2 and 6.3 respectively (All figures for this Chapter are located in Appendix J).

The measured values of σ_s used in the nonlinear regression fittings should be viewed as an approximation of the soil surface conductivity. These values were used because the models could not be fitted with σ_s as a fitting parameter. In the case of Eq.[6.9] σ_s was overestimated, resulting in σ_s values much greater than the lowest values of σ_a, which violates a physical constraint of the models. In the case of Eq.[6.14] the addition of σ_s as a fitting parameter resulted in nonuniqueness caused by overparameterization in the nonlinear regression procedure and thus the model could not be fitted. Both issues were resolved when measured values of σ_s were included in the nonlinear models. Rhoades et al. (1976) used a graphical approach to calculate σ_s which resulted in relatively high values when compared to our measurements. The soil solid phase conductivity was taken as the value of the apparent conductivity where the pore solution conductivity is zero (Rhoades et al., 1976). Amente et al. (2000) used the same procedure of Rhoades et al. (1976) and found a positive relationship between σ_s and volumetric water content. The problems associated with fitting σ_s by nonlinear regression using Eq.[6.5] were also experienced by Hamed et al. (2003). The estimated values of σ_s had a wide range of variability and in many cases the fittings resulted in negative values, which are not physically meaningful (Hamed et al., 2003). Although our approach of measuring σ_s in dry soil may be an approximation to the true value, we found that the best fits of Eqs.[6.9] and [6.14] were found when these values were used. These issues indicate that more research is needed to physically define the soil surface conductivity, its range of values for different soils, and to investigate its potential relationship with volumetric water content.

Volumetric water content independence

The predictive models presented in this research are based on the hypothesis that the pore solution conductivity (σ_w) estimates are independent of volumetric water content (θ_v). Pore water conductivity predictions versus volumetric water content plots are presented in Fig. 6.4 for

Eqs.[6.11] and [6.16] fitted on a soil and disturbance basis. The graphs for the general fits were very similar to the plots for soil and disturbance fittings and thus are not shown. Figures 6.4a, 6.4b and 6.4c present the estimates of σ_w for the whole range of water contents, from zero to about 0.55 cm^3 cm^{-3} using Eqs.[6.11] and [6.16] cases I and II. With all the models the σ_w predictions increase as the water contents decreases. Overall, the models resulted in undesirable variability in σ_w predictions for $\theta_v < 0.1$ cm^3 cm^{-3}. When values of ε_r and σ_a corresponding to water contents < 0.1 cm^3 cm^{-3} are removed from the data set, the predictions are more stable, with little or no dependence on volumetric water content. The average standard deviation of the data dropped from 0.25 to 0.18 cm^3 cm^{-3} for Eq.[6.11] and 0.24 to 0.17 cm^3 cm^{-3} for Eq.[6.16] case I, when $\theta_v < 0.1$ cm^3 cm^{-3} data was removed. The only exception is Eq.[6.16] case II where some residual dependence on water content remains. Although data shown in Figure 6.4c was cut at 6 dS m^{-1} (with the purpose of representing all plots in the same scale) the predicted values of σ_w go up to 18.5 dS m^{-1}. However there was still a substantial decrease in the variability of the data, as the average standard deviation dropped from 0.59 to 0.33 cm^3 cm^{-3} in Eq.[6.16] case II. Similar results were found for the general fittings for all models. Therefore, for Eqs.[6.11] and [6.16] case I these results lead us to believe that the estimates of pore solution conductivity at $\theta_v < 0.1$ cm^3 cm^{-3} are uncertain and thus we choose to use this water content value as a cutoff criterion for our models. Our cutoff criterion for water content is the same as that of Hilhorst (2000). Although estimations from Eq. [6.16] case II are not entirely independent of water content (Figure 6.4c) we decided to investigate its predictive capabilities along with the other models in the following section as the procedure employed in its development might have important implications in future research on estimation of water content and electrical conductivity relationships in soils.

Predictive capability of Eqs.[6.11] and [6.16]

Since the initial conductivity of the saturating solution is known we compared the average predictions of σ_w for the range of ε_r and σ_a values to the initial σ_w values (that is the pure solution conductivity before being introduced into the soils). If the effects of interactions between the solutions and soil are in fact small, the model should provide average predictions

that are close to the initial saturating solutions. The average predictions are presented in Table 6.2 for Eqs.[6.11] and [6.16] cases I and II for coefficients obtained on both a soil and disturbance basis, and on a general (all data) basis by using nonlinear regression. The coefficient of determination (R^2) and root mean square error (RMSE) for predicted versus average observed values for the models are presented in Figure 6.5. Two of the new models, Eqs.[6.11] and [6.16] case I, had very good predictive capabilities as indicated by the RMSE and R^2 values both for the soil and disturbance and general fittings (Figure 6.5). Equation [6.16] case II had an R^2 of 0.81 and an RMSE of 0.87 cm^3 cm^{-3} when fitted on a soil and disturbance basis and an R^2 of 0.71 and an RMSE of 1.01 cm^3 cm^{-3} when fitted to all data indicating that this model was somewhat less accurate than Eq.[6.11] and Eq.[6.16] case I.

It should be noted that for all models the predictions of pore solution conductivity for an initial saturating solution conductivity of ~0 dS m^{-1} are much higher than the actual value (Table 6.2). The estimations were only lower in the sandy loam disturbed treatment, and the average among all models developed in this research was 0.56 dS m^{-1}. Overall, the accuracy of the soil and disturbance specific models increases as the conductivity of the soil solution increases (Table 6.2). In other words, for Eqs.[6.11] and [6.16] fitted in a soil and disturbance basis, the average predicted conductivity tends to be closer to the actual solution conductivity as the pore solution conductivity increases. This can be explained by the fact that soil specific effects on the estimates are more pronounced when the soil solution conductivity is lower than about 2 dS m^{-1}. In essence as σ_w approaches higher values, σ_a will be dominated mainly by σ_w, minimizing any soil specific variability (Table 6.2). This has potential implications for the development of general models for predicting σ_w, since it is likely that the accuracy of any predictive function will be higher at higher pore solution conductivity values. Although this problem is likely a mathematical limitation of the models, it has physical implications, in that any zero conductivity solution in contact with a soil with salts precipitated in it or adsorbed to its exchange phase will acquire conductivity as the solution reaches equilibrium with the solid phase. The general models also overestimated the σ_w values at low conductivity values, but contrary to the soil and disturbance specific models, the accuracy of the predictions did not increase with increasing conductivity of the saturating solution (Table 6.2).

The precision of the models developed in this research is represented by the standard deviations of the model predictions of σ_w (Table 6.3). In any scenario, the standard deviations were very similar for Eq.[6.11] and Eq.[6.16] case I and substantially higher for Eq.[6.16] case II, indicating that including coefficients from Eq.[6.6] into Eq.[6.16] resulted in a decrease in precision for this model (Table 6.3). In the soil and disturbance fittings the standard deviations remained fairly constant with the increase of the initial saturating solution conductivity while for the general models the standard deviations were minimum at σ_w = 2.02 dS m^{-1}, increasing both toward lower (0 dS m^{-1}) and higher (3.96 dS m^{-1}) conductivities. The reasons for the increase in the precision of the general models at this specific conductivity value are unclear. We speculate that it might be related to the fact that a general predictive model will produce more accurate predictions at midpoint values of the variable being predicted, which is likely related to sensitivity to extreme observations in both ends of the conductivity spectrum during the parameterization process.

The values of the coefficients A = 0.1017 and B = -0.127 fitted to a general model independent of water content (Eq.[6.16] case I) were somewhat close to the range of values of these parameters reported in the literature for calibration equations in the form of Eq.[6.6]. Data presented in Chapter V resulted in fitted general values of A = 0.1188 and B = -0.2190, Seyfried et al. (2005) reported average values of A = 0.110 and B = -0.180, while Topp and Ferre (2002) reported A = 0.115 and B = -0.176 for a calibration to a TDR sensor. Given these results, it is recommended that further investigation of the relationships among the fitting parameters of Eqs.[6.6] and [6.14] should be sought in future research as this procedure seems to have potential applications in both water content and soil solution conductivity estimations.

Comparison to other models

The accuracy of predictions based on the models developed in this research was compared to that of two water content independent models published in the literature, the Malicki and Walczak (1999) and Hilhorst (2000) equations (Eqs.[6.17] and [6.18]). The average predictions for both models are presented in Table 6.2 and the standard deviation of the estimates is presented in Table 6.3. These models were also compared using the R^2 and RMSE among

average pore solution conductivity predictions from each of the models and the conductivity of the solution initially saturating the soil. Here we sought not to demonstrate that our models are better than previous models, because we are aware that a calibration equation developed for a specific dataset will always out perform general equations developed from different datasets (Seyfried et al., 2005). Therefore we used the Malicki-Walczak and Hilhorst models as standards to which each of the new models were compared.

A set of general R^2 and RMSE values for all models developed or evaluated in this research is presented in Figure 6.5. The Malicki-Walzack model Eq.[6.17] had lower R^2 and higher RMSE values than any of the models developed in this research, while the Hilhorst model performed better than Eq.[6.16] case II fitted on a general basis. For our data the Hilhorst model had accuracy comparable to our general models (Figure 6.5). The precision of Eq.[6.18] was in most cases higher than that of the models developed in this research (Table 6.3). This might be due to the fact that the Hilhorst model includes the value of pore solution real dielectric conductivity in the estimation process (Eq.[6.18]). This variable was not included in our models because it is not an easily measured soil property under normal field conditions. The R^2 when average predictions from Eq.[6.18] were compared to the initial saturating solution conductivity was 0.78. In all likelihood the estimates from Eq.[6.18] would be even more accurate if ε_h (i.e. offset) values were defined for each soil setting, instead of the "universal" value of $\varepsilon_h = 4.1$ (Persson, 2002; Hamed et al., 2003).

One of the reasons why the model of Malicki and Walczak (1999) (Eq.[6.17]) had a lower accuracy might be because it was devised for different soils and conditions and because it was used as a general model, rather than having coefficients fitted to each soil/disturbance setting. In some cases, the extremely high standard deviation in the Malicki-Walczak model are due to the fact that this model has a mathematical discontinuity at water contents lower than 0.2 $cm^3\ cm^{-3}$ where estimates reach asymptotic values. This is clear from the values of average predicted σ_w and standard deviation for the ~0 dS m^{-1} conductivity treatments corresponding to Eq.[6.17] (Tables 6.2 and 6.3). As discussed by Malicki and Walczak (1999), Eq.[6.17] should only be used to water contents > 0.2 $cm^3\ cm^{-3}$. However for this research, in order to compare the models estimates we chose the volumetric water content cutoff criterion that suited most of the models, i.e. volumetric water contents < 0.1 $cm^3\ cm^{-3}$ were excluded.

Conclusions

Two new semi-empirical models for calculating the electrical conductivity of the soil pore solution have been presented. These new models are mathematically independent of soil volumetric water content, and can be considered dielectric equivalents of Rhoades type models for calculating and/or predicting soil bulk and pore solution conductivities. The first case (Eq.[6.11]) is based on a linear transmission coefficient (Rhoades et al., 1976) while the second case (Eq.[6.16]) was derived using a power law function (Amente et al., 2000). Both models fitted the observed data of ε_r and ε_i well on a soil and disturbance and general (all data) basis. The inverse predictive capability of the models was very similar when used to predict pore solution conductivity from ε_r and ε_i. While not completely water content independent for our dataset, the predictions from Eq.[6.16] when using A and B parameters previously fitted to a form of Hydra Probe calibration equation (Eq.[6.6]) were also satisfactory. This is promising, as it could lead to the development of simpler methods for predicting soil conductivity and soil volumetric water content. The new models also performed well when compared to models previously published in the literature (Malicki and Walczak, 1999; Hilhorst, 2000). Based on our data, the soil effect on the model predictions decreases as the pore solution conductivity increases. Also, our models overestimated soil pore solution conductivity at very low solution conductivities (σ_w approaching zero). These results indicate that it is likely that pore solution predictive functions will perform better at higher pore solution conductivities (σ_w greater than about 1.23 dS m^{-1} for our data). In any case, further research using measured values of in situ soil solution conductivity (σ_w) should be employed in the future to validate the new models. The parameterized versions of our models are limited by the fact that we did not have pore solution conductivity measurements. The difficulties in extracting and measuring pore solution conductivity greatly limit the possibilities of obtaining good measurements for this variable. However they should be sought in future research in order to increase the accuracy and precision of parameterized versions of Eqs.[6.11] and [6.16] especially for soils saturated with low conductivity solutions. Further research on the measurement and inverse estimation of σ_w is also recommended.

Acknowledgements

This research was funded by the US Army Corps of Engineering – Engineering Research and Development Center, contract: BR05-0001C, UT – USACE/ERDC.

CHAPTER VII. CONCLUDING REMARKS

Summary

The interactions among soil physicochemical and electrical properties were the central theme of this research. The investigation was based on measurements of soil complex permittivity acquired using a 50 MHz impedance sensor, the Hydra Probe. Data were collected using disturbed and undisturbed duplicate samples from a range of soil textures (Clay, Silty Clay Loam, and Sandy Loam) saturated with distilled-deionized water and saline solutions at four concentrations: KCl and $CaCl_2$ at 0.01 and 0.02 Mol L^{-1} for three days and then air dried under laboratory conditions, generating monotonic drying curves. Real and imaginary components of the dielectric permittivity were measured by the Hydra Probe. Load cells recorded changes in sample weight over time, which were later converted into volumetric water content. Soil bulk apparent conductivity was calculated from soil imaginary permittivity.

Soil characterization analyses have shown that the logarithm of saturated hydraulic conductivity, and the residual and saturation volumetric water contents were significantly different for soils, disturbances and their interaction, but not for salt treatments. The α parameter from the van Genucthen model was not significantly different among soil textures, disturbances or salt treatments, while the van Genuchten n parameter was significantly different for soil texture, disturbance, the soil texture x disturbance interaction and salt treatment. Numerical simulations of the air drying experiments have shown that the variability in volumetric water content distribution in space within the cores was much less than the variability over time. Overall the variability in space within the cores was small and it was assumed to be negligible for further analyses.

Part of the study was focused on investigating the effect of soil texture, disturbance, and salinity of soil solution on the estimation of volumetric water content at 50 MHz. Data were also used to develop and evaluate models for predicting soil pore solution conductivity at 50 MHz. The main advantage of using dielectric methods to predict soil pore solution conductivity is that they provide estimations that are mathematically independent of soil volumetric water content.

I found that there was no benefit in including the imaginary dielectric permittivity, or a correction for the loss tangent, in models for estimating water content at 50 MHz. Based on the results, Clay soils should be assessed independently when developing calibration equations for the Hydra Probe. Furthermore, the sensor's water content estimations are sensitive to soil disturbance. The resulting models for estimating pore solution conductivity are dielectric equivalents of Rhoades type two-pathway models based on linear and power law solutions for the transmission coefficient. Overall the average soil solution conductivity predicted by the new models compared well to the saturating solution conductivities.

Conclusions

The main conclusions of this research are:

i. The residual and saturated volumetric water contents as well as the logarithm of the saturated hydraulic conductivity were not influenced by salt treatments, but responded to the soil and disturbance treatments

ii. The α parameter from the van Genuchten model was not responsive to soil texture, disturbance and salt treatments, while the n parameter was responsive to soil texture, disturbance, their interaction, and the salt treatment

iii. Numerical simulations using Hydrus 2D software have shown that the distribution of water content at any time increment within the soil samples was small relative to the changes over time and was thus neglected in further analyses

iv. It is possible to precisely and accurately estimate soil volumetric water content from the real component of soil dielectric permittivity at 50 MHz using a square root linear calibration equation

v. The estimation of volumetric water content is independent of the imaginary component of soil dielectric permittivity. In other words, the increase in soil conductive losses with the addition of salt to the soil saturating solution did not influence the accuracy of the estimations of volumetric water contents in soils saturated with solutions of conductivities up to 3.96 dS m^{-1}

vi. The estimation of volumetric water content at 50 MHz using the Hydra Probe was independent of soil texture for soils with clay content less than 34.4%

vii. Estimations of volumetric water content at 50 MHz using the Hydra Probe are sensitive to soil disturbance. However, I found only weak correlations between the parameters from the model for estimating water content at 50 MHz and soil structural properties

viii. It is possible that a more extensive dataset containing a wider range of soils and disturbance treatments would improve the chances of finding significant correlations among water retention and structural parameters and parameters from the water content estimation model from electrical properties at 50 MHz

ix. Two new models for predicting soil pore solution conductivity at 50 MHz using the Hydra Probe have been developed and evaluated. The resulting models for estimating pore solution conductivity are dielectric equivalents of Rhoades type two-pathway models based on linear and power law solutions for the transmission coefficient

x. The new models provide accurate and precise predictions of soil pore solution conductivity when the conductivity of the saturating solution was greater than about 1.23 dS m^{-1} and for water contents greater than 0.1 cm^3 cm^{-3}

Recommendations for Future Research

The influence of soil texture and structure (disturbance) on the estimation of volumetric water content at 50 MHz needs to be further investigated by using a data set from a variety of soils, with a broader range of soil textures, mineralogies and structural properties. More accurate and precise models, which can potentially be included as defaults in the commercial version of the probe, could be developed with this procedure.

Regarding the pore solution electrical conductivity estimation models, it is recommended that the models developed here should be validated with an independent dataset, accounting for different soils and a range of pore solution conductivities. The soil pore solution conductivities should be measured in-situ by independent methods and compared to model predictions.

Disclaimer

Mention of products and software's brand and commercial names are provided solely on the purpose of specific information for reproducibility of experiments and data analyses and should not be construed as product endorsement by the author or the University of Tennessee.

REFERENCES

REFERENCES

Amente, G., J.M. Baker, and C.F. Reece. 2000. Estimation of soil solution conductivity from bulk soil electrical conductivity in sandy soils. Soil Sci. Soc Am. J. 64:1931-1939.

Blake, C.R., and K.H. Hartge. 1986a. Bulk density. p. 363–375. In A. Klute (ed.) Methods of soil analysis. Part 1, 2nd ed. Agron. Monogr. 9. ASA and SSSA, Madison. WI.

Blake G.R., and K.H. Hartge. 1986b. Particle density. p. 377–382. In A. Klute (ed.) Methods of soil analysis. Part 1, 2nd ed. Agron. Monogr. 9. ASA and SSSA, Madison. WI.

Bosch, D.D. 2004. Comparison of capacitance-based soil water probes in coastal plain soils. Vadose Zone J. 3:1380-1389.

Brouder, S.M., B.S. Hoffmann, and D.K. Morris. 2005. Mapping soil pH: Accuracy of common soil sampling strategies and estimation techniques. Soil Sci. Soc. Am. J. 69:427-442.

Campbell, J.E. 1990. Dielectric properties and influence of conductivity in soils at one to fifty megahertz. Soil Sci. Soc. Am. J. 54:332-341.

Corwin, D.L., and S.M. Lesch. 2005. Apparent soil electrical conductivity measurements in agriculture. Comput. Electron. Agr. 46:11-43.

Davis, J.L., and A.P. Annan. 1977. Electromagnetic detection of soil moisture: Progress report 1. Can. J. Remote Sensing 3(1):76-86.

Ferre, P.A., and G.C. Topp. 2002. Time domain reflectometry. p. 434–446. In J.H. Dane and G.C. Topp (ed.) Methods of soil analysis. Part 4. SSSA Book Ser. 5. SSSA, Madison, WI.

Friedman, S.P. 1998. A saturation degree-dependent composite spheres model for describing the effective dielectric constant of unsaturated porous media. Water Resour. Res. 34:2949-2961.

Friedman, S.P. 2005. Soil properties influencing apparent electrical conductivity: a review. Comput. Electron. Agr. 46:45-70.

Gee, G.W., and D. Or. 2002. Particle-size analysis. p. 255–293. In J.H. Dane and G.C. Topp (ed.) Methods of soil analysis. Part 4. SSSA Book Series No. 5. SSSA, Madison, WI.

Griffin, T.S., C.W. Honeycutt, and Z. He. 2003. Changes in soil phosphorous from manure application. Soil Sci. Soc. Am. J. 67:645-653.

Hamed, Y., M. Persson, and R. Berndtsson. 2003. Soil solution electrical conductivity measurements using different dielectric techniques. Soil Sci. Soc Am. J. 67:1071-1078.

Hao, X., and A.N. Kravchenko. 2007. Management practice effects on surface soil total carbon: differences along a textural gradient. Agron. J. 99:18-26.

Heuscher, S.A., C.C. Brandt, and P.M. Jardine. 2005. Using soil physical and chemical properties to estimate bulk density. Soil Sci. Soc. Am. J. 69:51-56.

Hilhorst, M.A. 2000. A pore water conductivity sensor. Soil Sci. Soc Am. J. 64:1922-1925.

Hillel, D. 1998. Environmental soil physics. Academic Press, 771p.

Huisman, J.A., C. Sperl, W. Bouten, and J.M. Verstraten. 2001. Soil water content measurements at different scales: accuracy of time domain reflectometry and ground penetrating radar. J. Hydrol. 245:48-58.

James, J.W. 1964. Comparing regression and correlation coefficients. Appl. Stat. – J. Roy. St. C 13:127-132.

Jenkins R. 1999. X-ray Fluorescence Spectrometry. Wiley-Interscience, New York.

Jones, S.B., J.M. Wraith, and D. Or. 2002. Time domain reflectometry measurement principles and applications. Hydrol. Process. 16: 141-153.

Kao, C.K. 2004. Dielectric phenomena in solids. Elsevier Academic Press, San Diego, CA. 581p.

Kraus, J.D. 1992. Electromagnetics. McGraw Hill, Inc. 847p.

Leao T.P., and E. Perfect. 2007. Water content estimation from dielectric permittivity measured using the hydra probe in disturbed and undisturbed soil samples. In: Paltineanu, I.C. (ed.) The second international symposium on soil water measurement using capacitance, impedance and time domain transmission. Paltin International Inc. Beltsville, USA.

Legates, D.R., and G.J. McCabe. 1999. Evaluating the use of "goodness of fit" measures in hydrologic and hydroclimatic model validation. Water Resour. Res. 35:233-241.

Malicki, M.A., and R.T. Walczak. 1999. Evaluating soil salinity status from bulk electrical conductivity and permittivity. Eur. J. Soil Sci. 50:505-514.

Miller, R.W., and R.L. Donahue. 1995. Soils in our environment. 7th ed. Prentice-Hall Inc., New Jersey 649p.

Mualem, Y., and S.P. Friedman. 1991. Theoretical prediction of electrical conductivity in saturated and unsaturated soil. Water Resour. Res. 27:2771-2777.

Neter, J., W. Wasserman, and M.H. Kutner. 1990. Applied linear statistical models. Irwin Inc. 1181p.

Nimmo, J.R. 1997. Modeling structural influences on soil water retention. Soil Sci. Soc Am. J. 61: 712-719.

Paltineanu, I.C. (ed.). 2007. Transactions of the second international symposium on soil water measurement using capacitance, impedance and time domain transmission. Paltin International Inc. Beltsville, USA.

Pashley, R.M., M. Rzechowicz., L.R. Pashley, and M.J. Francis. 2005. De-gassed water is a better cleaning agent. J. Phys. Chem. B 109:1231-1238.

Pedhazur, E.J. 1997. Multiple regression in behavioral research: Explanation and prediction. 3rd ed. Harcourt Brace: Forth Worth, 1058p.

Pennell, K.D. 2002. Specific Surface Area. p. 295–315. In J.H. Dane and G.C. Topp (ed.) Methods of soil analysis. Part 4. SSSA Book Series No. 5. SSSA, Madison, WI.

Persson, M. 2002. Evaluating the linear dielectric constant-electrical conductivity model using time domain reflectometry. Hydrol. Sci. J. 45:833-847.

Raju, G.G. 2003. Dielectrics in electric fields. Dekker. 578p.

Rassam, D., J. Simunek, and M.Th. van Genuchten. 2003. Modeling variable saturated flow with Hydrus 2-D. ND Consult: Brisbane, Australia.

Regalado, C.M. 2004. A physical interpretation of logarithmic TDR calibration equations of volcanic soils and their solid fraction permittivity based on Lichtenecker's mixing formulae. Geoderma 123:41-50.

Reynolds W.D., and D.E. Elrick. 2002. Falling head soil core (tank) method. p. 809–812. In J.H. Dane and G.C. Topp (ed.) Methods of Soil Analysis. Part 4. Physical methods. SSSA Book Series No. 5. SSSA, Madison, WI.,

Rhoades, J.D., P.A.C. Raats, and R.J. Prather. 1976. Effects of liquid-phase electrical conductivity, water content, and surface conductivity on bulk soil electrical conductivity. Soil Sci. Soc. Am. J. 40:651-655.

Rhoades, J.D., N.A. Manteghi, P.J. Shouse, and W.J. Alves. 1989. Soil electrical conductivity and soil salinity: new formulations and calibrations. Soil Sci. Soc. Am. J. 53:433-439.

Robinson, D.A. 2004. Measurement of the solid dielectric permittivity of clay minerals and granular samples using a time domain reflectometry immersion method. Vadose Zone J. 3:705-713.

Robinson, D.A., S.B. Jones, J.M. Wraith, D. Or, and S.P. Friedman. 2003. A review of advances in dielectric and electrical conductivity measurements in soils using time domain reflectometry. Vadose Zone J. 2: 444-475.

Scanlon, B.R., B.J. Andraski, and J. Bilskie. 2002. Miscellaneous methods for measuring matric or water potential. In: J.H. Dane and G.C. Topp (eds) Methods of soil analysis: Part 4: Physical Methods. SSSA Book Series, No. 5. p. 643-670.

Seyfried, M.S., and M.D. Murdock. 2004. Measurement of soil water content with a 50 MHz soil dielectric sensor. Soil Sci. Soc. Am. J. 68:394-403.

Seyfried, M.S., and L.E. Grant. 2007. Temperature effects on soil dielectric properties measured at 50 MHz. Vadose Zone J. 6:759-765.

Seyfried, M.S., L.E. Grant, E. Du, and K. Humes. 2005. Dielectric loss and calibration of the hydra probe water sensor. Vadose Zone J. 4:1070-1079.

Soil Survey Staff, Natural Resources Conservation Service, United States Department of Agriculture. 2008. Official Soil Series Descriptions [Online WWW]. Available URL: "http://soils.usda.gov/technical/classification/osd/index.html" USDA-NRCS, Lincoln, NE. Accessed: 06-02-2008, verified: 09-08-2008.

Stevens Water Monitoring System. 2007. The Hydra Probe Soil Sensor. Online document: “http://www.stevenswater.com/catalog/stevensProduct.aspx?SKU='93640'” Accessed: 02-01-2008, verified: 06-08-2008.

Thompson, R.B., M. Gallardo, M.D. Fernandez, L.C. Valdez, and C. Martinez-Gaitan. 2007. Salinity effects on soil moisture measurement made with a capacitance sensor. Vadose Zone J. 71:1647-1657.

Topp, G.C., and P.A. Ferre. 2002. Scope of methods and brief description. p. 419–422. In J.H. Dane and G.C. Topp (ed.) Methods of soil analysis. Part 4. SSSA Book Ser. 5. SSSA, Madison, WI.

Topp, G.C., J.L. Davis, and A.P. Annan. 1980. Electromagnetic determination of soil water content: determination in coaxial transmission lines. Water Resour. Res. 24:945-952.

Topp, G.C., S. Zegelin, and I. White. 2000. Impacts of the real and imaginary components of relative permittivity on time domain reflectometry measurements in soils. Soil Sci. Soc. Am. J. 64: 1244-1252.

Topp, G.C., J.L. Davis, and A.P. Annan. 2003. The early development of TDR for soil measurement. Vadose Zone J. 2: 492-499.

UMS. 2001. T5 miniature pressure transducer tensiometer. User Manual version 1.8. UMS GmnH, München, Germany, 27p.

van Genuchten. 1980. A closed-from equation for predicting the hydraulic conductivity of unsaturated soils. Soil Sci. Soc. Am. J. 44:892-898.

Whittig L.D., and W.R. Allardice. X-ray diffraction techniques. In: Klute A., ed. Methods of soil analysis, Part 1, 2nd ed Madison, WI: ASA and SSSA, 1986:331-362 Agron. Monogr. 9

APPENDICES

APPENDIX A. Experimental Setup and Devices

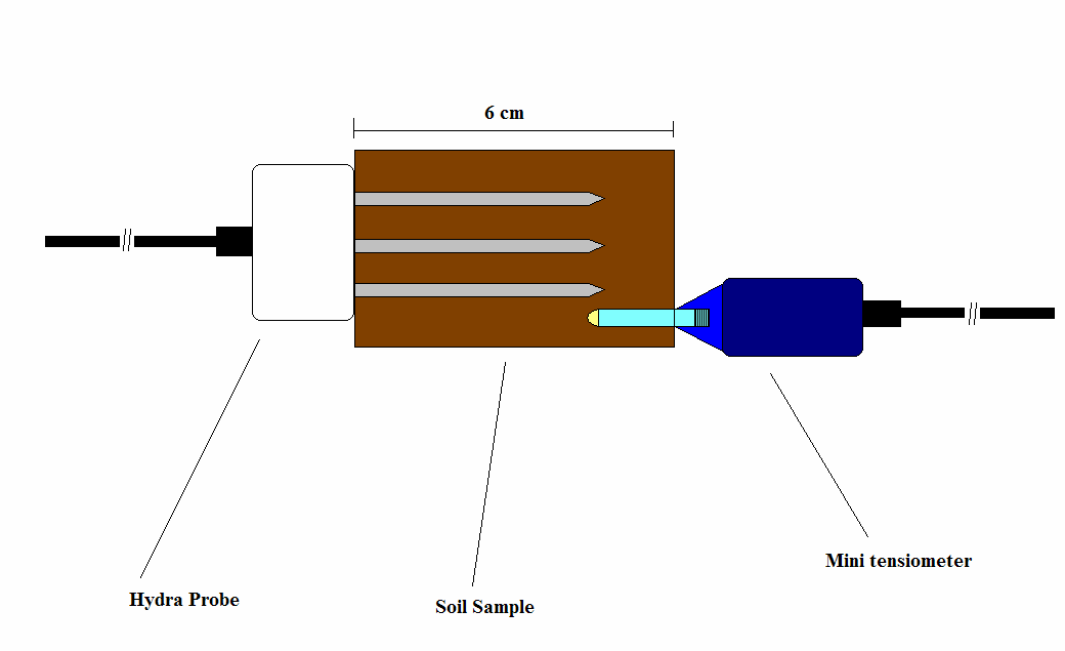

Setup of equipment within soil samples

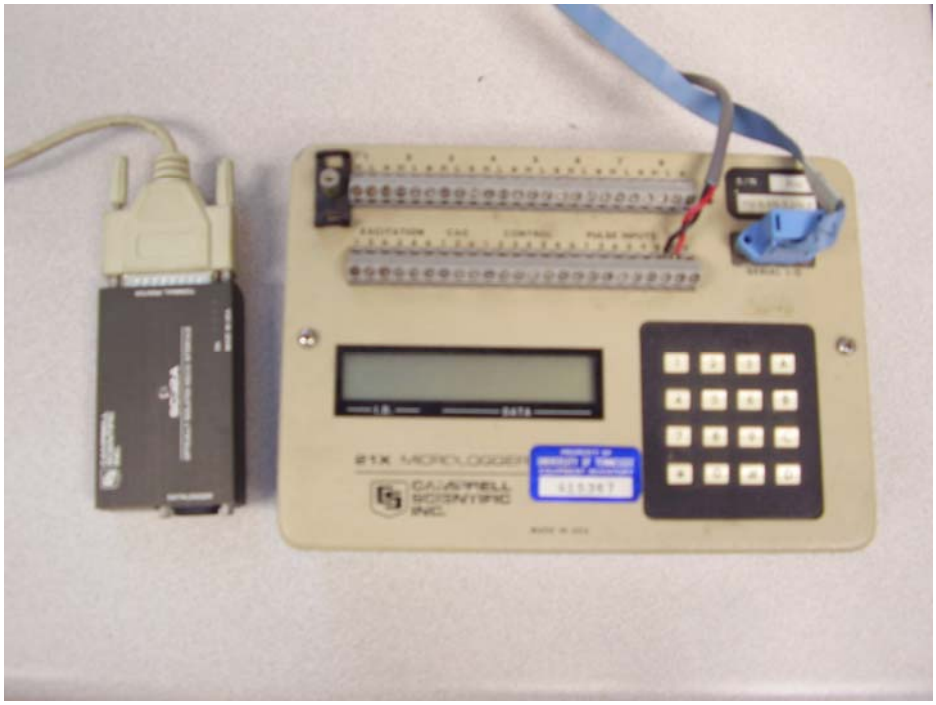

Campbell 21X Datalogger

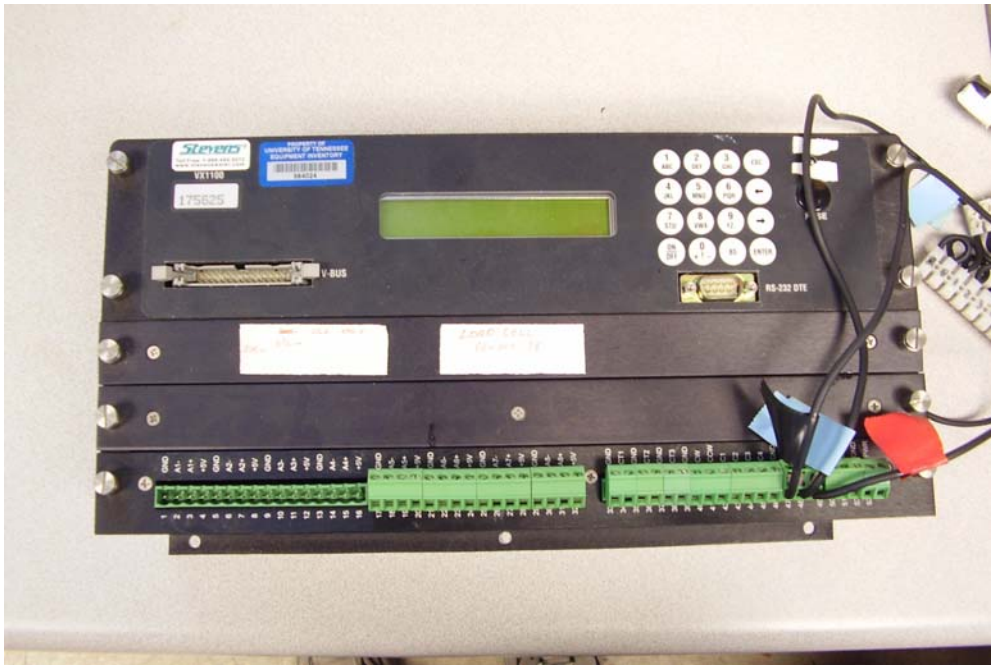

Vitel VX1100 Datalogger

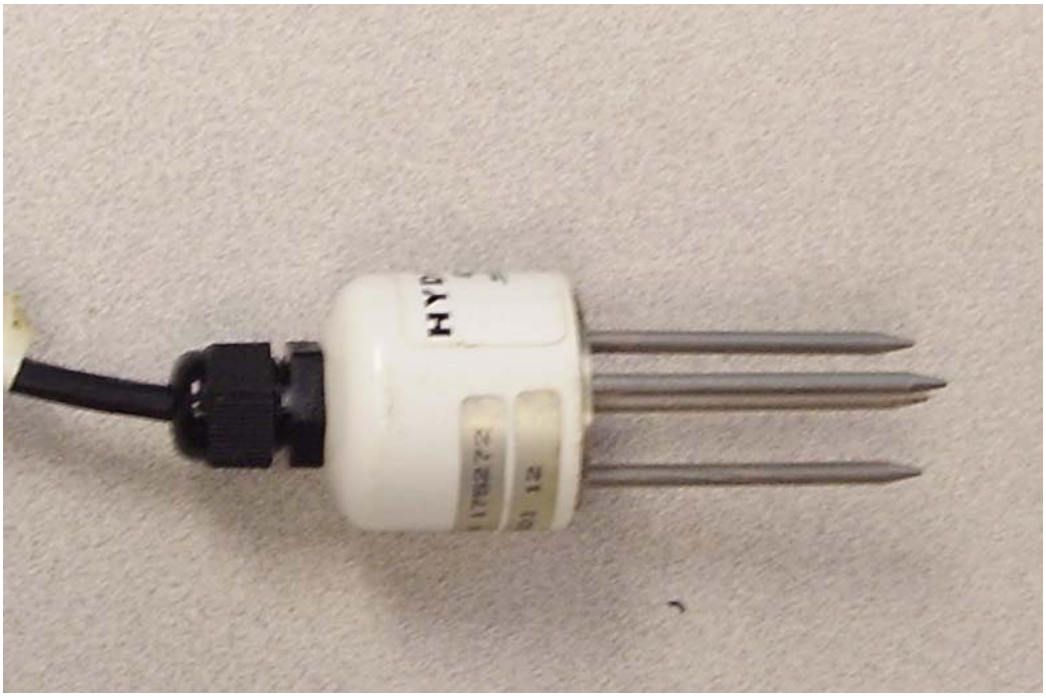

Stevens Water Hydra Probe

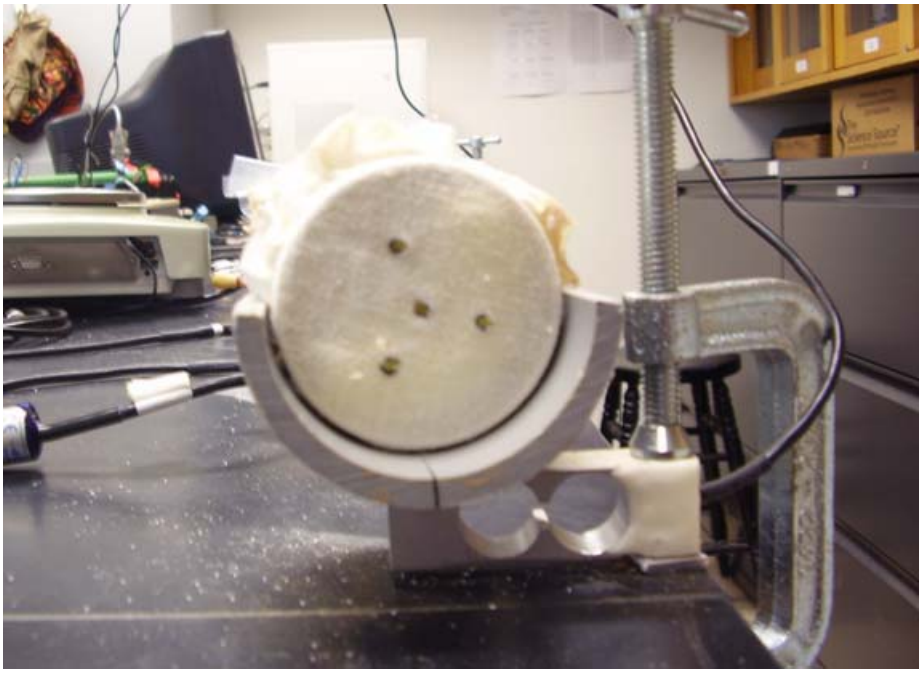

Transducer Techniques LSP-1 Load Cell system loaded with soil core

Decagon T5 Mini-Tensiometer

APPENDIX B. Soil Series Official Descriptions

LINDSIDE SERIES

The Lindside series consists of very deep, moderately well drained soils formed in alluvium washed mainly from lime influenced soils on uplands. They occur on nearly level flood plains. Saturated hydraulic conductivity is moderately high to high. Slope ranges from 0 to 3 percent.

TAXONOMIC CLASS: Fine-silty, mixed, active, mesic Fluvaquentic Eutrudepts

TYPICAL PEDON: Lindside silt loam - cultivated. (Colors are for moist soil.)

Ap--0 to 8 inches; dark grayish brown (10YR 4/2) silt loam; moderate fine granular structure; friable; few roots; strongly acid;clear wavy boundary. (6 to 12 inches thick)

BA--8 to 17 inches;brown (10YR 4/3) silt loam; weak fine granular structure; friable; few roots; strongly acid; clear wavy boundary. (0 to 10 inches thick)

Bw--17 to 30 inches; brown (10YR 4/3) silty clay loam; weak coarse subangular blocky structure parting to moderate medium subangular blocky; firm; few roots; many fine and medium distinct yellowish red (5YR 4/6) masses of oxidized iron and few fine and medium distinct grayish brown (10YR 5/2) iron depletions on faces peds; moderately acid; gradual wavy boundary. (10 to 30 inches thick)

BC--30 to 44 inches; brown (10YR 4/3) silt loam; moderate coarse subangular blocky structure parting to moderate medium subangular blocky; firm; few roots; common medium distinct yellowish red (5YR 4/6) masses of oxidized iron and dark grayish brown (10YR 4/2) iron depletions on faces peds; moderately acid; gradual wavy boundary. (0 to 20 inches thick)

C--44 to 65 inches; yellowish brown (10YR 5/4) weakly stratified silt loam and light silty clay loam; massive; firm; few black concretions; common medium faint grayish brown (10YR 5/2) iron depletions and distinct yellowish red (5YR 5/6) masses of oxidized iron on faces of peds; moderately acid.

TYPE LOCATION: Wood County, West Virginia; Boaz, about 150 yards east of Ohio River, 1 1/2 miles north of Keller Lane.

RANGE IN CHARACTERISTICS: Solum thickness ranges from 25 to 60 inches. The soil ranges from strongly acid to mildly alkaline in the upper part, unless limed, and from moderately acid to mildly alkaline in the lower part of the profile. Rock fragments range from 0 to 5 percent within a depth of 40 inches and from 0 to 30 percent below. Depth to redoximorphic depletions ranges from 14 to 24 inches.

The Ap horizon has hue of 7.5YR or 10YR, value of 3 through 5, and chroma of 2 or 3. Dry value is 6 or more. Undisturbed areas have a thin A horizon with hue of 7.5YR or 10YR, value of 2 or 3, and chroma of 1 to 3. The A horizon is silt loam, silty clay loam, or loam.

The BA, Bw, and BC horizons have hue of 7.5YR to 2.5Y, value of 4 or 5, and chroma of 3 to 6, above a depth of 20 inches and 1 to 4 below. Some pedons have moist value of 3 and chroma of 2 where dry value is 6 or more. They are silt loam or silty clay loam, and in some pedons there are thin strata of very fine sandy loam, fine sandy loam, loam, or clay loam.

The C horizon has hue of 7.5YR to 2.5Y, value of 4 to 6, and chroma of 1 to 4, except chroma of 6 and 8 are allowed if colors are mixed. Texture of the fine-earth fraction is silty clay loam, silt loam, loam, clay loam, very fine sandy loam, fine sandy loam, and sandy loam and may be stratified.

COMPETING SERIES: The Boonewood, Hontas and Senecaville series are in the same family. Boonewood soils are moderately deep with depth to the bedrock range from 20 to 40 inches. They formed in alluvium derived from limestone, siltstones, shales, and other silty material. The Hontas soils have subhorizons less than 40 inches with chroma of 2 or less. They formed in silty alluvium. Senecaville soils have hue of 5YR or redder throughout the B horizon, they formed in alluvium from dominantly interbedded shale and siltstone, and some interbedding of sandstone.

The Dockery, Hamblen, Hamlin, Huntington, Lobdell, Nolin, Rahm, Ray, Steff, Teel, Wakeland, and Weaver series are similar soils in related families. Dockery, Rahm, and Wakeland soils do not have a cambic horizon. Hamblen, Lobdell, and Weaver soils have more than 15 percent coarser particles than very fine sand in the particle-size control section. Hamlin and Teel soils have less than 18 percent clay in the particle-size control section. Huntington soils have a mollic epipedon. Nolin and Ray soils do not have low chroma mottles within a depth of 24 inches of the surface. Steff soils have less than 60 percent base saturation in all subhorizons between a depth of 10 and 30 inches below the soil surface.

GEOGRAPHIC SETTING: Lindside soils are nearly level soils on flood plains and in upland drainageways. Slopes are mostly 0 to 3 percent. The soils formed in recent alluvium washed mainly from limestone influenced uplands. Average annual precipitation ranges from 35 to 55 inches, and temperature ranges from 45 to 57 degrees F.

GEOGRAPHICALLY ASSOCIATED SOILS: These are the Ashton, Chagrin, Clarksburg, Dunning, Huntington, Linden, Melvin, Newark, Nolin, Sciotoville, and Wheeling soils. Ashton, Sciotoville, and Wheeling soils are on terraces and have argillic horizons. Chagrin soils are well drained. Dunning and Melvin soils are poorly drained. Huntington soils formed in alluvium on flood plains. Linden are very deep, well drained soils formed in alluvial sediments washed from nearby uplands that are underlain by red and brown shales, sandstones, and in some areas, conglomerate. Newark soils are somewhat poorly drained. Clarksburg soils have a fragipan. Nolin formed in alluvium derived from limestones, sandstones, siltstones, shales, and loess

DRAINAGE AND SATURATED HYDRAULIC CONDUCTIVITY: Moderately well drained. Runoff is low to medium and saturated hydraulic conductivity is moderately high to high.

USE AND VEGETATION: Most areas are cleared and cultivated or pastured. Original vegetation was mixed hardwoods.

DISTRIBUTION AND EXTENT: West Virginia, Pennsylvania, Maryland, Virginia, Ohio, Kentucky, Indiana, Tennessee, Arkansas, and Missouri. Extent is large. MLRA's 116A, 120, 121, 122, 125, 126, 127, 128, 130, 147, and 148.

MLRA OFFICE RESPONSIBLE: Morgantown, West Virginia

SERIES ESTABLISHED: Monroe County, West Virginia, 1925.

REMARKS: Diagnostic horizons and features recognized in this pedon are: 1. Ochric epipedon - the zone from 0 to 17 inches (Ap and BA horizons). 2. Cambic horizon - the zone from 17 to 30 inches (Bw horizon).

ETOWAH SERIES

The Etowah series consists of very deep, well drained, moderately permeable soils on high stream terraces, alluvial fans and foot slopes. These soils formed in alluvium or colluvium that is commonly underlain by limestone residuum below 40 inches. The slopes range from 0 to 35 percent.

TAXONOMIC CLASS: Fine-loamy, siliceous, semiactive, thermic Typic Paleudults

TYPICAL PEDON: Etowah silt loam--cultivated. (Colors are for moist soil unless otherwise stated.)

Ap--0 to 7 inches; dark brown (7.5YR 3/2) silt loam; moderate fine granular structure; very friable; common fine roots; medium acid; clear smooth boundary. (5 to 12) inches thick)

Bt1--7 to 13 inches; yellowish red (5YR 4/6) silty clay loam; moderate medium subangular blocky structure; friable; common fine roots and pores; few thin patchy clay films on faces of peds; strongly acid; gradual smooth boundary.

Bt2--13 to 24 inches; yellowish red (5YR 4/6) silty clay loam; moderate medium subangular blocky structure; friable; few fine roots and pores; many thin patchy clay films on faces of peds; few fine fragments of chert; strongly acid; clear smooth boundary.

Bt3--24 to 38 inches; yellowish red (5YR 4/6) silty clay loam; moderate medium subangular blocky structure; friable; many thin patchy clay films on faces of peds; few fragments of chert; strongly acid; gradual smooth boundary.

Bt4--38 to 54 inches; strong brown (7.5YR 5/6) silty clay loam, common fine and medium distinct red (2.5YR 4/6) mottles; moderate fine subangular blocky structure; firm; few fine roots and pores; many thin patchy clay films on faces of peds; few fragments of chert; strongly acid; gradual wavy boundary.

Bt5--54 to 70 inches; strong brown (7.5YR 5/6) silty clay loam, common fine distinct red and few fine distinct light yellowish brown mottles; strong fine subangular blocky structure; firm; few fine roots and pores; thin patchy clay films on faces of peds; few fine and medium fragments of chert; strongly acid. (Combined thickness of the Bt horizon ranges from 50 to more than 60 inches.)

TYPE LOCATION: Meigs County, Tennessee; 300 yards west of Flag Pond Bridge across Sugar Creek on River Road.

RANGE IN CHARACTERISTICS: The solum is more than 60 inches thick. Depth to bedrock, commonly limestone, ranges from 6 to 15 feet or more. Coarse fragments are commonly less than 5 percent, but range from 0 to 15 percent in each horizon, except the A horizon ranges to 20

percent. Some pedons contain some fine mica flakes. Reaction is strongly acid or very strongly acid except the surface layer is less acid in recently limed areas.

The A horizon has hue of 10YR or 7.5YR, value of 3 or 4 and chroma of 2 to 4. The fine earth texture is dominantly silt loam, but the range includes loam and silty clay loam.

Some pedons have a transitional horizon between the A or E horizon and the Bt horizon.

The Bt horizon has hue of 7.5YR to 2.5YR, value of 4 or 5, and chroma of 6 to 8. The lower part has few to common mottles in shades of red, yellow, and brown. The texture is silty clay loam or clay loam.

The 2Bt horizon, where present, has the same color as the Bt horizon. The texture is silty clay or clay.

COMPETING SERIES: Soils in the same family are the Addielou, Allen, Avilla, Bama, Holston, Leesburg, Minvale, Nella, Norfork, Octavia, Orangeburg, Pikeville, Ruston, and Smithdale series. Addielou soils have A horizons more than 20 inches thick. Allen, Avilla, Holston, and Leesburg soils have A horizons with value of 4 or more. Bama soils have sandy A horizons. Holston, Leesburg, and Norfork soils have hues of 7.5YR or yellower in the Bt horizon. Minvale, Nella, Octavia, and Pikeville soils have more than 15 percent fragments in the B horizon. Orangeburg, Ruston, and Smithdale soils have a higher sand content throughout the solum.

GEOGRAPHIC SETTING: Etowah soils are on stream terraces, alluvial fans, and foot slopes. Some areas have karst to semikarst topography. Slopes range from 0 to 35 percent. These soils formed in alluvium or colluvium that is commonly underlain by limestone residuum below 40 inches. Average annual precipitation is about 50 inches, and the average annual temperature is about 60 degrees F. near the type location.

GEOGRAPHICALLY ASSOCIATED SOILS: These are the competing Minvale series, and the Decatur, Dewey, Emory, Sequatchie, and Waynesboro series. Decatur, Dewey, and Waynesboro soils have more than 35 percent clay in the argillic horizons. Emory soils lack argillic horizons. Sequatchie soils have less than 18 percent clay in the B horizon and thinner sola.

DRAINAGE AND PERMEABILITY: Well drained; runoff is medium; moderate permeability.

USE AND VEGETATION: Practically all is cleared and used primarily for growing hay, pasture, corn, and small grain. Original vegetation was oaks, hickory, tulip poplar, elm, beech, and shortleaf, and Virginia pine.

DISTRIBUTION AND EXTENT: Highland Rim, and Southern Appalachian Ridges and Valleys of Tennessee; northwestern Georgia, northern Alabama and Maryland. The series is of moderate extent.

MLRA OFFICE RESPONSIBLE: Lexington, Kentucky

SERIES ESTABLISHED: Bartow County, Georgia; 1926.

REMARKS: Diagnostic horizons recognized in this pedon are:

Ochric epipedon - from 0 to 7 inches (Ap horizon)

Argillic horizon - from 7 to 70 inches (Bt horizon)

SEQUATCHIE SERIES

The Sequatchie series consists of very deep, well drained, moderately permeable soils that formed in loamy alluvium. These soils are on low terraces, foot slopes, and benches. Water runs off the surface at a moderate or slow rate. Slopes range from 0 to 12 percent but are dominantly less than 6 percent.

TAXONOMIC CLASS: Fine-loamy, siliceous, semiactive, thermic Humic Hapludults

TYPICAL PEDON: Sequatchie loam--cultivated. (Colors are for moist soil unless otherwise stated.)

Ap--0 to 9 inches; dark brown (10YR 3/3) loam; weak medium granular structure; friable; many fine roots; strongly acid; clear smooth boundary. (6 to 9 inches thick)

BA--9 to 12 inches; brown (7.5YR 4/4) loam; weak medium subangular blocky structure; friable; many fine roots; strongly acid; gradual smooth boundary. (0 to 8 inches thick)

Bt1--12 to 28 inches; brown (7.5YR 4/4) loam; weak fine and medium subangular blocky structure; friable; many roots; discontinuous clay films on faces of peds; strongly acid; gradual smooth boundary.

Bt2--28 to 38 inches; brown (7.5YR 4/4) loam; few fine faint brown mottles; weak fine and medium subangular blocky structure; friable; few roots; 5 percent by volume sandstone pebbles up to 3 inches in diameter; discontinuous clay films on faces of peds; very strongly acid; gradual smooth boundary. (Combined thickness of the Bt horizon is 18 to 40 inches.)

BC--38 to 46 inches; strong brown (7.5YR 5/6) loam; weak medium subangular blocky structure; friable; about 5 percent by volume sandstone pebbles up to 3 inches in diameter; very strongly acid; gradual smooth boundary. (0 to 12 inches thick)

C--46 to 72 inches; strong brown (7.5YR 5/6) sandy loam; structureless; friable; about 10 percent pebbles and cobbles up to 6 inches in diameter; very strongly acid.

TYPE LOCATION: Sequatchie County, Tennessee; 1 1/2 miles north of Dunlap; east of Hwy. U.S. 127; 100 yards east of old paved road.

RANGE IN CHARACTERISTICS: Thickness of the solum ranges from 32 to 60 inches. Depth to bedrock is more than 60 inches. The soil is strongly acid or very strongly acid except the A and B1 horizons are less acid in recently limed areas. Gravel and cobbles range from 0 to 15 percent by volume in the solum. Coarse fragments in the C horizon average from 0 to 35 percent by volume, but some subhorizons within the C horizon may contain as much as 50 percent of coarse fragments by volume.

The A horizon has hue of 10YR or 7.5YR, value of 3 and chroma of 2 to 4. It is loam, fine sandy loam, or silt loam.

The BA horizon, where present, has hue of 10YR, value of 4 and chroma of 3 or 4; hue of 7.5YR, value of 4 or 5, and chroma of 4 or 6; hue of 5YR, value of 4, and chroma of 4. It is loam, silt loam, or fine sandy loam.

The Bt horizon has hue of 7.5YR or 10YR, value of 4 or 5, and chroma of 4 to 8; hue of 5YR, value of 4, and chroma of 4 or 6. Mottles in shades of brown range from none to common in the upper part and mottles in shades of brown, yellow, gray, and red range from none to common in the lower part. It is loam, clay loam, or silt loam. Some pedons have a silty clay loam texture, however, the weighted average clay content of the upper 20 inches averages between 18 and 30 percent, and the content of sand coarser than very fine sand is more than 15 percent.

The BC horizon has hue of 10YR or 7.5YR, value of 4 or 5, and chroma of 3 to 8. Mottles in shades of brown, gray, yellow, or red range from none to common. It is loam, clay loam, fine sandy loam, or sandy loam.

The C horizon has hue of 10YR or 7.5YR, value of 4 or 5, and chroma of 3 to 6. Mottles range from none to many in shades of brown, gray, and yellow. The fine earth texture is fine sandy loam, sandy loam, or loam and contains thin strata of loamy sandy.

COMPETING SERIES: These are the Humphreys soils. Similar soils are the Chavies, Hayter, State, Statler, and Whitwell series. Chavies and Hayter soils have base saturation more than 35 percent and soil temperature less than 59 degrees F. Humphreys soils have more than 15 percent chert fragments. State soils have an Ap horizon with moist color value of 4 or more and have mixed mineralogy. Statler soils have mixed mineralogy. Whitwell soils have mottles with chroma of 2 or less in the upper part of the B horizon.

GEOGRAPHIC SETTING: Sequatchie soils are on low terraces, foot slopes, and benches. Slopes are mainly 0 to 6 percent but range from 0 to 12 percent. Near the type location mean annual air temperature is 60 degrees F. and mean annual precipitation is 53 inches.

GEOGRAPHICALLY ASSOCIATED SOILS: These are the similar Humphreys and Whitwell series and the Cartecay, Hamblen, and Bruno series. Humphreys soils are on slightly higher terraces. Whitwell soils are on slightly lower, slightly depressional areas. Cartecay, Hamblen, and Bruno soils are on slightly lower adjacent flood plains and lack argillic horizons.

DRAINAGE AND PERMEABILITY: Sequatchie soils are well drained. Runoff is medium or slow and permeability is moderate. The lower lying more level areas of Sequatchie soils are subject to occasional flooding.

USE AND VEGETATION: Most of these soils are cleared and used for growing hay, pasture, corn, tobacco, small grains, and vegetables. The native vegetation was mixed hardwoods.

DISTRIBUTION AND EXTENT: The Great Valley, and Highland Rim in Tennessee, Alabama, Georgia, Maryland and Arkansas.

MLRA OFFICE RESPONSIBLE: Lexington, Kentucky

SERIES ESTABLISHED: Hamilton County, Tennessee; 1937.

REMARKS: Diagnostic horizons and features recognized in this pedon are: Ochric epipedon - 0 to 9 inches (Ap horizon) Argillic horizon - 12 to 38 inches (Bt horizon)

APPENDIX C. Soil Mineralogical and Chemical Data

X-ray Fluorescence Spectroscopy Results

XRF RUN FOR TAIRONE LEAO JULY 13, 2005
CALIBRATION USED:
CALSOILS_090204
EXCEL FILE SAVED AS: leao_071305

Sample	Sum of conc. (%)	Al2O3 Al (%)	CaO Ca (%)	Fe2O3 Fe (%)	K2O K (%)	MgO Mg (%)	MnO Mn (%)	Na2O Na (%)	P2O5 P (%)	SiO2 Si (%)	TiO2 Ti (%)
GSD-11	95.982	10.294	0.440	4.193	3.134	0.579	0.304	0.494	0.065	75.866	0.353
SOIL-1	89.177	20.895	0.080	6.443	2.220	0.789	0.096	0.157	0.185	56.882	1.262
SOIL-2	85.841	11.998	0.915	2.507	2.702	0.915	0.067	0.879	0.223	64.443	1.028
SOIL-3	92.271	14.817	0.298	3.888	1.532	0.585	0.213	0.181	0.252	68.927	1.407

GSD-11 is standard

SOIL-1 Clay
SOIL-2 Sandy Loam
SOIL-3 Silty Clay Loam

X-ray Fluorescence Spectroscopy Results (Continued)

XRF RUN FOR TAIRONE LEAO JULY 13, 2005
CALIBRATION USED: CALSOILS_090204
EXCEL FILE SAVED AS: leao_071305

Sample	As As (ppm)	Ba Ba (ppm)	Co Co (ppm)	Cr Cr (ppm)	Cu Cu (ppm)	Hf Hf (ppm)	Nb Nb (ppm)	Ni Ni (ppm)	Pb Pb (ppm)	Rb Rb (ppm)	S S (ppm)	Sr Sr (ppm)
GSD-11	108	238	14	46	72	6	25	16	777	401	188	30
SOIL-1	16	460	11	57	21	12	23	35	6	122	211	45
SOIL-2	14	580	-10	33	5	15	15	13	-7	56	170	105
SOIL-3	17	510	-2	51	15	11	29	25	17	99	245	58

Minus sign indicates measurement below background noise (do not use)

GSD-11 is standard

SOIL-1 Clay
SOIL-2 Sandy Loam
SOIL-3 Silty Clay Loam

X-ray Fluorescence Spectroscopy Results (Continued)

XRF RUN FOR TAIRONE LEAO JULY 13, 2005
CALIBRATION USED: CALSOILS_090204
EXCEL FILE SAVED AS: leao_071305

Sample	V V (ppm)	W W (ppm)	Y Y (ppm)	Zn Zn (ppm)	Zr Zr (ppm)
GSD-11	35	105	39	363	146
SOIL-1	73	-40	26	106	497
SOIL-2	32	-39	25	40	591
SOIL-3	65	-39	58	94	455

Minus sign indicates measurement below background noise (do not use)

GSD-11 is standard

SOIL-1 Clay
SOIL-2 Sandy Loam
SOIL-3 Silty Clay Loam

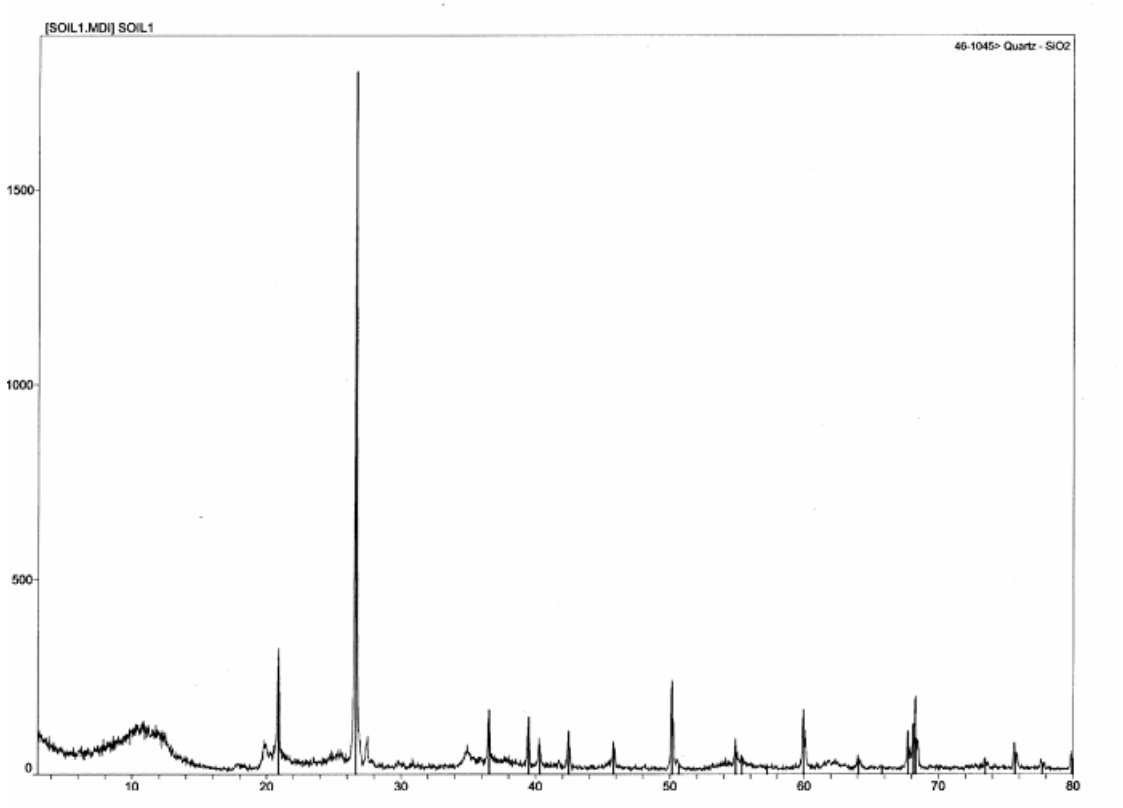

X-ray Diffraction Results: Clay

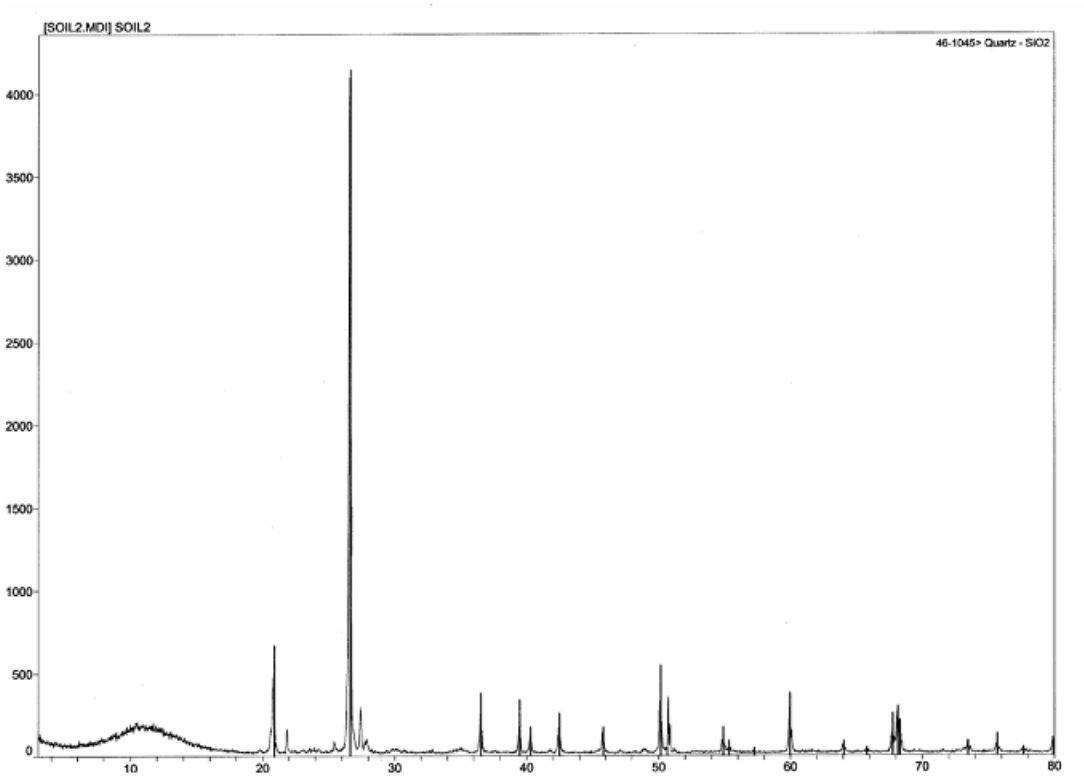

X-ray Diffraction Results: Sandy Loam

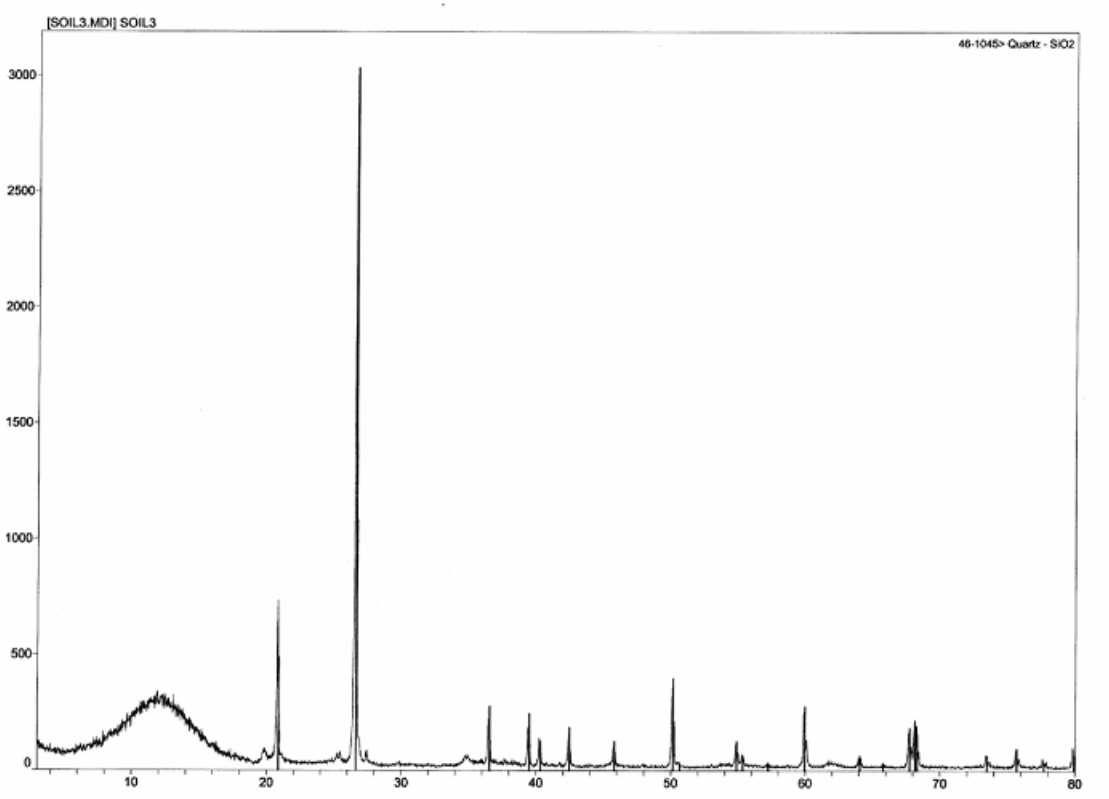

X-ray Diffraction Results: Silty Clay Loam

Basic Chemical Characterization Results

THE UNIVERSITY of TENNESSEE Extension

SOIL TEST REPORT

TAIRONE LEAO
306 EARTH & PLANETARY SCI. BLDG

KNOXVILLE, TN 379961410

Deborah K. Joines
Extension Assistant
Biosystems Engineering and Environmental Science
5201 Marchant Drive
Nashville, TN 37211-5112
(615) 832-5850
djoines2@utk.edu

Date Tested: 7/21/2005

County: Knox **Lab Number:** 273248

Mehlich 1 SOIL TEST RESULTS and RATINGS*

(Pounds Per Acre)

Sample Number	Water pH	Buffer Value	P Phosphorus		K Potassium		Ca Calcium		Mg Magnesium		Zn Zinc		Cu Copper		Fe Iron		Mn Manganese		Organic Matter %	Soluble Salts PPM**
SOIL 1	5.1	7.4	8	L	46	L	15	S	46	S	0.87	S	0.14	S	25	S	47	S	0.2%	42

RECOMMENDATIONS

Sample Number	Crop	Fertilizer/Lime Application Rate and Timing
SOIL 1	Results Only	
		$N / P_2O_5 / K_2O$
	Nitrogen/Phosphate/Potash:	- / - / -
	Limestone:	Lime is not recommended at this time

Results Only

County: Knox **Lab Number:** 273249

Mehlich 1 SOIL TEST RESULTS and RATINGS*

(Pounds Per Acre)

Sample Number	Water pH	Buffer Value	P Phosphorus		K Potassium		Ca Calcium		Mg Magnesium		Zn Zinc		Cu Copper		Fe Iron		Mn Manganese		Organic Matter %	Soluble Salts PPM**
SOIL 2	6.0	7.6	32	H	52	L	140	S	45	S	2.1	S	0.31	S	25	S	20	S	0.5%	56

RECOMMENDATIONS

Sample Number	Crop	Fertilizer/Lime Application Rate and Timing
SOIL 2	Results Only	
		$N / P_2O_5 / K_2O$
	Nitrogen/Phosphate/Potash:	- / - / -
	Limestone:	Lime is not recommended at this time

Results Only

County: Knox **Lab Number:** 273250

Mehlich 1 SOIL TEST RESULTS and RATINGS*

(Pounds Per Acre)

Sample Number	Water pH	Buffer Value	P Phosphorus		K Potassium		Ca Calcium		Mg Magnesium		Zn Zinc		Cu Copper		Fe Iron		Mn Manganese		Organic Matter %	Soluble Salts PPM**
SOIL 3	6.2		18	L	44	L	310	S	53	S	3.5	S	0.22	S	21	S	110	S	1.8%	84

RECOMMENDATIONS

Sample Number	Crop	Fertilizer/Lime Application Rate and Timing
SOIL 3	Results Only	
		$N / P_2O_5 / K_2O$
	Nitrogen/Phosphate/Potash:	- / - / -
	Limestone:	Lime is not recommended at this time

LEAO - Page 1

*Ratings: Indicates relative availability of nutrients to plants. (See back of this form for detailed explanation.)

**PPM = Parts per Million

If you have questions about these recommendations, contact your County Extension office.

Visit our web site at http://bioengr.ag.utk.edu/soiltestlab for additional information.

Legend: Soil 1 = Clay, Soil 2 = Sandy Loam and Soil 3= Silty Clay Loam

APPENDIX D. Chapter III Figures

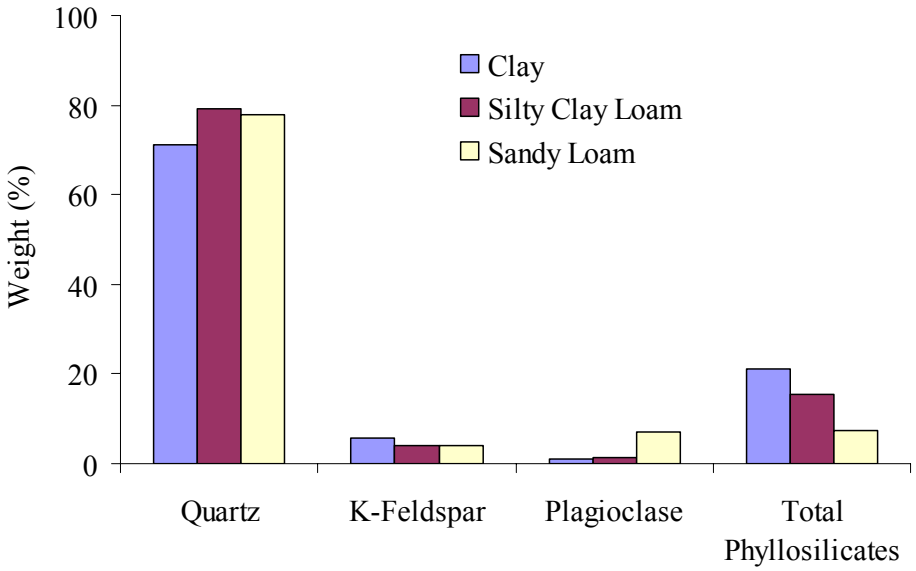

Figure 3.1. Mineralogical composition of bulk soil samples.

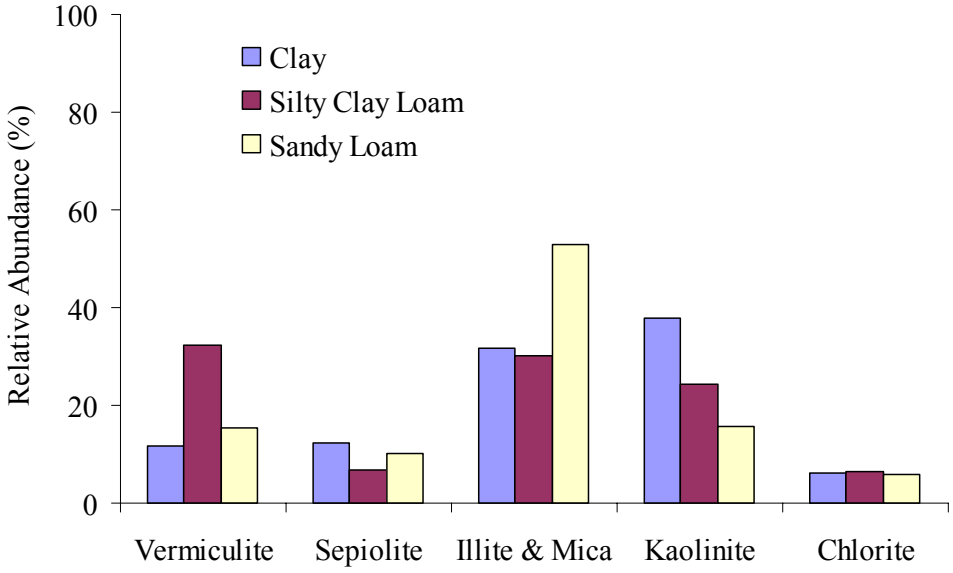

Figure 3.2. Relative abundance of minerals in phyllosilicate fraction of soil samples (Other minor constituents: Clay soil: 0.21% Calcite and 0.92% Hematite; Sandy Loam: 3.76% Amphibole).

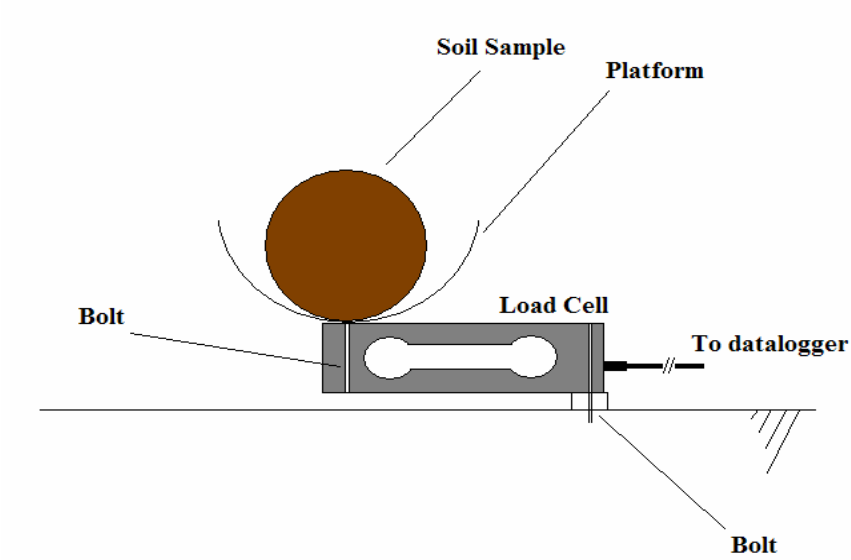

Figure 3.3. Schematic view of the load cell used to calculate mass change in the soil samples.

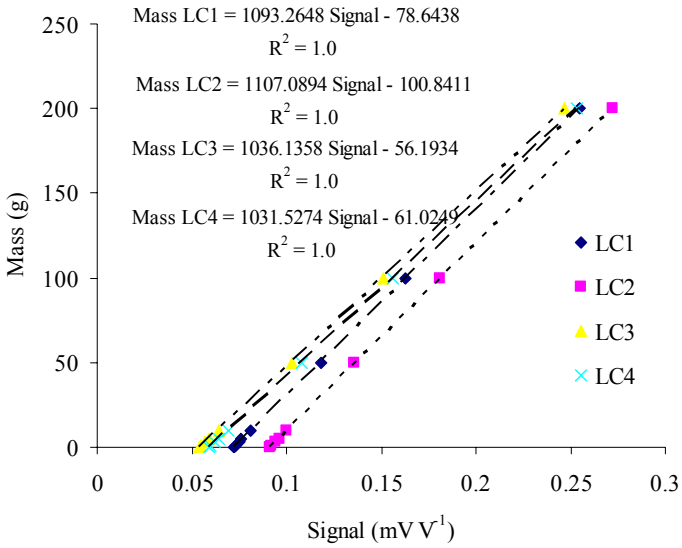

Figure 3.4. Calibration equations (mass versus signal) for the four load cells used in the experiments.

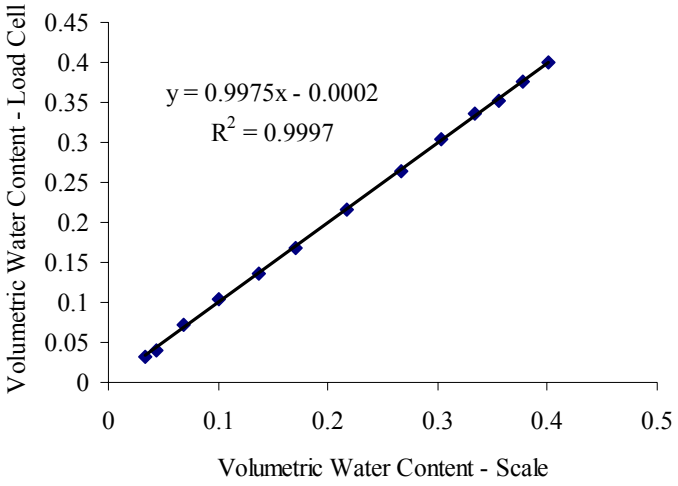

Figure 3.5. Volumetric water content measured using Load Cell 1 versus Scale.

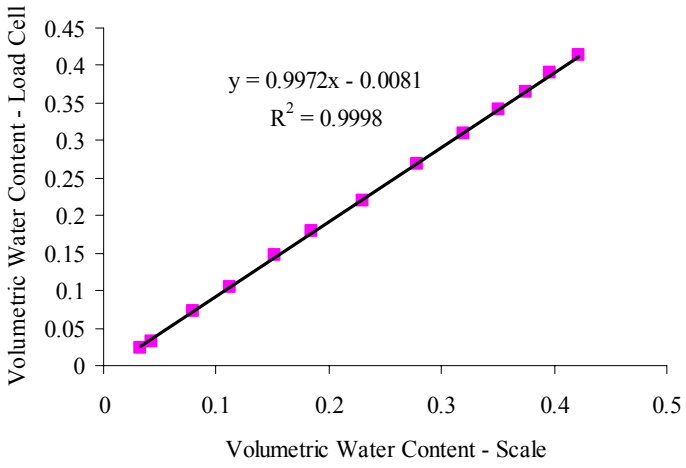

Figure 3.6. Volumetric water content measured using Load Cell 2 versus Scale.

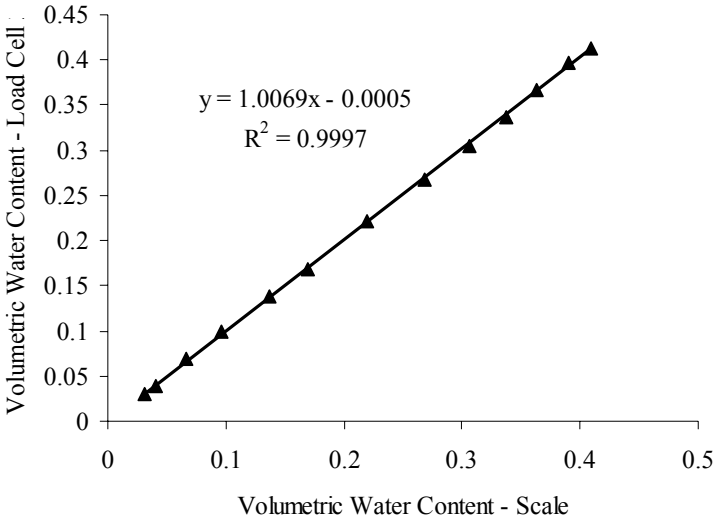

Figure 3.7. Volumetric water content measured using Load Cell 3 versus Scale.

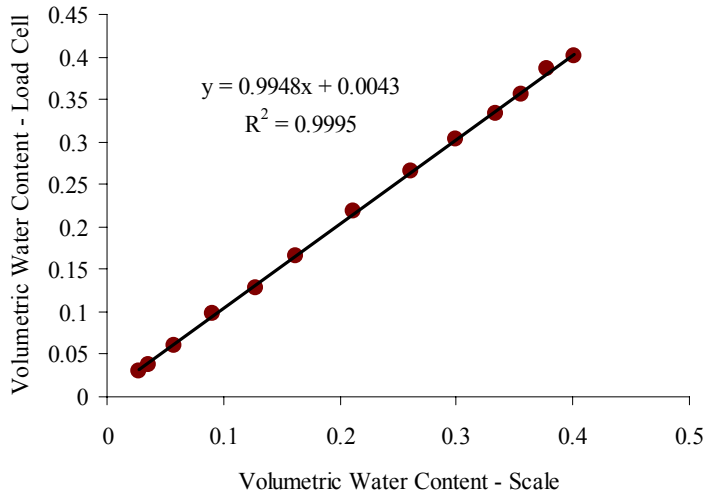

Figure 3.8. Volumetric water content measured using Load Cell 4 versus Scale.

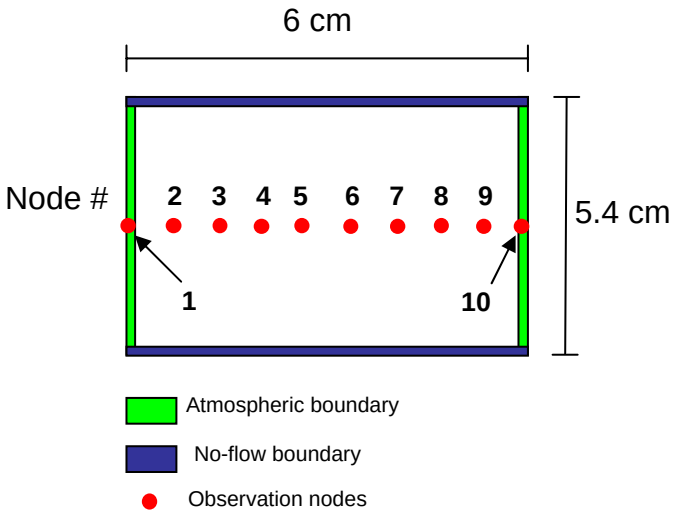

Figure 3.9. Model domain and boundary conditions of the numerical simulation of the air drying experiments.

APPENDIX E. Chapter IV Tables

Table 4.1. Soil physicochemical properties[†].

Soil	Sand	Silt	Clay	Total C	pH in water	Bulk density		Particle density	Hydraulic conductivity*		Specific surface area	Residual water content[‡]
						Undist.	Dist.		Undist.	Dist.		
	%			%		g cm^{-3}		g cm^{-3}	cm s^{-1}		m^2 g^{-1}	g g^{-1}
Clay	20.35	34.06	45.59	0.1347 (0.0105)	5.1	1.45 (0.04)	1.30 (0.02)	2.731 (0.008)	$1.21x10^{-5}$ ($4.27x10^{-5}$)	$3.03x10^{-3}$ ($1.31x10^{-3}$)	34.678 (0.007)	0.13
Silty Clay Loam	13.03	52.59	34.38	0.8660 (0.0188)	6.2	1.46 (0.02)	1.31 (0.01)	2.669 (0.004)	$1.78x10^{-3}$ ($5.85x10^{-3}$)	$1.80x10^{-3}$ ($4.76x10^{-4}$)	16.389 (0.337)	0.09
Sandy Loam	74.41	19.32	6.27	0.2329 (0.0067)	6.0	1.65 (0.02)	1.55 (0.02)	2.685 (0.005)	$4.04x10^{-4}$ ($7.00x10^{-4}$)	$3.81x10^{-3}$ ($4.40x10^{-3}$)	2.176 (0.056)	0.03

[†] Standard deviations of mean estimates are shown in parentheses

* Geometric means

[‡] Gravimetric water content at 1500 kPa

Table 4.2. Inverse modeling parameters used in Hydrus 2D simulation.

Texture	Disturbance	Hcrit*	Evaporation Rate	Model Bulk Density
		|kPa|	cm h^{-1}	g cm^{-3}
Clay	Undist	1500	0.015	1.42
Clay	Dist	1500	0.015	1.2
Sandy Loam	Undist	500	0.02	1.66
Sandy Loam	Dist	500	0.02	**
Silty Clay Loam	Undist	1500	0.012	1.46
Silty Clay Loam	Dist	1500	0.02	1.29

*Maximum water potential at boundary condition
**Simulation performed without parameterizing for bulk density

APPENDIX F. Chapter IV Figures

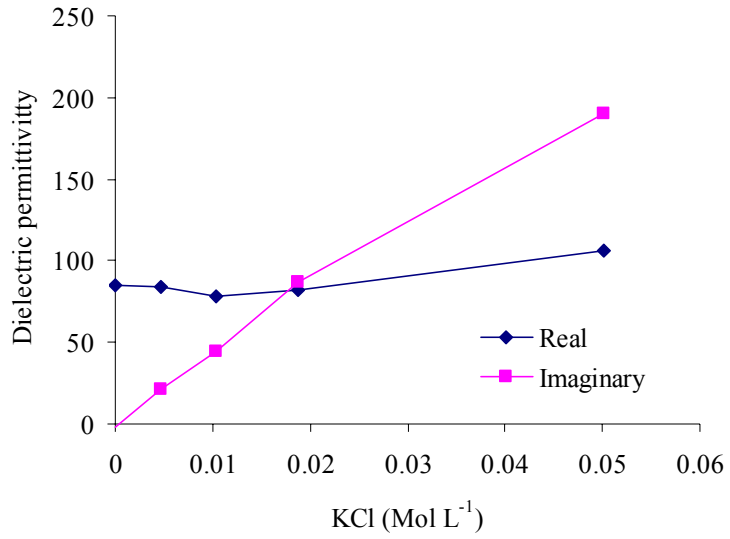

Figure 4.1. Response of the Hydra Probe to increasing KCl concentration in aqueous solution.

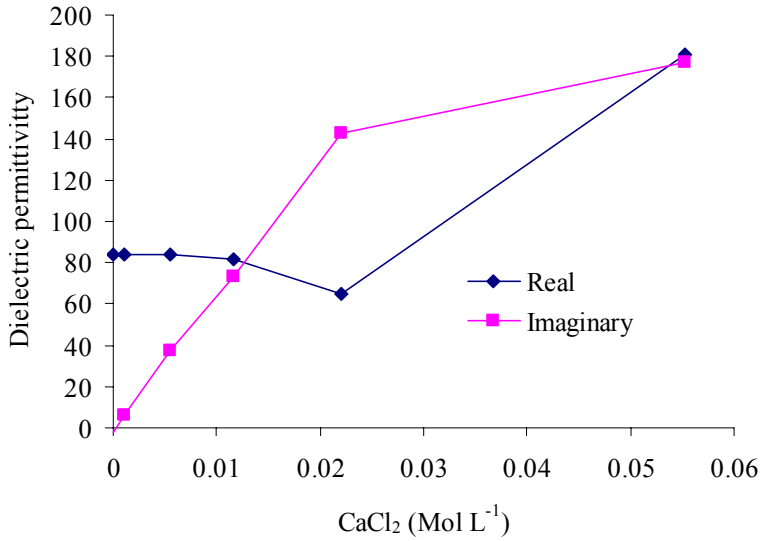

Figure 4.2. Response of the Hydra Probe to increasing $CaCl_2$ concentration in aqueous solution.

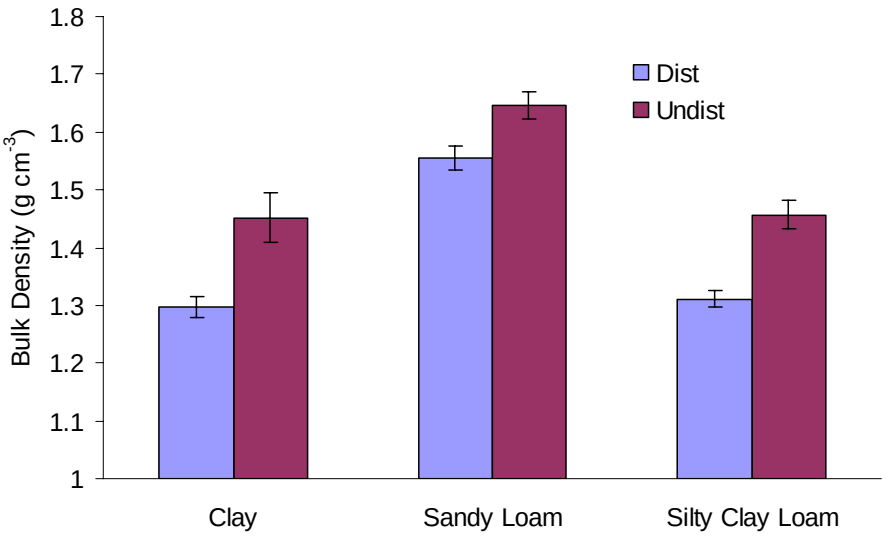

Figure 4.3. Averages of bulk density for each soil texture and disturbance. Error bars represent standard deviation of estimates.

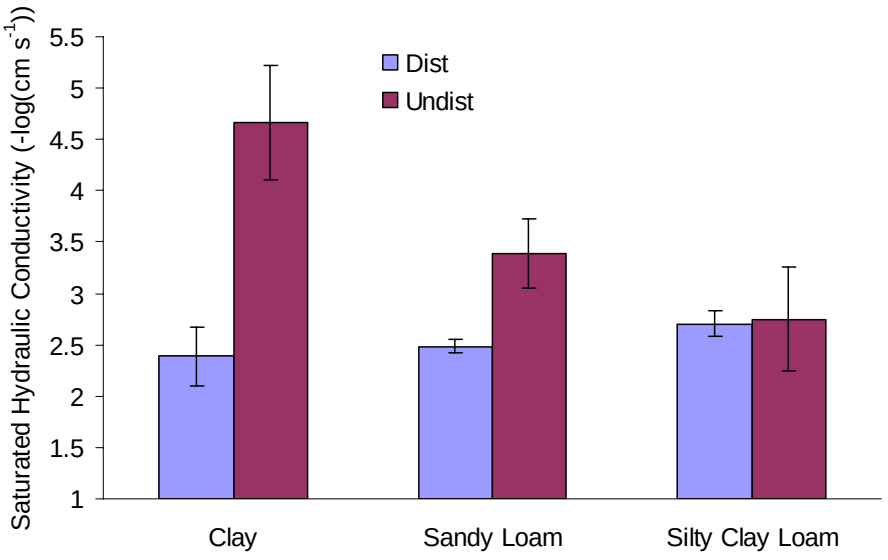

Figure 4.4. Averages of absolute value of the logarithm of saturated hydraulic conductivity for each soil texture and disturbance. Error bars represent standard deviation of estimates.

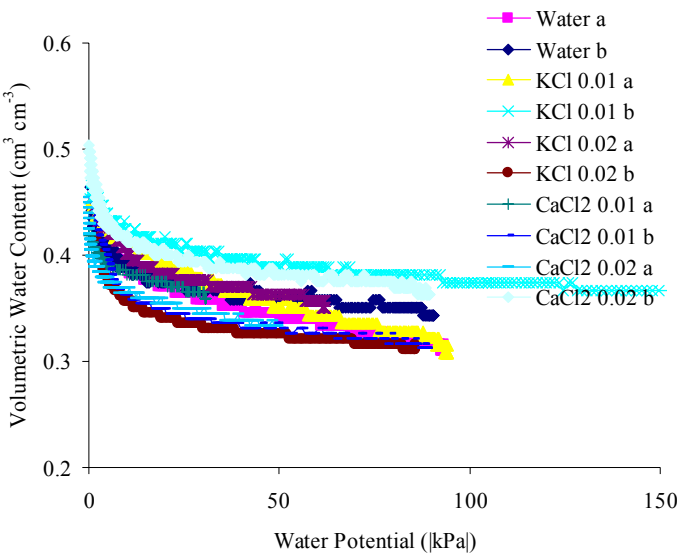

Figure 4.5. Volumetric water content as a function of water potential in undisturbed Clay soil samples (a and b are duplicate samples).

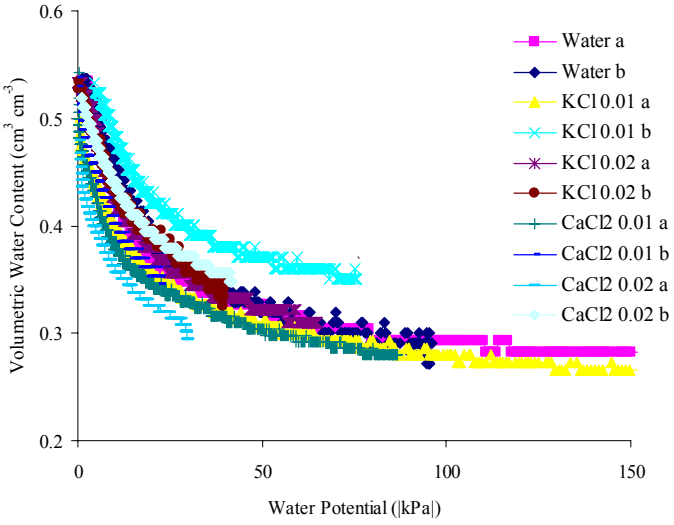

Figure 4.6. Volumetric water content as a function of water potential in disturbed Clay soil samples (a and b are duplicate samples).

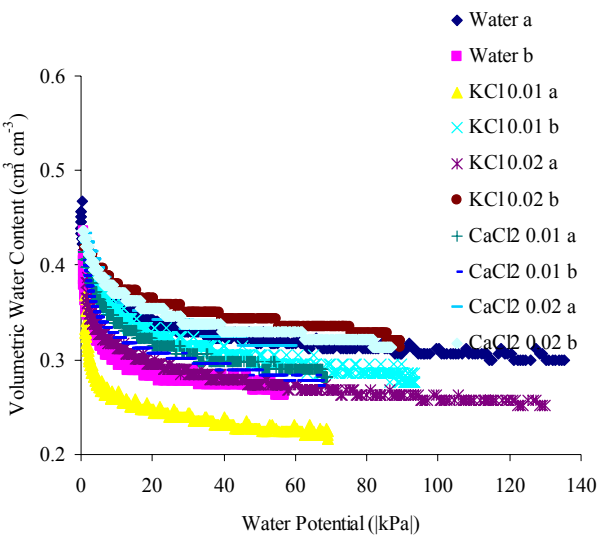

Figure 4.7. Volumetric water content as a function of water potential in undisturbed Silty Clay Loam soil samples (a and b are duplicate samples).

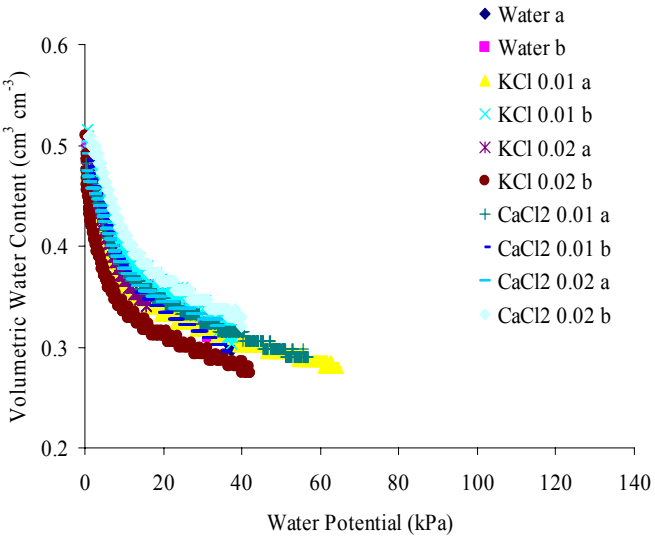

Figure 4.8. Volumetric water content as a function of water potential in disturbed Silty Clay Loam soil samples (a and b are duplicate samples).

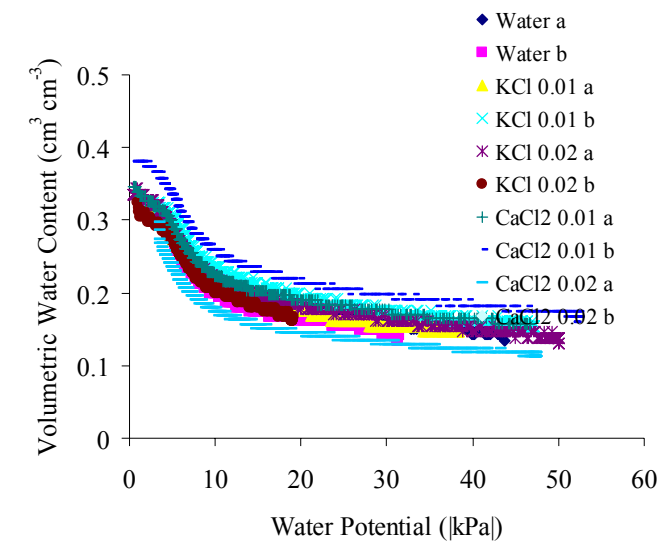

Figure 4.9. Volumetric water content as a function of water potential in undisturbed Sandy Loam soil samples (a and b are duplicate samples).

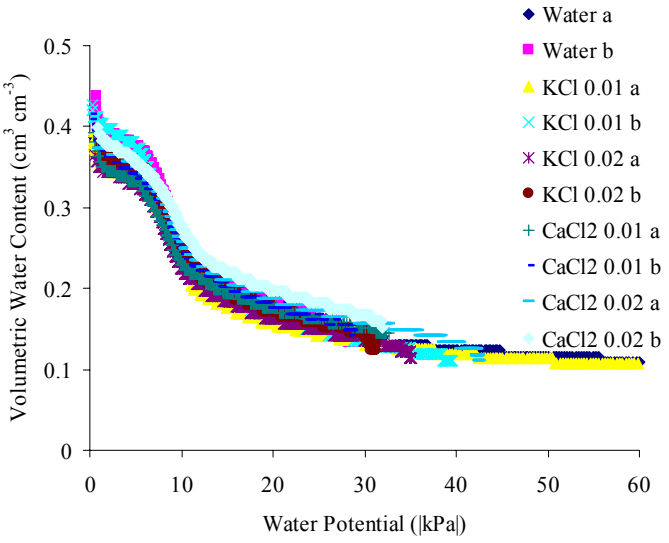

Figure 4.10. Volumetric water content as a function of water potential in disturbed Sandy Loam soil samples (a and b are duplicate samples).

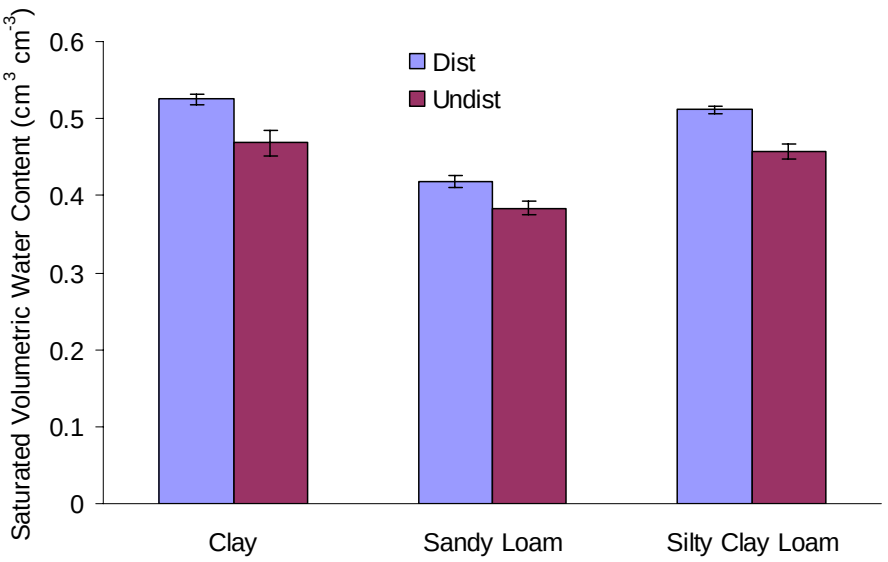

Figure 4.11. Averages of saturated volumetric water content for each soil texture and disturbance. Error bars represent standard deviation of estimates.

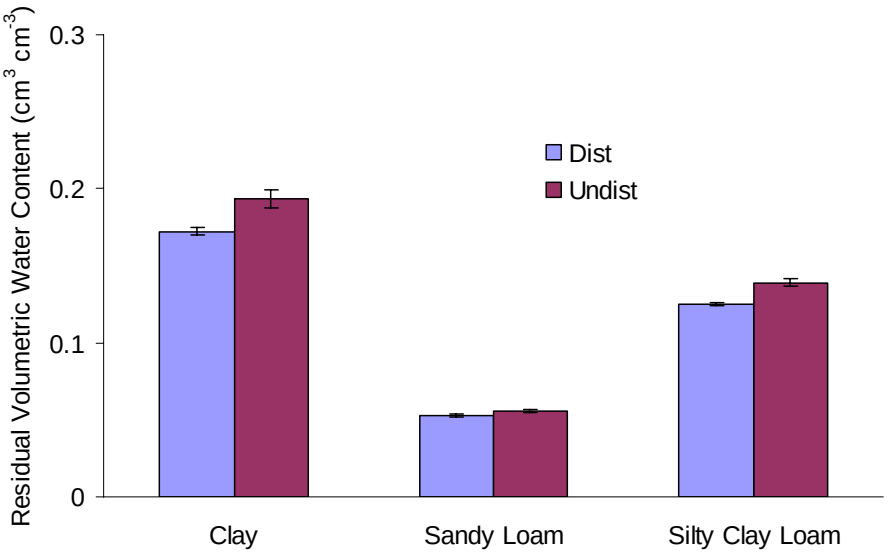

Figure 4.12. Averages of residual volumetric water content for each soil texture and disturbance. Error bars represent standard deviation of estimates.

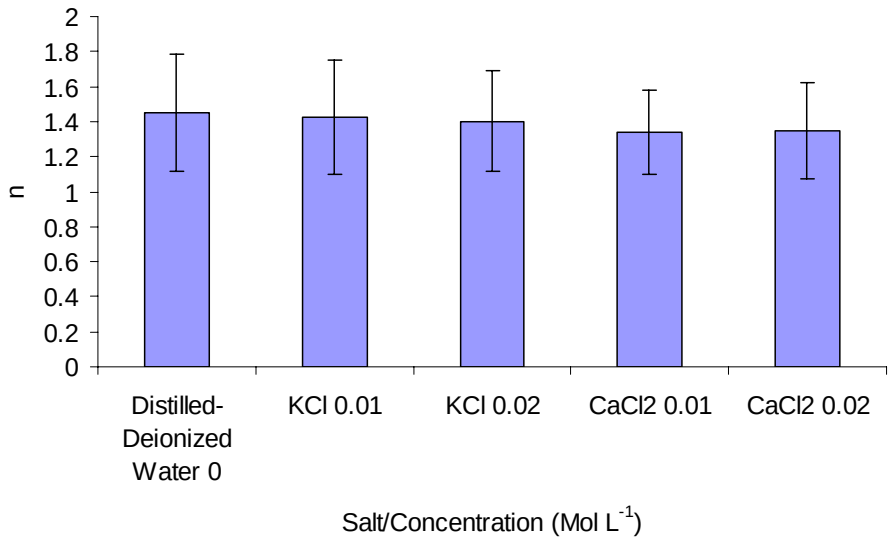

Figure 4.13. Averages of n parameter for each salt treatment. Error bars represent standard deviation of estimates.

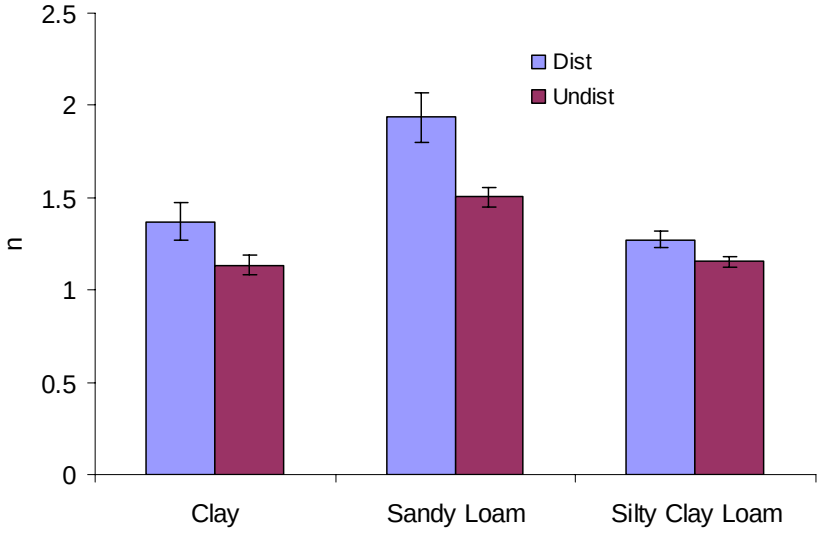

Figure 4.14. Averages of n parameter for each soil texture and disturbance. Error bars represent standard deviation of estimates.

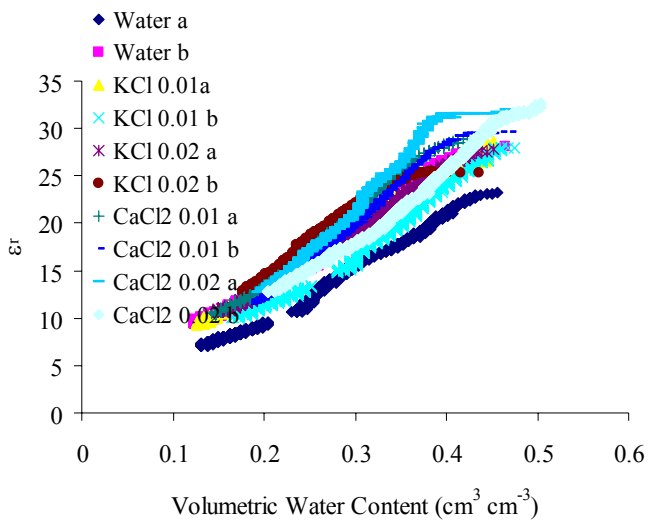

Figure 4.15. Real dielectric permittivity response (ε_r) as a function of volumetric water content in undisturbed Clay soil samples (a and b are duplicate samples).

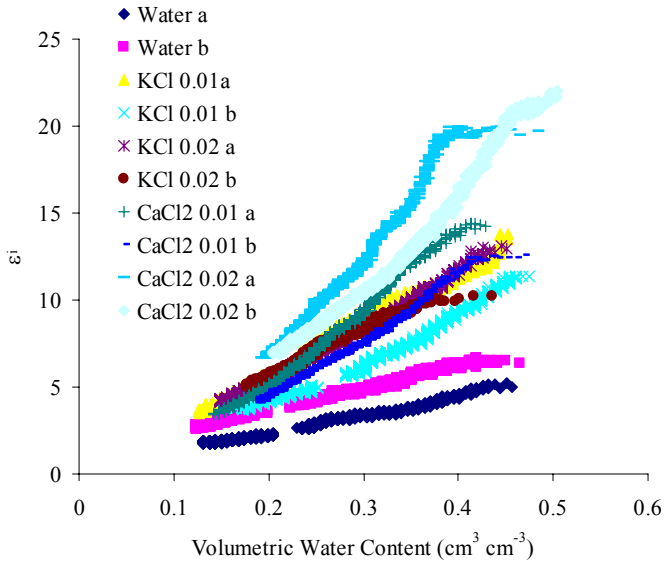

Figure 4.16. Imaginary dielectric permittivity response (ε_i) as a function of volumetric water content in undisturbed Clay soil samples (a and b are duplicate samples).

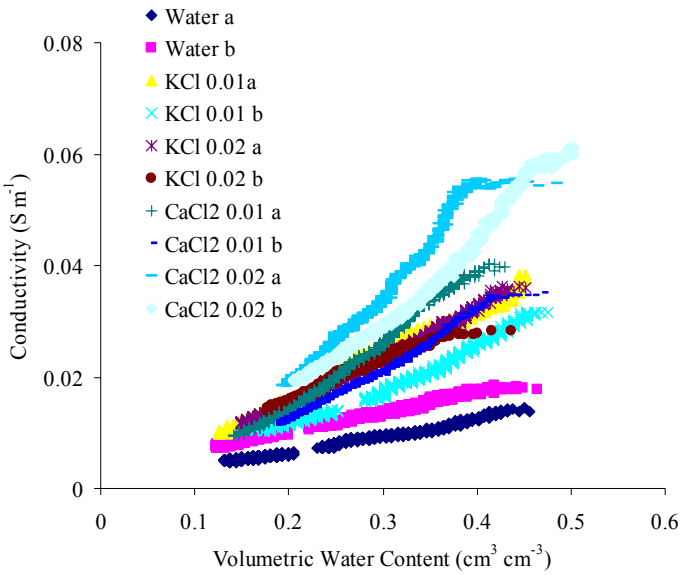

Figure 4.17. Electrical conductivity response as a function of volumetric water content in undisturbed Clay soil samples (a and b are duplicate samples).

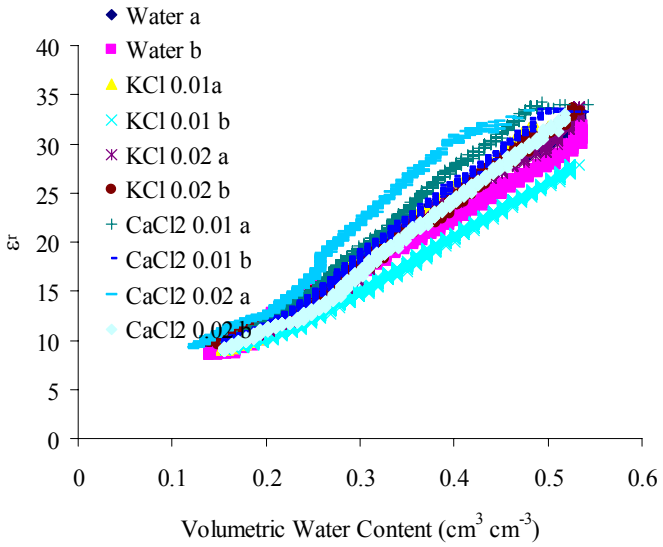

Figure 4.18. Real dielectric permittivity response (ε_r) as a function of volumetric water content in disturbed Clay soil samples (a and b are duplicate samples).

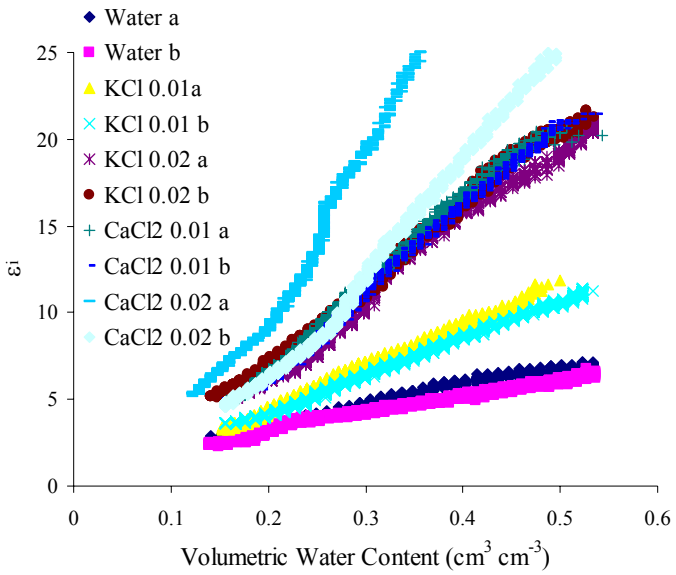

Figure 4.19. Imaginary dielectric permittivity response (ε_i) as a function of volumetric water content in disturbed Clay soil samples (a and b are duplicate samples).

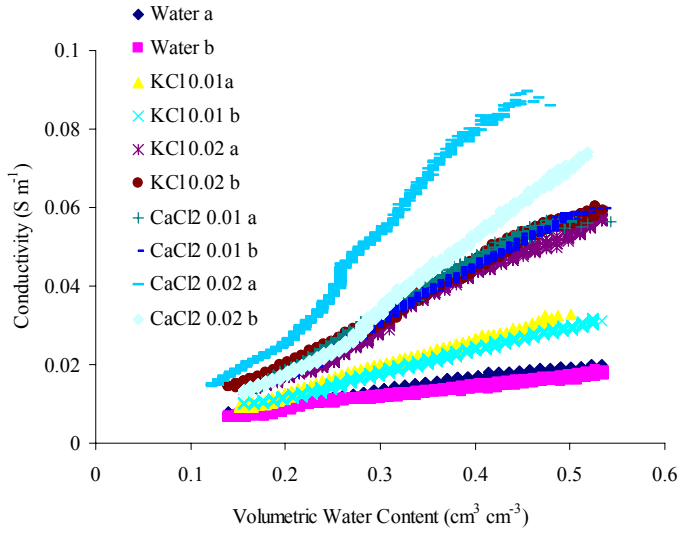

Figure 4.20. Electrical conductivity response as a function of volumetric water content in disturbed Clay soil samples (a and b are duplicate samples).

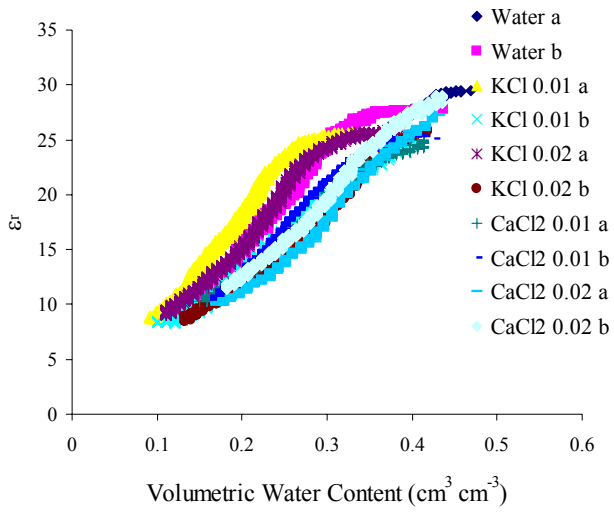

Figure 4.21. Real dielectric permittivity response (ε_r) as a function of volumetric water content in undisturbed Silty Clay Loam soil samples (a and b are duplicate samples).

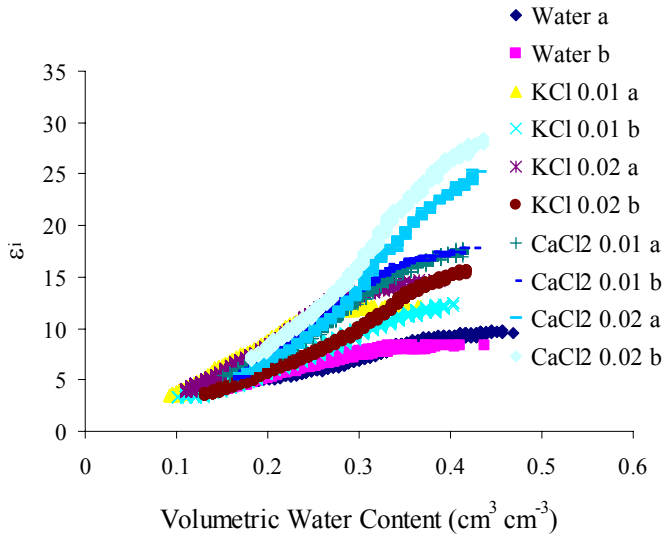

Figure 4.22. Imaginary dielectric permittivity response (ε_i) as a function of volumetric water content in undisturbed Silty Clay Loam soil samples (a and b are duplicate samples).

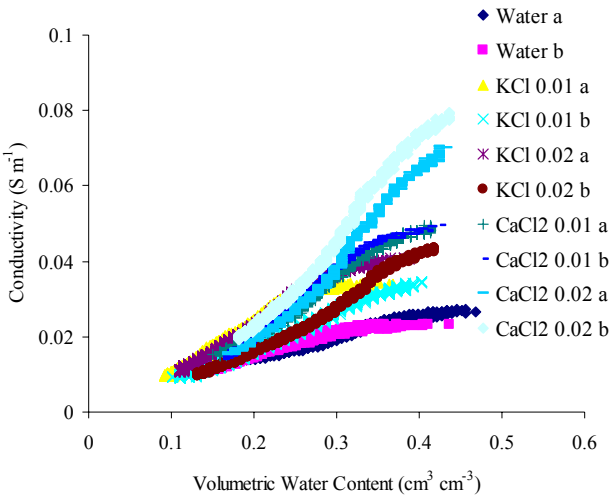

Figure 4.23. Electrical conductivity response as a function of volumetric water content in undisturbed Silty Clay Loam soil samples (a and b are duplicate samples).

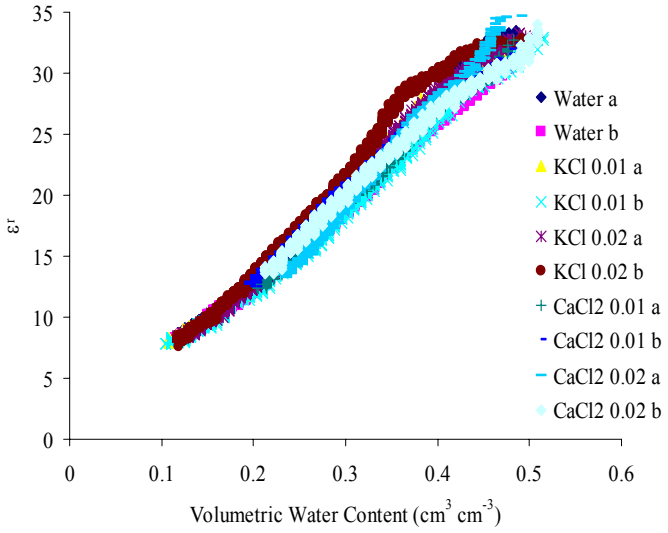

Figure 4.24. Real dielectric permittivity response (ε_r) as a function of volumetric water content in disturbed Silty Clay Loam soil samples (a and b are duplicate samples).

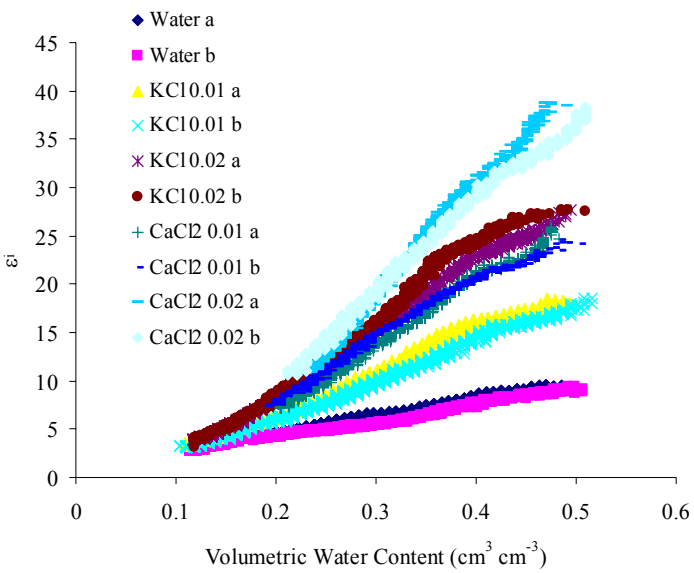

Figure 4.25. Imaginary dielectric permittivity response (ε_i) as a function of volumetric water content in disturbed Silty Clay Loam soil samples (a and b are duplicate samples).

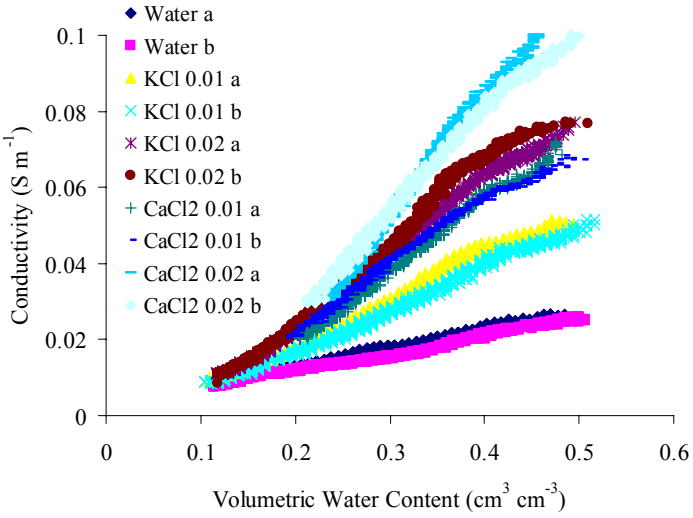

Figure 4.26. Electrical conductivity response as a function of volumetric water content in disturbed Silty Clay Loam soil samples (a and b are duplicate samples).

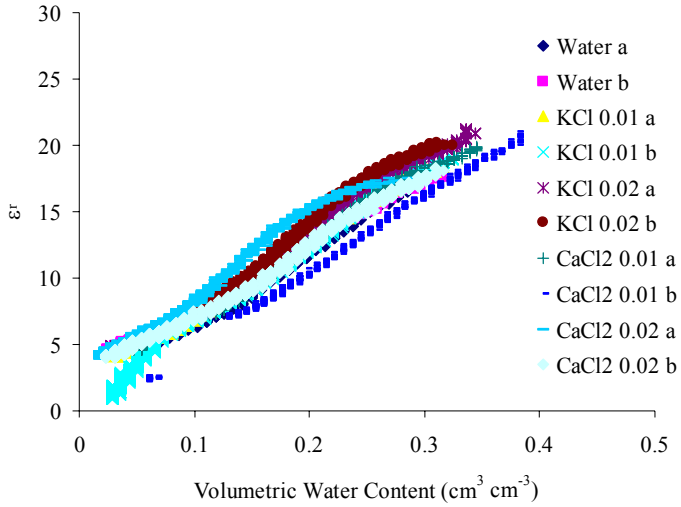

Figure 4.27. Real dielectric permittivity response (ε_r) as a function of volumetric water content in undisturbed Sandy Loam soil samples (a and b are duplicate samples).

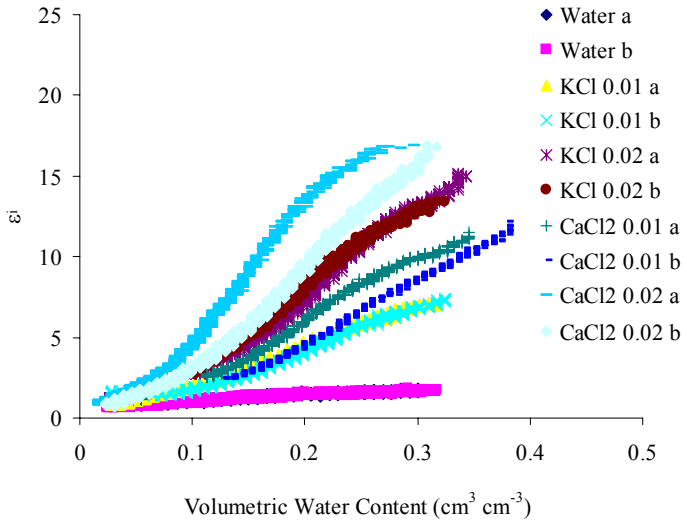

Figure 4.28. Imaginary dielectric permittivity response (ε_i) as a function of volumetric water content in undisturbed Sandy Loam soil samples (a and b are duplicate samples).

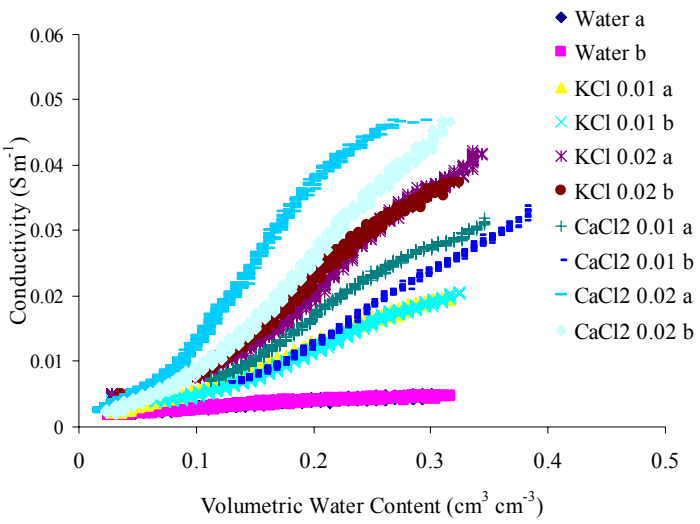

Figure 4.29. Electrical conductivity response as a function of volumetric water content in undisturbed Sandy Loam soil samples (a and b are duplicate samples).

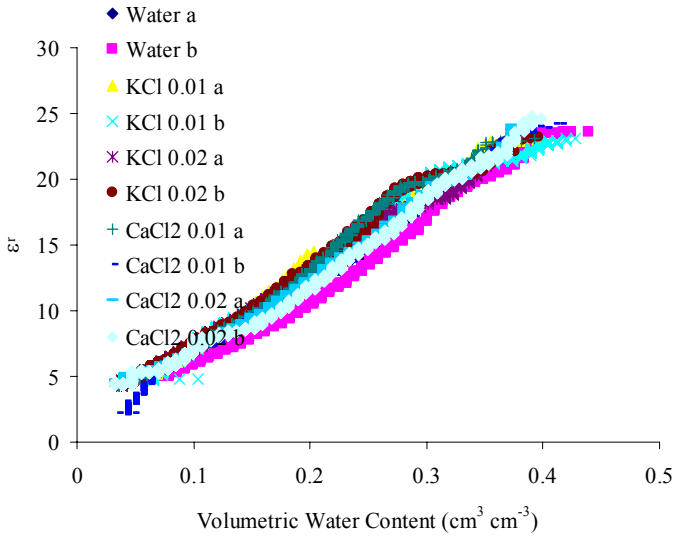

Figure 4.30. Real dielectric permittivity response (ε_r) as a function of volumetric water content in disturbed Sandy Loam soil samples (a and b are duplicate samples).

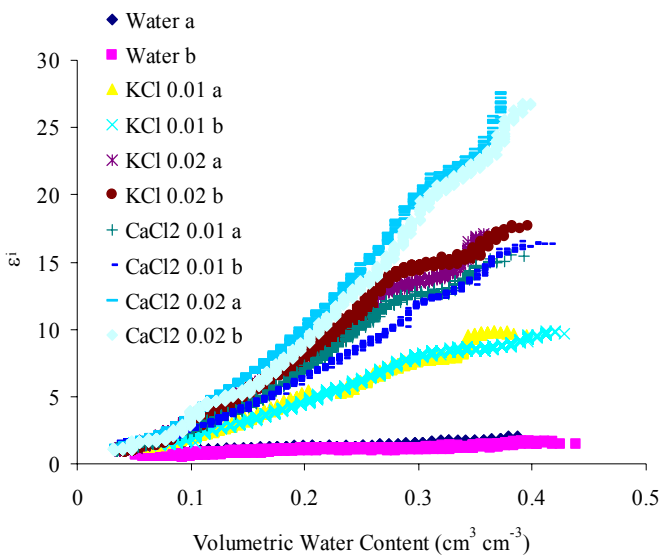

Figure 4.31. Imaginary dielectric permittivity response (ε_i) as a function of volumetric water content in disturbed Sandy Loam soil samples (a and b are duplicate samples).

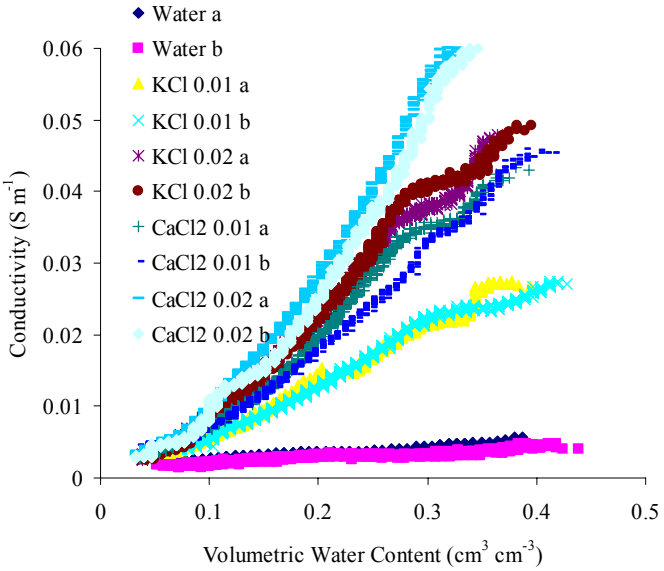

Figure 4.32. Electrical conductivity response as a function of volumetric water content in disturbed Sandy Loam soil samples (a and b are duplicate samples).

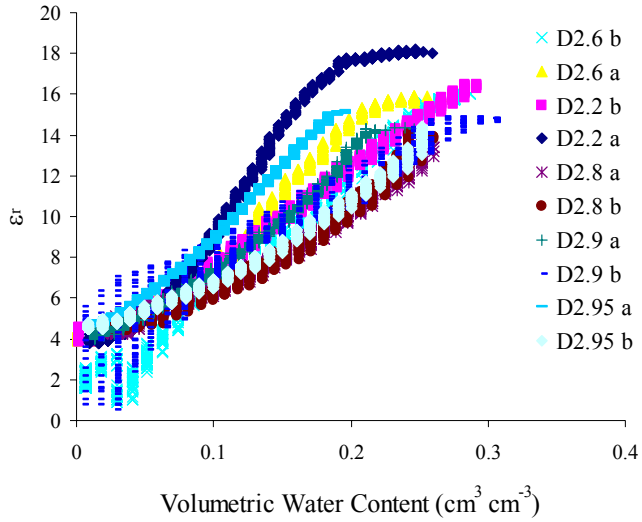

Figure 4.33. Real dielectric permittivity response (ε_r) as a function of volumetric water content in glass beads samples (a and b are duplicate samples).

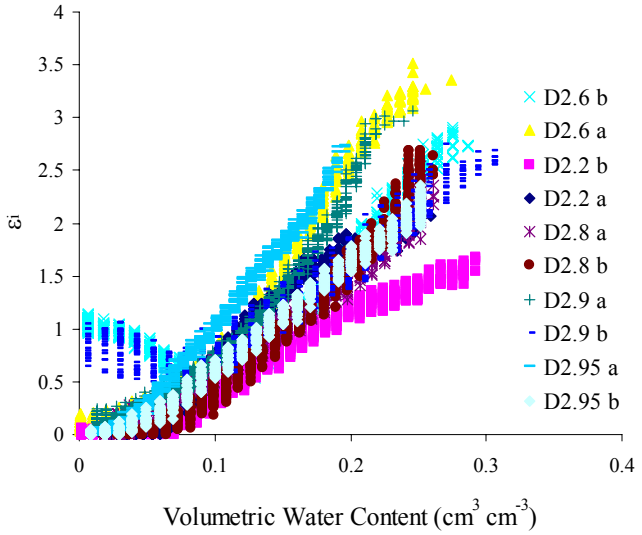

Figure 4.34. Imaginary dielectric permittivity response (ε_i) as a function of volumetric water content in glass beads samples (a and b are duplicate samples).

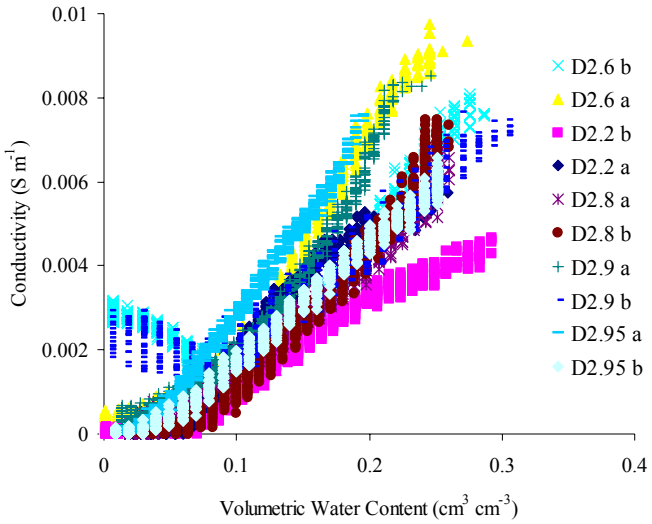

Figure 4.35. Electrical conductivity response as a function of volumetric water content in glass beads samples (a and b are duplicate samples).

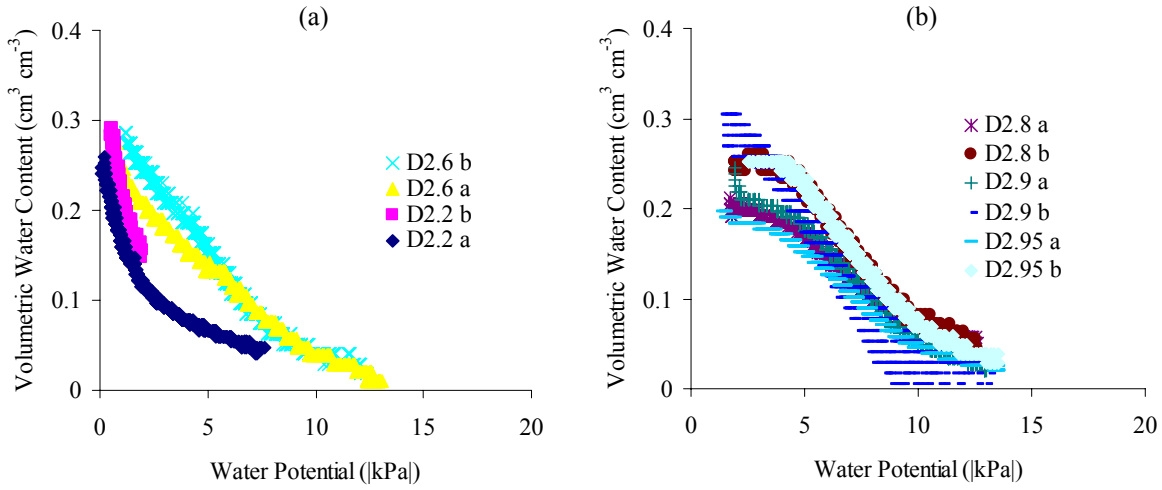

Figure 4.36. Volumetric water content as a function of water potential in glass beads samples. In (a) samples D2.2 and D2.6 and in (b) samples D2.8, D2.9 and D2.95 (a and b in the legend following each sample name indicate replicates).

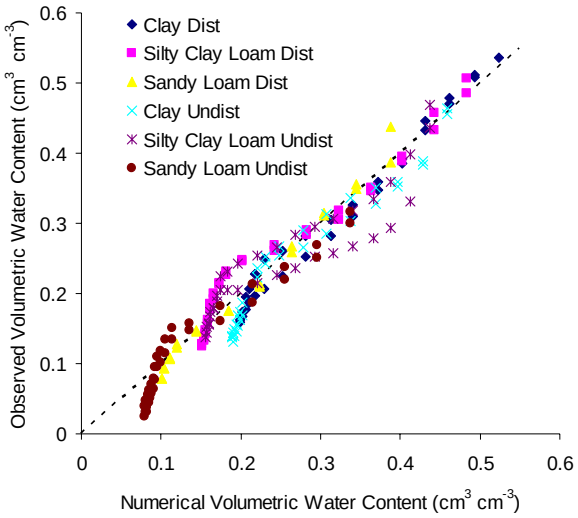

Figure 4.37. Observed versus numerically simulated volumetric water content.

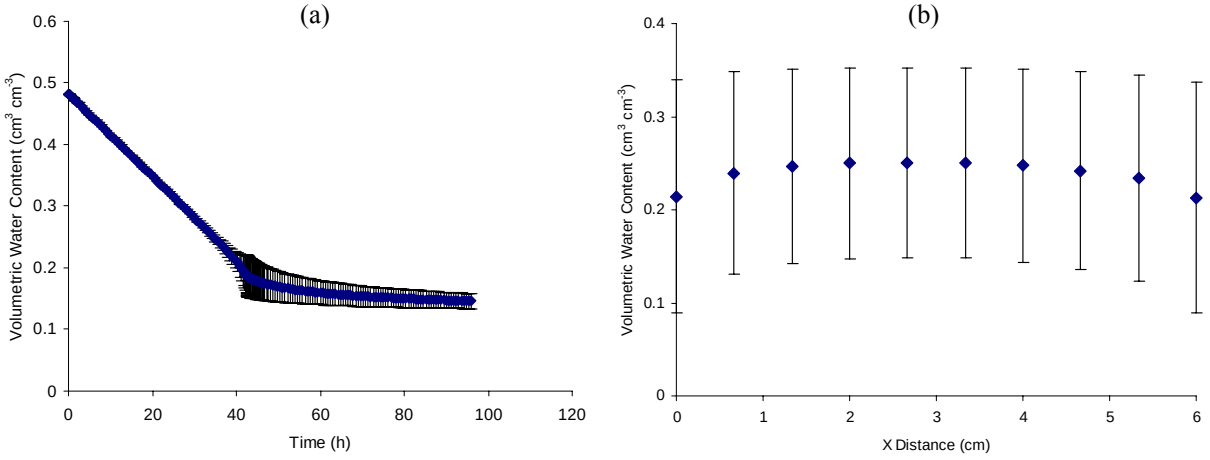

Figure 4.38. Numerical model average and standard deviation of volumetric water contents in time (a) and in space (b) for a Silty Clay Loam disturbed soil simulation.

APPENDIX G. Chapter V Tables

Table 5.1. Soil physicochemical properties[†].

Series	Soil	Sand	Silt	Clay	Total C	pH in water	Bulk density		Particle density	Hydraulic conductivity		Specific surface area
							Undist	Dist		Undist	Dist	
		%			%		g cm^{-3}		g cm^{-3}	cm s^{-1}		m^2 g^{-1}
Etowah	Clay	20.35	34.06	45.59	0.1347 (0.0105)	5.1	1.45 (0.04)	1.30 (0.02)	2.731 (0.008)	$3.00x10^{-5}$ ($4.27x10^{-5}$)	$3.24x10^{-3}$ ($1.31x10^{-3}$)	34.678 (0.007)
Lindside	Silty Clay Loam	13.03	52.59	34.38	0.8660 (0.0188)	6.2	1.46 (0.02)	1.31 (0.01)	2.669 (0.004)	$3.62x10^{-3}$ ($5.85x10^{-3}$)	$1.85x10^{-3}$ ($4.76x10^{-4}$)	16.389 (0.337)
Sequatchie	Sandy Loam	74.41	19.32	6.27	0.2329 (0.0067)	6.0	1.65 (0.02)	1.55 (0.02)	2.685 (0.005)	$5.79x10^{-4}$ ($7.00x10^{-4}$)	$4.71x10^{-3}$ ($4.40x10^{-3}$)	2.176 (0.056)

[†] Standard deviations of mean estimates are shown in parentheses

Table 5.2. Statistical summary of numerical simulation data as compared to observed volumetric water content data.

Soil	Disturbance	Average maximum error	Maximum error	Peak time	$R^{2\dagger}$
		Numerical Simulation			
		$cm^3\ cm^{-3}$		h	
Clay	Dist	0.013	0.027	58	0.98
Clay	Undist	0.017	0.029	44	0.93
Sandy Loam	Dist	0.017	0.030	40	0.98
Sandy Loam	Undist	0.018	0.030	32	0.90
Silty Clay Loam	Dist	0.016	0.032	42	0.95
Silty Clay Loam	Undist	0.017	0.032	65	0.85

† Calculated from predicted (mass balance) versus observed data

Table 5.3. Coefficients of the model $\theta_v = \beta_0 + \beta_1\sqrt{\varepsilon_r}$ fitted to data from Sandy Loam, Silty Clay Loam and Clay soils†.

Soil	N	β_0	β_1
Sandy Loam	20	-0.2102a	0.1169b
Silty Clay Loam	20	-0.2112a	0.1139b
Clay	20	-0.2369b	0.1261a

† Values in the same column followed by the same letter are not significantly different at $p = 0.05$

Table 5.4. Coefficients of the model $\theta_v = \beta_0 + \beta_1\sqrt{\varepsilon_r}$ fitted to data from disturbed and undisturbed soil samples†.

Disturbance	N	β_0	β_1
Undist	30	-0.2092a	0.1148b
Dist	30	-0.2297b	0.1232a

† Values in the same column followed by the same letter are not significantly different at $p = 0.05$

Table 5.5. Coefficients of the model $\theta_v = \beta_0 + \beta_1\sqrt{\varepsilon_r}$ hierarchically fitted to data for different soils and disturbances.

Soil	Disturbance	N	β_0	β_1	R^2	ARMSE
Clay	Dist	12086	-0.2381	0.1288	0.94	0.0251
	Undist	12752	-0.1994	0.1136	0.89	0.0257
Loam	Dist	21507	-0.2098	0.1161	0.98	0.0134
	Undist	23126	-0.1934	0.1086	0.93	0.0248

Table 5.6. Root mean square errors between observed data and selected models.

Model	Clay		Loam	
	Dist	Undist	Dist	Undist
	RMSE ($cm^3\ cm^{-3}$)			
This Study (Eq.[5.5])	0.0251	0.0257	0.0134	0.0248
Seyfried	0.0345	0.0263	0.0163	0.0307
Man Sand	0.0336	0.0264	0.0139	0.0267
Topp	0.0305	0.0422	0.0353	0.0496

Table 5.7. Root mean square errors between glass beads observed data and selected models.

This Study (Eq.[5.5])[†]	Topp	Seyfried	Sand
RMSE ($cm^3\ cm^{-3}$)			
0.0110	0.0363	0.0208	0.0129

[†] Loam disturbed coefficients

APPENDIX H. Chapter V Figures

(a)

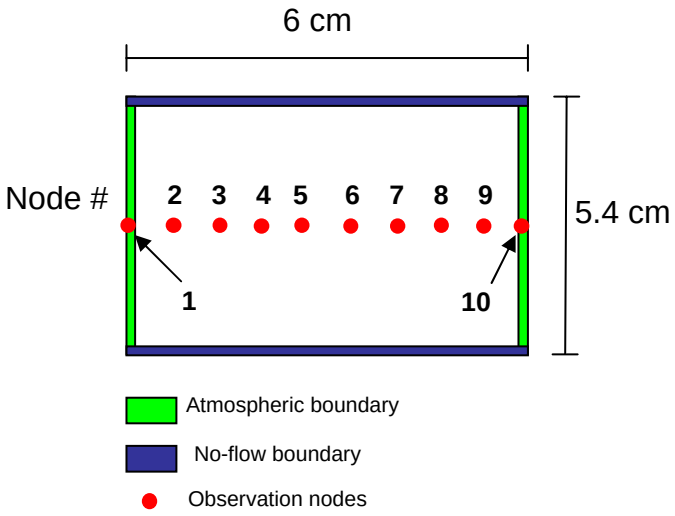

(b)

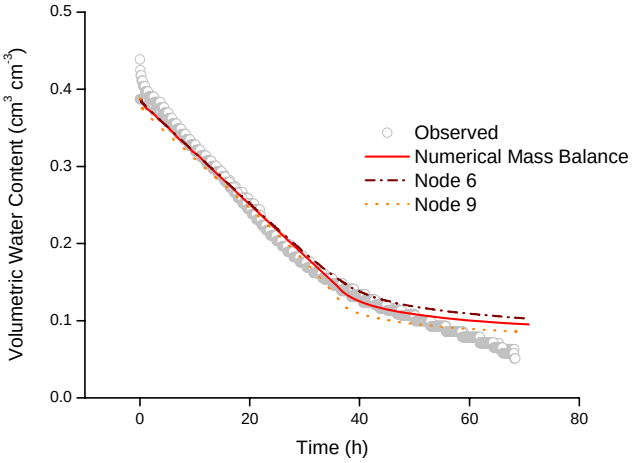

Figure 5.1. Model domain and boundary conditions of the numerical simulation of the drying experiments (a) and drying experiment results showing observed Sandy Loam disturbed data, numerical mass balance and maximum difference; i.e. outer (Node 9) and inner (Node 6) nodes over time (b).

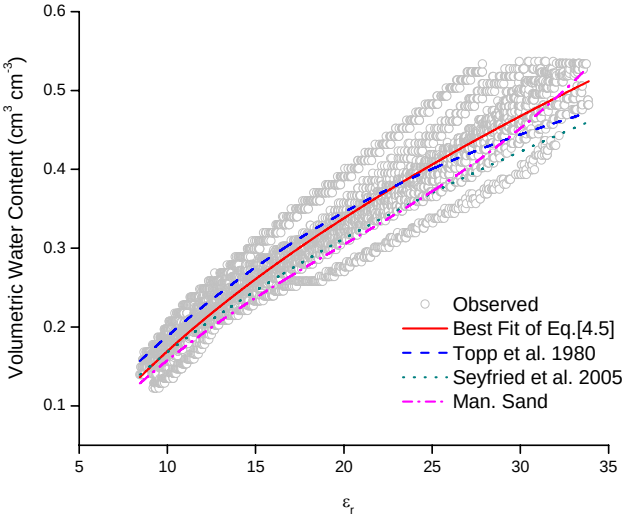

Figure 5.2. Disturbed Clay best fit regression line to $\theta_v = \beta_0 + \beta_1\sqrt{\varepsilon_r}$ and selected models for comparison.

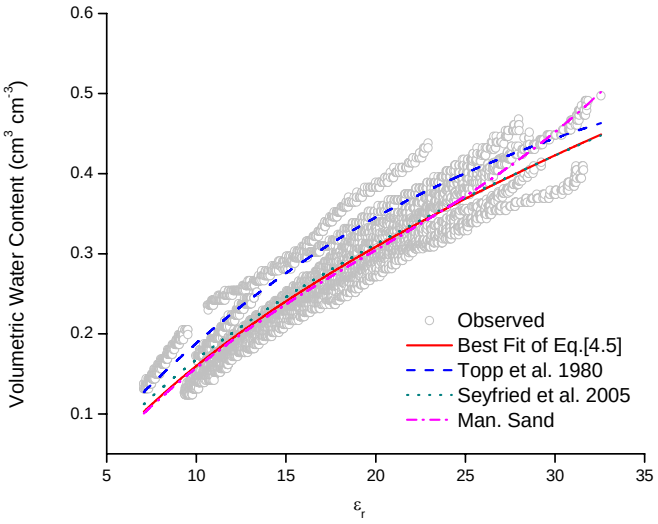

Figure 5.3. Undisturbed Clay best fit regression line to $\theta_v = \beta_0 + \beta_1\sqrt{\varepsilon_r}$ and selected models for comparison.

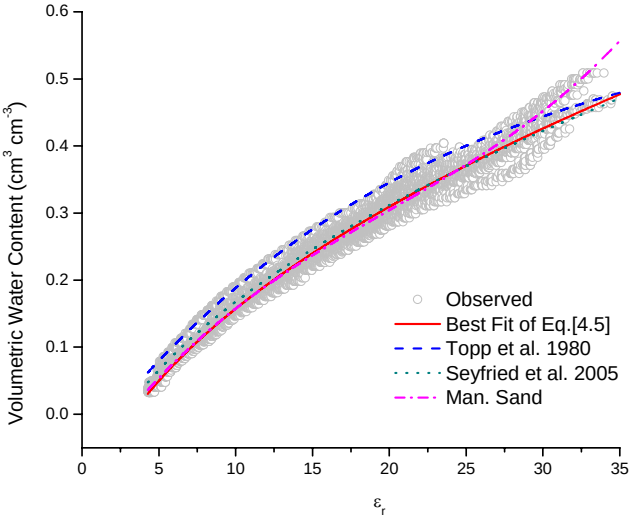

Figure 5.4 Disturbed Sandy Loam and Silty Clay Loam combined (Loam) best fit regression line to $\theta_v = \beta_0 + \beta_1\sqrt{\varepsilon_r}$ and selected models for comparison.

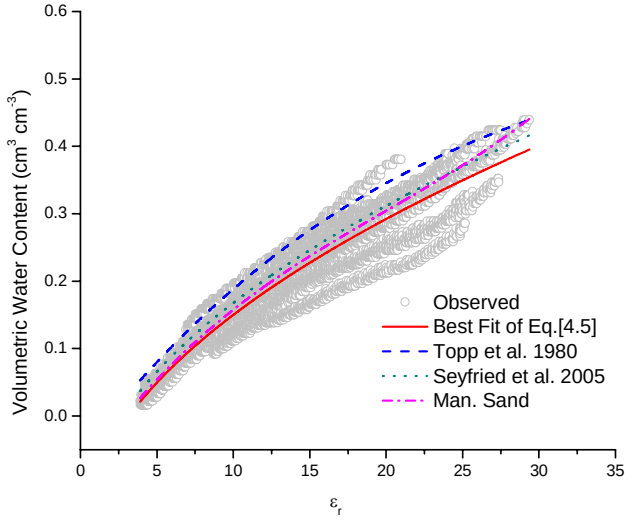

Figure 5.5 Undisturbed Sandy Loam and Silty Clay Loam combined (Loam) best fit regression line to $\theta_v = \beta_0 + \beta_1\sqrt{\varepsilon_r}$ and selected models for comparison.

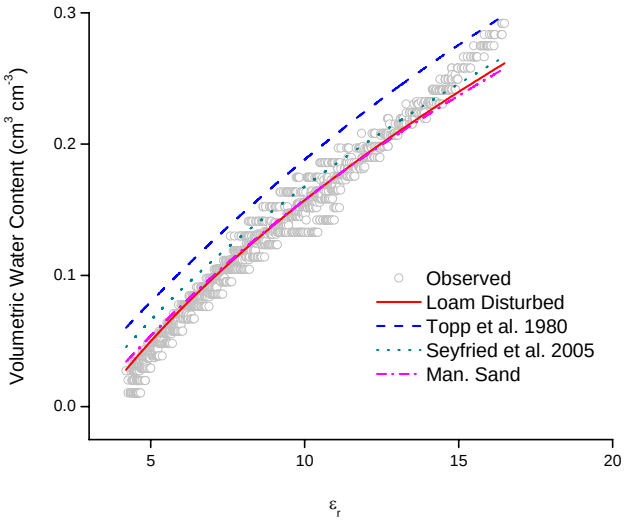

Figure 5.6. Glass beads observed data and predicted data using selected equations for estimating θ_v from ε_r.

APPENDIX I. Chapter VI Tables

Table 6.1. Soil physicochemical properties[†].

Series	Soil	Sand	Silt	Clay	Total C	pH in water	Bulk density		Particle density	Hydraulic conductivity		Specific surface area
							Undist.	Dist.		Undist.	Dist.	
		%			%		g cm^{-3}		g cm^{-3}	cm s^{-1}		m^2 g^{-1}
Etowah	Clay	20.35	34.06	45.59	0.1347 (0.0105)	5.1	1.45 (0.04)	1.30 (0.02)	2.731 (0.008)	$3.00x10^{-5}$ ($4.27x10^{-5}$)	$3.24x10^{-3}$ ($1.31x10^{-3}$)	34.678 (0.007)
Lindside	Silty Clay Loam	13.03	52.59	34.38	0.8660 (0.0188)	6.2	1.46 (0.02)	1.31 (0.01)	2.669 (0.004)	$3.62x10^{-3}$ ($5.85x10^{-3}$)	$1.85x10^{-3}$ ($4.76x10^{-4}$)	16.389 (0.337)
Sequatchie	Sandy Loam	74.41	19.32	6.27	0.2329 (0.0067)	6.0	1.65 (0.02)	1.55 (0.02)	2.685 (0.005)	$5.79x10^{-4}$ ($7.00x10^{-4}$)	$4.71x10^{-3}$ ($4.40x10^{-3}$)	2.176 (0.056)

[†] Standard deviations of mean estimates are shown in parentheses

Table 6.2. Mean soil pore solution conductivity values predicted using Eqs.[6.11], [6.16], [6.17] and [6.18].

Soil	Dist	σ_w	average predicted σ_w							
			Eq.[6.11]		Eq.[6.16]		Eq.[6.16]*		Eq.[6.17]	Eq.[6.18]
			Soil/Dist‡	Gen†	Soil/Dist	Gen	Soil/Dist	Gen		
		dS m^{-1}	dS m^{-1}							
Clay	D	3.96	3.28	3.25	3.28	3.26	3.80	3.55	3.62	2.30
		2.41	2.69	2.68	2.69	2.69	3.04	2.86	2.85	1.90
		2.02	2.55	2.54	2.55	2.55	2.89	2.72	2.65	1.71
		1.23	1.76	1.74	1.76	1.75	2.10	1.94	1.38	1.22
		5.45x10^{-7}	1.12	1.09	1.11	1.10	1.34	1.23	0.39	0.87
	U	3.96	3.50	2.45	3.50	2.45	3.76	2.49	2.58	1.71
		2.41	2.41	1.77	2.42	1.78	3.00	1.91	1.50	1.29
		2.02	2.29	1.68	2.31	1.69	2.84	1.81	1.35	1.17
		1.23	2.34	1.77	2.38	1.78	3.13	1.96	1.41	1.24
		5.45x10^{-7}	1.31	1.09	1.36	1.09	2.21	1.32	-0.25	0.93
Sandy Loam	D	3.96	3.53	4.16	3.54	4.18	3.60	4.96	3.22	2.84
		2.41	2.65	3.13	2.66	3.14	2.70	3.72	2.00	2.13
		2.02	2.29	2.69	2.29	2.70	2.34	3.22	1.40	1.74
		1.23	1.52	1.80	1.53	1.80	1.56	2.14	0.39	1.16
		5.45x10^{-7}	0.49	0.56	0.49	0.56	0.52	0.77	-3.65	0.40
	U	3.96	3.65	3.81	3.64	3.83	3.64	4.68	2.78	2.60
		2.41	2.62	2.77	2.61	2.78	2.62	3.34	1.53	1.89
		2.02	2.33	2.43	2.32	2.44	2.34	3.02	1.01	1.58
		1.23	1.75	1.79	1.74	1.80	1.77	2.31	-0.08	1.18
		5.45x10^{-7}	0.73	0.73	0.72	0.73	0.74	0.99	-1.78	0.52
Silty Clay Loam	D	3.96	3.48	4.18	3.48	4.19	3.48	4.16	5.23	2.82
		2.41	2.42	3.02	2.44	3.04	2.70	3.39	3.33	2.13
		2.02	2.47	2.97	2.47	2.98	2.50	3.02	3.45	1.92
		1.23	1.84	2.33	1.86	2.34	2.12	2.69	2.14	1.58
		5.45x10^{-7}	1.24	1.56	1.25	1.57	1.43	1.82	0.96	1.16
	U	3.96	3.32	3.40	3.33	3.41	3.40	3.59	4.02	2.33
		2.41	2.65	2.72	2.66	2.73	2.74	2.91	2.96	1.88
		2.02	2.27	2.37	2.29	2.37	2.47	2.67	2.26	1.58
		1.23	2.06	2.16	2.08	2.16	2.27	2.48	1.89	1.46
		5.45x10^{-7}	1.61	1.66	1.62	1.67	1.70	1.82	1.34	1.20

* With A and B from calibration equations
‡ Models fit on a soil and disturbance basis
† Model fit on a general basis (all data)

Table 6.3. Standard deviation of soil pore solution conductivity values predicted using Eqs.[6.11], [6.16], [6.17] and [6.18].

Soil	Dist	σ_w	Standard deviation							
			Eq.[6.11]		Eq.[6.16]		Eq.[6.16]*		Eq.[6.17]	Eq.[6.18]
			Soil/Dist‡	Gen†	Soil/Dist	Gen	Soil/Dist	Gen		
		dS m^{-1}	dS m^{-1}							
Clay	D	3.96	0.27	0.32	0.27	0.31	0.51	0.33	0.53	0.17
		2.41	0.14	0.13	0.14	0.14	0.59	0.40	0.17	0.13
		2.02	0.12	0.11	0.12	0.11	0.55	0.37	0.16	0.11
		1.23	0.23	0.19	0.23	0.19	0.55	0.41	0.23	0.18
		$5.45x10^{-7}$	0.26	0.22	0.25	0.22	0.51	0.40	0.34	0.22
	U	3.96	0.16	0.08	0.16	0.08	0.47	0.19	0.13	0.06
		2.41	0.17	0.13	0.15	0.13	0.57	0.26	0.19	0.12
		2.02	0.26	0.11	0.24	0.11	0.42	0.17	0.34	0.07
		1.23	0.25	0.16	0.22	0.16	0.76	0.34	0.30	0.15
		$5.45x10^{-7}$	0.19	0.17	0.17	0.18	0.80	0.38	1.20	0.22
Sandy Loam	D	3.96	0.16	0.35	0.16	0.35	0.14	0.51	0.45	0.16
		2.41	0.10	0.14	0.10	0.14	0.17	0.51	0.53	0.07
		2.02	0.08	0.10	0.09	0.10	0.17	0.51	0.77	0.06
		1.23	0.14	0.08	0.14	0.08	0.20	0.47	0.86	0.09
		$5.45x10^{-7}$	0.22	0.22	0.23	0.22	0.26	0.46	26.75§	0.18
	U	3.96	0.14	0.28	0.14	0.28	0.15	0.37	0.49	0.12
		2.41	0.13	0.13	0.13	0.13	0.18	0.41	0.57	0.07
		2.02	0.17	0.06	0.17	0.06	0.24	0.48	0.71	0.07
		1.23	0.19	0.08	0.19	0.08	0.25	0.46	1.17	0.10
		$5.45x10^{-7}$	0.25	0.20	0.25	0.20	0.29	0.44	2.18	0.17
Silty Clay Loam	D	3.96	0.17	0.20	0.18	0.20	0.12	0.15	0.32	0.13
		2.41	0.24	0.16	0.22	0.15	0.13	0.35	0.51	0.06
		2.02	0.08	0.08	0.08	0.08	0.07	0.17	0.20	0.04
		1.23	0.10	0.11	0.08	0.12	0.29	0.52	0.44	0.14
		$5.45x10^{-7}$	0.21	0.33	0.22	0.34	0.43	0.64	0.27	0.30
	U	3.96	0.25	0.23	0.25	0.22	0.10	0.11	0.44	0.13
		2.41	0.11	0.10	0.10	0.09	0.13	0.22	0.27	0.06
		2.02	0.11	0.07	0.08	0.08	0.21	0.34	0.39	0.08
		1.23	0.10	0.14	0.11	0.14	0.31	0.44	0.29	0.14
		$5.45x10^{-7}$	0.26	0.29	0.27	0.29	0.39	0.49	0.14	0.23

* With A and B from calibration equations
‡ Models fit on a soil and disturbance basis
† Model fit on a general basis (all data)
§ Extreme value associated with discontinuity in the model

APPENDIX J. Chapter VI Figures

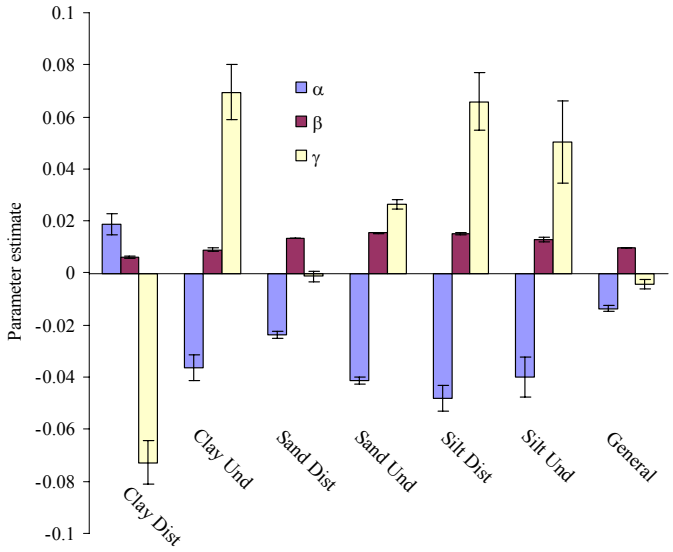

Figure 6.1. Values of the parameters α, β and γ obtained by fitting Eq.[6.9] by nonlinear least squares. Error bars represent the standard error of the estimates.

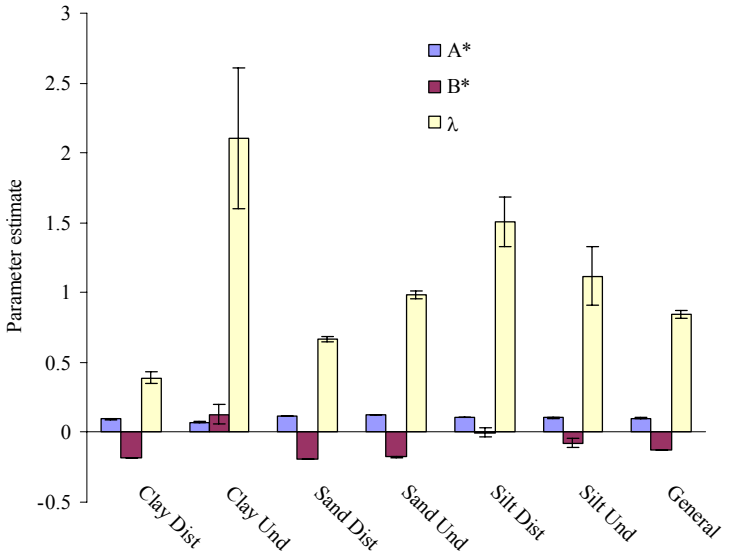

Figure 6.2. Values of the parameters A, B and λ obtained by fitting Eq.[6.14] by nonlinear least squares. The asterisk (*) indicates the A and B parameters were estimated by nonlinear regression. Error bars represent the standard error of the estimates.

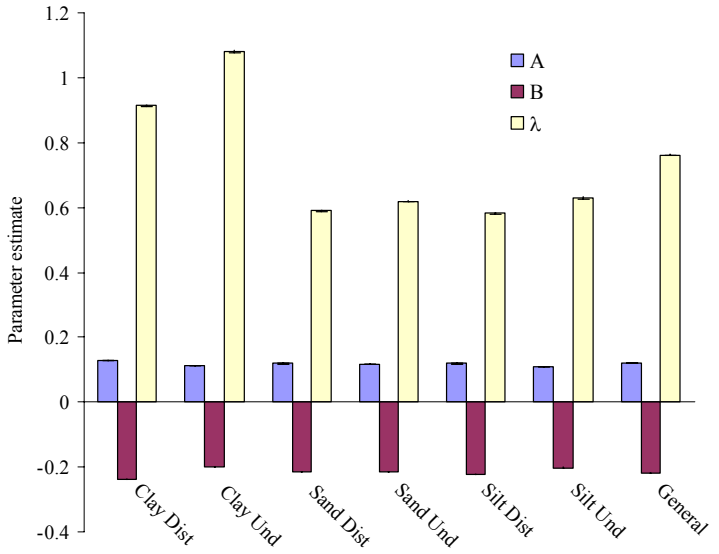

Figure 6.3. Values of the parameter λ obtained by fitting Eq.[6.14] by nonlinear least squares. The parameters A and B were previously fitted to Eq.[6.6] by using linear least squares and are also presented. Error bars represent the standard error of the estimates.

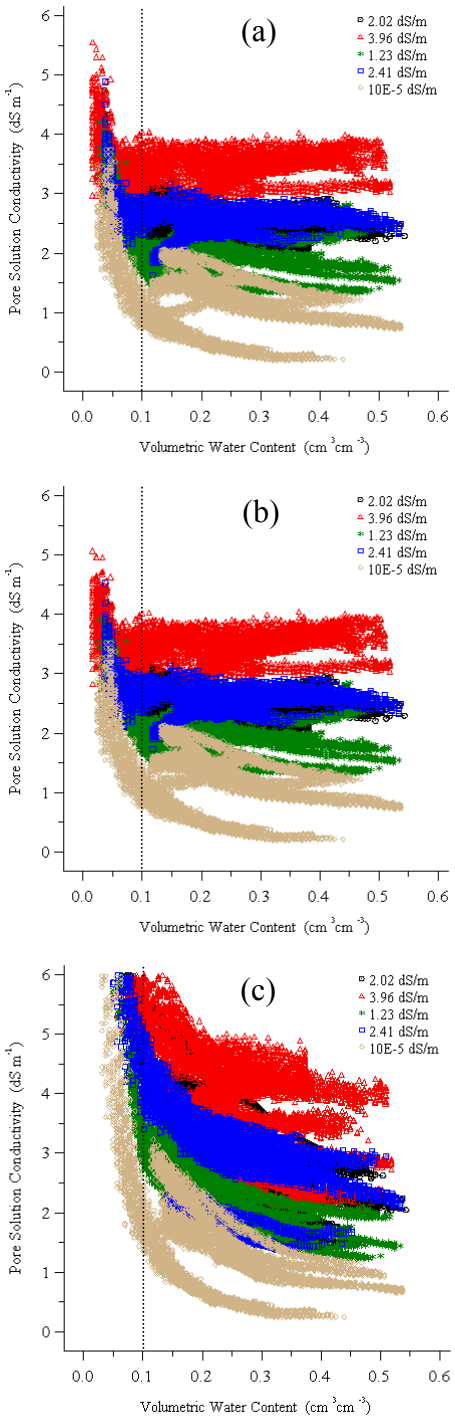

Figure 6.4. Soil pore solution conductivity predictions as a function of volumetric water content. Figure 6.4(a, b and c) shows predictions for Eqs.[6.11] and [6.16] cases I and II, respectively. Dashed vertical line represents the cutoff criterion for volumetric water content employed in this research ($\theta_v = 0.10$ cm^3 cm^{-3}).

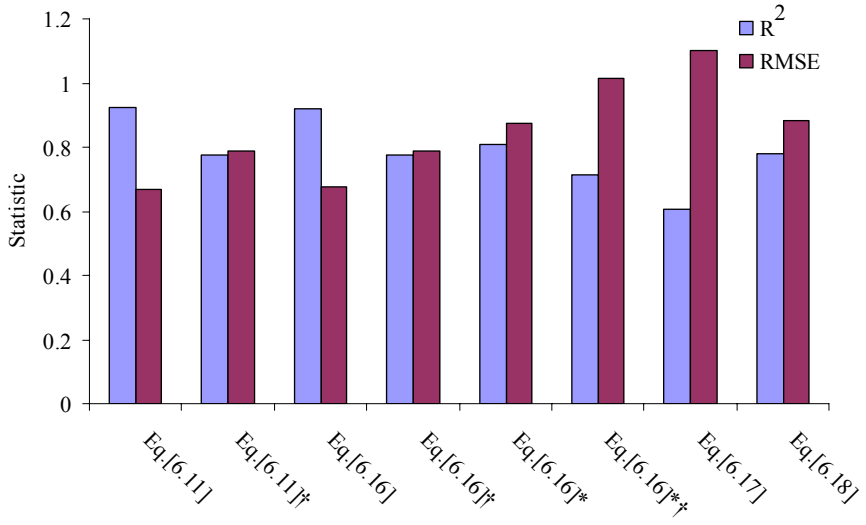

Figure 6.5. Root mean square error (RMSE) and coefficient of determination (R^2) from average pore solution conductivity predictions from Eqs.[6.11], [6.16], [6.17] and [6.18] compared to initial saturating solution conductivities. *With A and B from soil/disturbance specific calibration equations (Eq.[6.6]). † Models fit on a general basis (all data).

VITA

Tairone Paiva Leão was born in Rio Verde, Goiás, Brazil in 1979. After high school he attended the University of Rio Verde, pursuing a bachelor's degree in Agronomy. He graduated in 2001 and joined the University of São Paulo – Escola Superior de Agricultura Luiz de Queiroz to pursue a Masters Degree in Agronomy with emphasis in Soil Physics. He obtained his Masters Degree in 2002 and in 2003 started his first Ph.D. degree at the University of São Paulo – Escola Superior de Agricultura Luiz de Queiroz. In August 2004 he started his Ph.D. in Earth and Planetary Sciences with emphasis in Soil Physics at the University of Tennessee. In August 2005 he obtained his first Ph.D. degree in Agronomy at the University of São Paulo and returned to continue his degree at the University of Tennessee. He was supported as a graduate teaching assistant and as a graduate research assistant, funded by a joint grant of the U.S. Army Corps of Engineers and the University of Tennessee.